

**CONTACTLESS SMART BODY TEMPERATURE SCANNER  
SYSTEM**

**ALVIN KU ZI QIAN**


**A project report submitted in partial fulfilment of the  
requirements for the award of Bachelor of Engineering  
(Honours) Electrical and Electronic Engineering**

**Lee Kong Chian Faculty of Engineering and Science  
Universiti Tunku Abdul Rahman**

**April 2021**

## DECLARATION

I hereby declare that this project report is based on my original work except for citations and quotations which have been duly acknowledged. I also declare that it has not been previously and concurrently submitted for any other degree or award at UTAR or other institutions.

Signature :   
\_\_\_\_\_

Name : ALVIN KU ZI QIAN  
\_\_\_\_\_

ID No. : 1602914  
\_\_\_\_\_

Date : 13 APRIL 2021  
\_\_\_\_\_


## APPROVAL FOR SUBMISSION

I certify that this project report entitled "**CONTACTLESS SMART BODY TEMPERATURE SCANNER SYSTEM**" was prepared by **ALVIN KU ZI QIAN** has met the required standard for submission in partial fulfilment of the requirements for the award of Bachelor of Engineering (Honours) Electrical and Electronic Engineering at Universiti Tunku Abdul Rahman.

Approved by,

Signature

:

  
\_\_\_\_\_

Supervisor

:

DR. TAN CHUN HUI  
\_\_\_\_\_

Date

:

13 APRIL 2021  
\_\_\_\_\_

The copyright of this report belongs to the author under the terms of the copyright Act 1987 as qualified by Intellectual Property Policy of Universiti Tunku Abdul Rahman. Due acknowledgement shall always be made of the use of any material contained in, or derived from, this report.

© 2021, Alvin Ku Zi Qian. All right reserved.

## **ACKNOWLEDGEMENTS**

I would like to thank everyone who had contributed to the successful completion of this project. I would also like to deliver my deepest gratitude to my research supervisor, Dr. Tan Chun Hui, for his valuable time and invaluable guidance, comments, and suggestions throughout the development of this research.

In addition, I would also like to dedicate my gratitude towards my loving parents and friends. They had helped me emotionally by giving constant encouragement in completing this final year project.

## ABSTRACT

Fever is the early sign of infection. Therefore, body temperature screening has always been deployed to detect suspected individuals with infectious diseases. The current temperature scanner is distance-dependent, which introduces errors when the temperature is measured at various distances. Also, some contactless temperature scanners can only measure body temperature at a fixed distance. Besides, many studies are mainly focused on building additional features for the temperature scanner system rather than improving the performance of the temperature sensor. In addition, the typical contactless temperature scanner is also not equipped with an automatic data logging feature for contact tracing purposes. This project aims to set up a low-cost, functional distance-independent contactless temperature scanner system with an automated data logging feature. Next, a calibration approach is introduced to ensure accurate contactless temperature measurement at various distances. The proposed system consists of integrating subsystems, which are the temperature scanner system and data logging system. The prototype is first calibrated at a fixed distance of 3 cm to improve its accuracy. It is then further calibrated at multiple distances of 3.5 cm, 4 cm, 4.5 cm, and 5 cm to obtain a minimal trade-off between measuring distance and accuracy. The data logging feature can store user's information such as barcode, temperature, check-in time, and date on an SD card. The alarming system is activated if the user's temperature is not within the normal range. Overall, the prototype developed can provide temperature measurement with an accuracy of  $\pm 0.2$  °C and automatically record the user's information. The prototype is envisioned to be deployed at public or private places, which a barcode is used for identification purpose.

## TABLE OF CONTENTS

<b>DECLARATION</b>	<b>iii</b>
<b>APPROVAL FOR SUBMISSION</b>	<b>iv</b>
<b>ACKNOWLEDGEMENTS</b>	<b>vi</b>
<b>ABSTRACT</b>	<b>vii</b>
<b>TABLE OF CONTENTS</b>	<b>i</b>
<b>LIST OF SYMBOLS / ABBREVIATIONS</b>	<b>ix</b>
<b>LIST OF APPENDICES</b>	<b>x</b>

### CHAPTER

<b>1</b>	<b>INTRODUCTION</b>	<b>1</b>
	1.1 Background	1
	1.2 Motivation of the Study	2
	1.3 Problem Statement	4
	1.4 Aim and Objectives	5
	1.5 Scope and Limitation of the Study	5
<b>2</b>	<b>LITERATURE REVIEW</b>	<b>7</b>
	2.1 Temperature of a Human Body	7
	2.2 Body Temperature Measurement Location and Invasiveness	10
	2.3 Comparison of Different Measurement Sites for Body Temperature	11
	2.4 Thermometer	15
	2.4.1 Comparison of Contact and Contactless Thermometer	15
	2.4.2 Comparison of Different Contactless Infrared Thermometer	18
	2.4.3 Commercially Available Handheld and Automatic Contactless Infrared Thermometer	22
	2.5 Principle of Contactless Infrared Temperature Measurement	23

2.5.1	Emissivity	24
2.5.2	Field of View	24
2.5.3	Distance to Spot Ratio	25
2.6	Review of Existing Prototype	26
2.6.1	Contactless Temperature Monitoring for Campus	26
2.6.2	Contactless Portable Infrared Thermometer	27
2.6.3	IoT Contactless Body Temperature Measurement System	28
<b>3</b>	<b>METHODOLOGY AND WORK PLAN</b>	<b>30</b>
3.1	Project Planning and Management	30
3.1.1	Workflow	30
3.1.2	Schedule	32
3.1.3	Cost Estimation	33
3.2	System Overview	34
3.3	Hardware	35
3.3.1	Arduino Mega 2560	35
3.3.2	USB Host Shield	37
3.3.3	HC-SR04 Ultrasonic Sensor	37
3.3.4	MLX90614 Non-Contact Infrared Temperature Sensor	38
3.3.5	16x2 LCD Module	40
3.3.6	I2C Serial Interface Board Module	41
3.3.7	DS3231 RTC Module	42
3.3.8	SD Card Module	43
3.3.9	Buzzer	44
3.3.10	LED	44
3.3.11	SSM Wired 1D Barcode Scanner	45
3.4	Software	46
3.4.1	Arduino IDE	46
3.4.2	Origin 2019b	47
3.5	Circuit Design	47
3.5.1	Contactless Temperature Scanner System	48
3.5.2	Tracking System	48



3.6	Sensor Calibration	49
3.6.1	Fixed Distance Calibration Setup and Procedure	49
3.6.2	Multiple Distances Calibration Setup and Procedure	54
3.7	System Integration	55
3.7.1	Final Circuit Design	56
3.7.2	Overall System Flowchart	56
<b>4</b>	<b>RESULTS AND DISCUSSION</b>	<b>59</b>
4.1	Introduction	59
4.2	Fixed Distance Calibration Setup	59
4.2.1	Data Collected	59
4.2.2	Curve Fitting	61
4.2.3	Verification	67
4.3	Multiple Distances Calibration Setup	68
4.3.1	Data Collected	68
4.3.2	Surface Fitting	69
4.3.3	Verification	76
4.4	Prototype Evaluation	77
4.4.1	Percentage of Escapees	78
4.4.2	Limitation of Operating Temperature Range	85
4.5	Final Prototype	87
4.5.1	Contactless Temperature Scanner System	87
	Figure 4.12 indicates the display of normal temperature reading on the LCD with the flashing green LED.	87
4.5.2	Barcode Tracking System	89
4.5.3	Prototype Setup	91
<b>5</b>	<b>CONCLUSIONS AND RECOMMENDATIONS</b>	<b>92</b>
5.1	Conclusion	92
5.2	Recommendations for Future Works	92
	<b>REFERENCES</b>	<b>94</b>
	<b>APPENDICES</b>	<b>98</b>

## LIST OF TABLES

Table 2.1: Human Body Temperature for Different Ages (Heng Yew Ling <i>et al.</i> , 2015)	8
Table 2.2: Comparison between Different Body Temperature Measurement Sites	11
Table 2.3: Comparison between Contact and Contactless Thermometer	17
Table 2.4: Comparison of Different Contactless Infrared Thermometer	21
Table 2.5: Review of Handheld and Automatic Infrared Thermometer	22
Table 3.1: Task Description	31
Table 3.2: Estimated Cost	33
Table 3.3: Specification of Arduino Mega 2560	36
Table 3.4: Pinout Description of HR-SR04	38
Table 3.5: Specification of Ultrasonic Sensor of HR- SR04	38
Table 3.6: Pinout Description of MLX90614	39
Table 3.7: Specification of MLX90614	40
Table 3.8: Pinout Description of 16x2 LCD	40
Table 3.9: Specification of 16x2 LCD	41
Table 3.10: Specification of I2C Serial Interface Board Module	41
Table 3.11: Pinout Description of RTC Module	42
Table 3.12: Specification of RTC Module	42
Table 3.13: Pinout Description of SD Card Module	43
Table 3.14: Specification of SD Card Module	43
Table 3.15: Specification of Buzzer	44
Table 3.16: Specification of Red and Green LEDs	45

Table 3.17: Specification of Barcode Scanner	46
Table 3.18: Method Applied to Manipulate the Temperature of Water Balloon	53
Table 4.1: Data Collected from Fixed Distance Calibration Setup	60
Table 4.2: Statistical Measures of Different Polynomial Models	62
Table 4.3: Percentage Error for 6 <sup>th</sup> Degree Polynomial Model	63
Table 4.4: Percentage Error Obtained using Different Decimal Places	64
Table 4.5: Average Temperature Measured at Different Measuring Distances	68
Table 4.6: Temperature Differences with Respect to Reference	69
Table 4.7: Statistical Measure of Selected Functions	71
Table 4.8: Percentage Error Calculation using Rational Taylor function	72
Table 4.9: Percentage Error of Different Built-in Functions	74
Table 4.10: Summarized Definition of Selected Functions	75
Table 4.11: Reference Table to Detect Escapee	79
Table 4.12: Data collected with Percentage Escapee Calculation	80
Table 4.13: Estimation of Allowable Measured Temperature Range	85

## LIST OF FIGURES

Figure 1.1: Statistic for infected and death cases( <i>Coronavirus: Comparing COVID-19, SARS and MERS / News / Al Jazeera</i> , no date)	2
Figure 1.2: Statistic for infected COVID-19 cases per million people (Ritchie <i>et al.</i> , 2021)	3
Figure 2.1: Body Temperature Measurement Range ( <i>Normal body temperature / definition of Normal body temperature by Medical dictionary</i> , no date)	9
Figure 2.2: Oesophagus Measurement (Naiman <i>et al.</i> , 2017)	10
Figure 2.3: Mercury-in-glass thermometer (Rani, 2015)	16
Figure 2.4: Handheld Infrared Thermometer (Kapoor, 2021)	18
Figure 2.5: Automatic Infrared Thermometer ( <i>Handsfree Non-contact Automatic Forehead Infrared Thermometer</i> , no date)	19
Figure 2.6: AI Infrared Thermometer (Smith, 2020)	20
Figure 2.7: Deployment of Infrared Thermography (Glaser, 2020)	20
Figure 2.8: Difference forms of infrared energy ( <i>What is Emissivity? / Fluke Process Instruments</i> , no date)	24
Figure 2.9: Field of View ( <i>IR Thermometers explained - FireCraft / ir-thermometers-explained-firecraft.pdf / PDF4PRO</i> , no date)	25
Figure 2.10: Relationship between Distance to Spot Area (Schneider, 2007)	26
Figure 2.11: System Overview (Tang and Hung, 2017)	27
Figure 2.12: Block diagram (Santoso and Dalu Setiaji, 2016)	28
Figure 2.13: Function block diagram (Rahimoon, Abdullah and Taib, 2020)	29

Figure 3.1: Project Workflow	30
Figure 3.2 Gantt chart for Phase 1	32
Figure 3.3 Gantt chart for Phase 2	32
Figure 3.4: Block diagram of the proposed system	35
Figure 3.5: Arduino Mega 2560 (Kumar <i>et al.</i> , 2015)	36
Figure 3.6: USB Host Shield ( <i>USB Host Shield 2.0 - Arduino Compatible</i> / <i>QQ Online Trading</i> , no date)	37
Figure 3.7: HS-SR04 Ultrasonic Sensor	37
Figure 3.8: MLX96014 Infrared Temperature Sensor	39
Figure 3.9: Internal block diagram of MLX96014 ( <i>MLX90614 IR Thermometer Hookup Guide</i> - <i>learn.sparkfun.com</i> , no date)	39
Figure 3.10: 16x2 LCD	40
Figure 3.11: I2C Serial Interface Board Module ( <i>Wiring I2C module on 16x2 LCD with SCL/SDA</i> / <i>14core.com</i> , no date)	41
Figure 3.12: RTC Module	42
Figure 3.13: SD Card Module	43
Figure 3.14: Buzzer	44
Figure 3.15: LED	45
Figure 3.16: SSM Wired Barcode Scanner	45
Figure 3.17: Arduino IDE	47
Figure 3.18: Origin 2019b	47
Figure 3.19: Temperature Scanner System Schematic Diagram	48
Figure 3.20: Tracking System Schematic Diagram	49
Figure 3.21: Filling the Water Balloon	50
Figure 3.22: Marking of Reference Line	51

Figure 3.23: Fixed Distance Calibration Setup	52
Figure 3.24: Manipulating the Temperature of Water Balloon	53
Figure 3.25: Multiple Distances Calibration Setup	55
Figure 3.26: Schematic Circuit of Prototype	56
Figure 3.27: Flowchart of the System	58
Figure 4.1: Graph of Reference Versus Prototype	61
Figure 4.2: Polynomial Fitting for Graph of Reference Versus Prototype	66
Figure 4.3: 6 <sup>th</sup> Polynomial Fitting's Coefficients	66
Figure 4.4: Verification for Temperature Measured by Reference and Prototype	67
Figure 4.5: Plotted Surface Graph	70
Figure 4.6: Rational Taylor's Fitting Coefficients	74
Figure 4.7: Temperature Measured at 3.5cm	76
Figure 4.8: Temperature Measured at 4cm	76
Figure 4.9: Temperature Measured at 4.5cm	77
Figure 4.10: Temperature Measured at 5cm	77
Figure 4.11: Prototype Evaluation using Human as Subject	78
Figure 4.12: Normal Temperature	87
Figure 4.13: High Temperature Within the Operating Range	87
Figure 4.14: Low Temperature Within the Operating Range	88
Figure 4.15: High Temperature Outside the Operating Range	88
Figure 4.16: Low Temperature Outside the Operating Range	89

Figure 4.17: System Inquiry of Barcode	89
Figure 4.18: Display of Scanned Barcode	90
Figure 4.19: Sample of Data Stored	90
Figure 4.20: Overview of Final Prototype	91

### **LIST OF SYMBOLS / ABBREVIATIONS**

H1NI	Hemagglutinin Type 1 and Neuraminidase Type 1
SARS	Severe Acute Respiratory Syndrome
COVID-19	Coronavirus Disease 2019
AI	Artificial Intelligence
EEPROM	Electrically Erasable Programmable Read-Only Memory
MOH	Medical Officer of Health
MERS	Middle East Respiratory Syndrome
WHO	World Health Organization
LCD	Liquid Crystal Display
USB	Universal Serial Bus
RTC	Real Time Clock
RFID	Radio-Frequency Identification
I2C	Inter-Integrated Circuit
ICU	Intensive Care Unit
IDE	Integrated Development Environment
SRAM	Static Random-Access Memory
SD Card	Secure Digital Card
FOV	Field of View
3D	Three-Dimensional
PCB	Printed Circuit Board

## LIST OF APPENDICES

APPENDIX A: Polynomial Curve Fitting Equation	98
APPENDIX B: Percentage Error Calculation for Curve Fitting	101
APPENDIX C: Data Collected for Multiple Distances Calibration	104
APPENDIX D: Surface Fitting Equation	106
APPENDIX E: Percentage Error Calculation for Surface Fitting	108
APPENDIX F: Arduino Source Code	112



## CHAPTER 1

### INTRODUCTION

#### 1.1 Background

The thermoscope is the earliest invention that enables humankind to measure temperature. However, the absence of scale in thermoscope only allows the user to illustrate the changes in temperature of the measured object but did not provide an accurate temperature reading. In 1593, an Italian inventor, Galileo Galilei, managed to invent the world's first version of thermoscope using the principle of buoyancy. After two decades, another Italian inventor, Santorio Santorio, decided to apply a numerical scale on the thermoscope. The invention leads to the born of the first rudimentary thermometer for medical usage. The further introduction of different scales such as Fahrenheit, Celsius, and Kelvins standardised and gave rise to a more accurate and consistent temperature measurement.

Next, thermometers have been widely used in the medical setting as a tool to measure body temperature. The body temperature is measured through several locations such as the mouth, rectum, axillary, tympanic and more. The body temperature is generally used as guidance during diagnosis as fever is one of the ordinary sign or symptoms that emerge during the tracking of several infectious diseases. The earliest method for body temperature measurement was done by using a contact mercury thermometer. The advancement of electronic technology causes the rise of different contact-type digital thermometers which are portable and have a digital display for convenient measurement reading. Also, the modern thermometer nowadays uses infrared technology, which makes contactless body temperature measurement possible.

Moreover, the importance of body temperature measurement is highlighted in mass fever screening. Mass fever screening has always been one of the government's proposed solution to break the transmission chain of infectious disease. This can be seen from the vast deployment of mass screening during the SARS outbreak in 2003, H1N1 attack in 2009, and the recent COVID-19 pandemic. The spread of the deadly COVID-19 virus has caused a global pandemic that exerted immense stress to both private and public healthcare

facilities. Also, the COVID-19 pandemic has contributed to a dramatic loss of human lives. According to statistics, more than 4 million peoples are infected globally with a record of more than 300,000 deaths reported across 188 countries worldwide (Teo, Tan and Prem, 2020). Figure 1.1 indicates the infection and death cases caused SARS, MERS, and COVID-19. Up until now, the case of COVID-19 is still increasing daily.

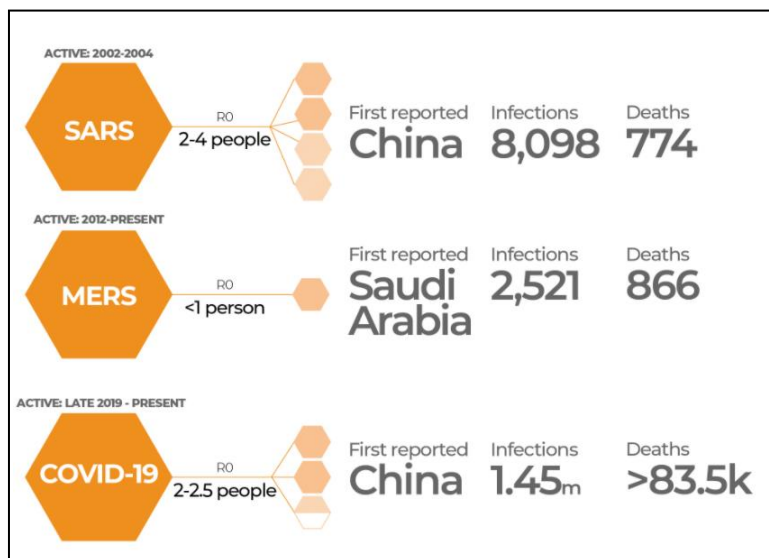


Figure 1.1: Statistic for infected and death cases(*Coronavirus: Comparing COVID-19, SARS and MERS / News / Al Jazeera, no date*)

Therefore, the WHO has issued a statement related to ways to protect oneself from the virus and help to halt its deadly spread. These include regular hand washing with soap, mask wearing in public area, and the most important body temperature checking. The body temperature screening for fever identification is crucial in the detecting the suspected individual with infectious disease.

## 1.2 Motivation of the Study

Most cases of infectious diseases such as SARS, H1N1, MERS, and current COVID-19 are due to the individual's concealment of travel histories and symptoms related to the disease. The individual may conceal information related to potential disease exposure because of fear or by intention. Nevertheless, this poor ethical action has caused the rapid spread of the deadly

virus to innocent citizens. Thus, body temperature screening has become the first level of infectious disease detection for all the places, especially for hotels, university campuses, hospitals, and the airport, which are usually crowded with people. Figure 1.2 indicates the global infection cases of COVID-19.

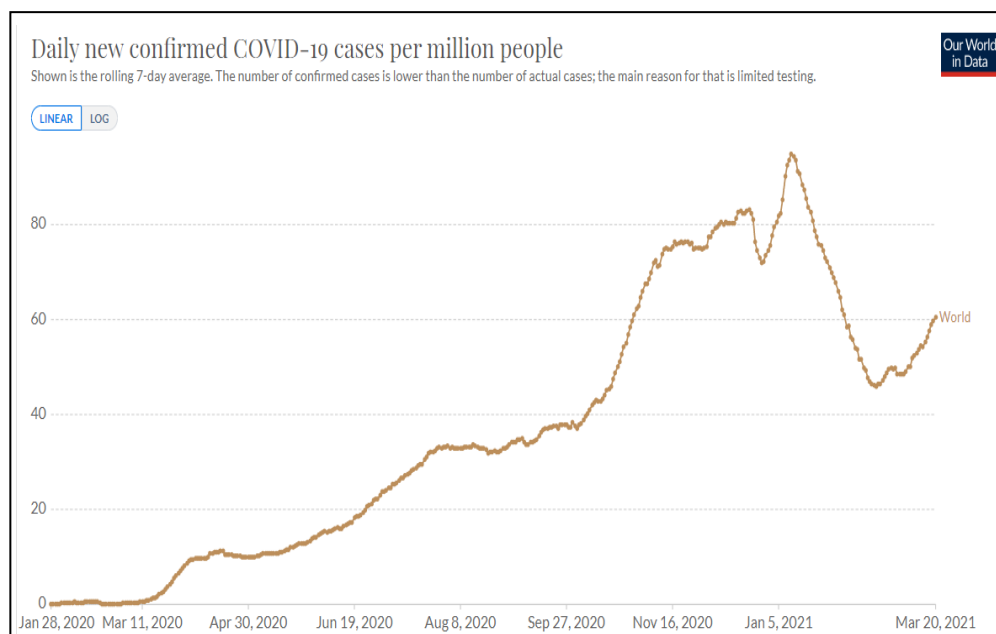


Figure 1.2: Statistic for infected COVID-19 cases per million people (Ritchie *et al.*, 2021)

In addition, body temperature screening is currently becoming the new normal to halt the wild spread of COVID-19. Malaysia's government has also declared that body temperature screening is an inevitable process before accessing any premises during the pandemic. The existence of the Prevention and Control of Infectious Disease Act 1998 causes the owner of a premise to abide strictly as the breaching of rules may cause the owner to get a monetary fine. Subsequently, this causes the increment demand for contactless body temperature screening. All the countries worldwide could not afford another wave of virus outbreak due to its severe impact on the economy, living lifestyle, education, and also shocking fatalities. Therefore, the deployment of a contactless temperature scanner system is essential and acts to prevent the current and future infectious disease outbreak.

Moreover, contact tracing is another crucial strategy to break the transmission chain and flatten the infection curve of COVID-19. The contact

tracing records the temperature, identity, time, date, and places visited of an individual. It allows early identification of the people who have contacted a COVID-19 patient and prevents any secondary cases. The early detection enables the government to detect the location of the new COVID-19 cluster and get those at risk to undergo self-isolation. Subsequently, contact tracing can help in reducing the spread of the COVID-19 virus.

### **1.3 Problem Statement**

The current temperature scanner available in the market is distance-dependent, which means the temperature measured varies accordingly to the measuring distance. The temperature measured tends to change according to the measuring distance. Therefore, no calibration is made to ensure accurate measurement at a different distance within the measuring range. Also, the current contactless temperature scanners can only measure body temperature at a fixed distance, which the measuring distance is minimal.

Next, a lot of works and studies have been conducted to develop a low-cost contactless temperature scanner. However, the studies mainly focus on adding extra functionality to the temperature scanner but less likely to improve the temperature scanner's accuracy and performance. Even if there are studies on improving the accuracy, most of the studies calibrate the prototype using a reference thermometer at a fixed distance. Hence, the measurement tends to be inaccurate if the object is not placed at a fixed distance. The temperature sensor's calibration to provide a minimal trade-off between increasing measuring distance and accuracy has not been done.

Nevertheless, the contactless temperature scanners available in the market are only designed for the sole purpose of body temperature measurement. It is not equipped with tracking features or data logging systems, which can track and record users' details. Therefore, extra human resources are needed to accomplish a repetitive task. The lack of an automated tracking feature in the current contactless temperature scanner system required people to fill in their information manually. The whole process of temperature screening and information recording requires quite an amount of time and often causes congestion, further increasing the risk of virus transmission. Some of the contactless temperature scanners equipped with infrared thermography provide

various useful functionalities such as face detection, mask detection, and alarming system. However, the cost of such a body temperature scanner is expensive.

The contactless temperature scanner system with data logging is essential, especially during the outbreak of contagious disease. The authority of a premise must abide by the law enforced by the government to record details such as body temperature, check-in time, and date of the people before entering a premise. In addition, an application, namely "MySejahtera," has been developed by the government for contact tracing purposes. However, all the data collected are only manageable by MOH and not the authority of premise. Therefore, a contactless temperature system with data logging features is needed.

#### **1.4 Aim and Objectives**

This project's main objective is to build a smart contactless body temperature scanner system utilizing low-cost commercially available microcontroller modules and sensors. The breakdowns of the main objective are:

1. To set up a low-cost functional distance-independent contactless temperature scanner system.
2. To introduce a calibration approach for accurate contactless temperature measurement at various distances.
3. To automate the contactless temperature scanner system with data recording.

#### **1.5 Scope and Limitation of the Study**

The project focuses on developing a low-cost functional contactless body temperature scanner system. The proposed system required the integration of both software and hardware. The details are as below:

- I. Hardware: Arduino UNO R3, USB Host Shield, LCD, SD Card Module, RTC Module, ultrasonic sensor, infrared temperature sensor, and barcode scanner.
- II. Software: Arduino IDE and OriginLab 2019b.

The prototype allows the automated monitoring, measuring, and recording of body temperature, identity with current date and time. The main objective of the project is to develop a contactless body temperature scanner

system. Thus, the accuracy of the prototype will be taken into consideration in this project. Besides, further improvement will be made on the measuring distance of the temperature scanner by taking the effect of measuring distance into consideration. The temperature scanner will also alert the authority for any detection of fever. Next, the tracking feature of the prototype will store the information of the user. The proposed system will only detect and record the users' identity in the form of a one-dimensional barcode. Thus, the prototype will only be applicable for university campuses, office, or places where one-dimensional barcode can represent an individual's identity on the identification card.

## CHAPTER 2

### LITERATURE REVIEW

#### 2.1 Temperature of a Human Body

Temperature is an indication of the degree of heat intensity. The human body temperature is undoubtedly one of the most important signs of health. It is often measured in the medical setting, preliminary to any diagnosis. The purpose of body temperature monitoring is to search for any sign of systemic or viral infection in the presence of fever, in which the body temperature of an individual is higher than the normothermia (Heng Yew Ling *et al.*, 2015). Fever is one of the earliest clinical symptoms of disease in humans and one of the most customary purposes for medical consultation. The human body defence system has the instinct to raise the body temperature to kill off bacteria or viruses and stimulate immune response during infection.

Next, the body temperature should be regulated within a very narrow allowable range so that the body's proper functionality is guaranteed. Hypothalamus is a part of the brain responsible for the continual adjustment and regulation of human body temperature to sustain an optimum body function environment. The thermoregulation mechanism ensures the body temperature is kept within a narrow range by controlling the loss and heat gain. The body temperature of a human is predominantly constant and independent of the surrounding temperature. However, it is also customary for the fluctuation of body temperature to occur throughout the day, provided that it should not be more than 1.0 °C (Heng Yew Ling *et al.*, 2015).

In healthy individuals, body temperatures may differ regarding environmental and biological factors such as surrounding temperature, activity level, ageing, and gender. However, the human body temperature is most highly influenced by the individual's age and the surrounding temperature (Geneva *et al.*, 2019). Table 2.1 shows the average body temperature range for different ages. Despite the variability, healthy human's body temperature should be regulated within the normothermia, which is ranges between 36.5 °C to 37.5 °C (Sessler, 2008).

Apart from the normal range for body temperature, hyperthermia and hypothermia are the two most extreme states of temperature loss or gain. Hyperthermia occurs as an individual's body temperature rises extensively and higher than the maximum limit of the average temperature range. On the other hand, hypothermia occurs when the body temperature of individual drops below the minimum limit of the normal temperature range. The failure to provide immediate medical treatment to both the hypothermia and hyperthermia condition may cause fatality. Figure 2.1 indicates the typical body temperature measurement range.

Table 2.1: Human Body Temperature for Different Ages (Heng Yew Ling *et al.*, 2015)

<b>Body Temperature Range</b>	<b>Hypothermia</b>	<b>Normal</b>	<b>Hyperthermia</b>
<b>Baby (Birth to 2 years old)</b>	36.00 °C	36.00 °C – 37.00 °C	37.00 °C – 38.00 °C
<b>Children (3 to 12 years old)</b>	36.00 °C	36.0 °C – 36.77 °C	38.00 °C
<b>Adult (13 to 40 years old)</b>	36.10 °C	36.1 °C – 37.20 °C	37.50 °C
<b>Elder (above 40 years old)</b>	35.00 °C	35.77 °C – 36.94 °C	37.44 °C – 37.94 °C



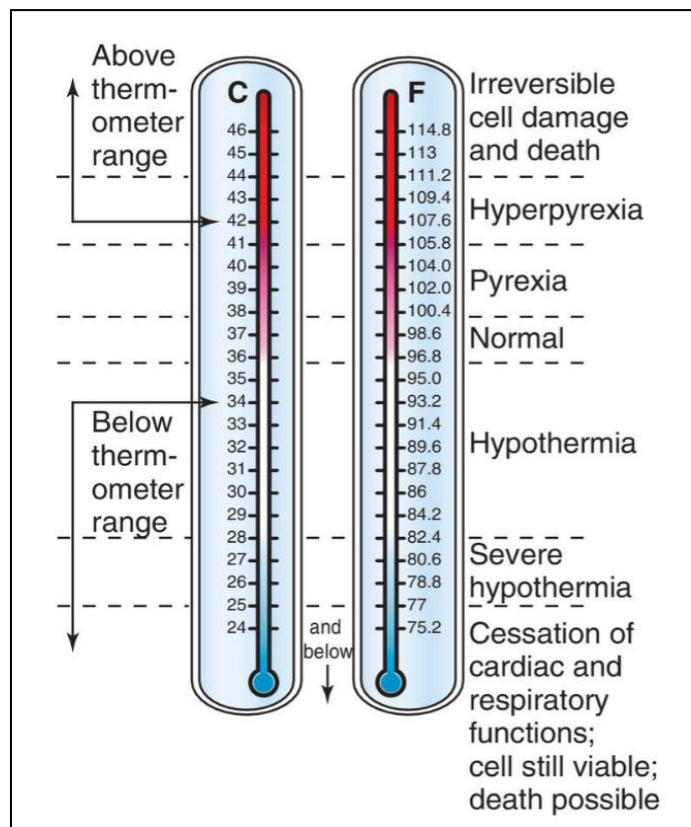


Figure 2.1: Body Temperature Measurement Range (*Normal body temperature / definition of Normal body temperature by Medical dictionary, no date*)

## 2.2 Body Temperature Measurement Location and Invasiveness

The locations for body temperature measurement can be categorized accordingly based on their invasiveness. The measure of temperature, which involves only the skin's surface, are known as non-invasive measurement. Next, the temperature measurement requiring the insertion of temperature probe into the natural body opening without extreme discomfort is minimally invasive measurement such as mouth, ear or rectum. Besides, the measure of body temperatures such as the insertion of temperature probe into the oesophagus, urinary bladder or pulmonary artery is considered invasive. Figure 2.2 shows the body temperature measurement by the insertion of a catheter from the mouth. The invasive measurements often cause undue discomfort and pain upon measurement and only reserved for an individual who is critically ill. However, the most accurate measurement of the core body temperature can only be obtained only by invasive means (Anuar and Leow, 2019). The non-invasive and minimally invasive measurements such as forehead, mouth and axilla are deemed to offer the finest approximation of the body temperatures (McCallum and Higgins, 2012). The following section shows the pros and cons of different measurement locations based on their invasiveness.

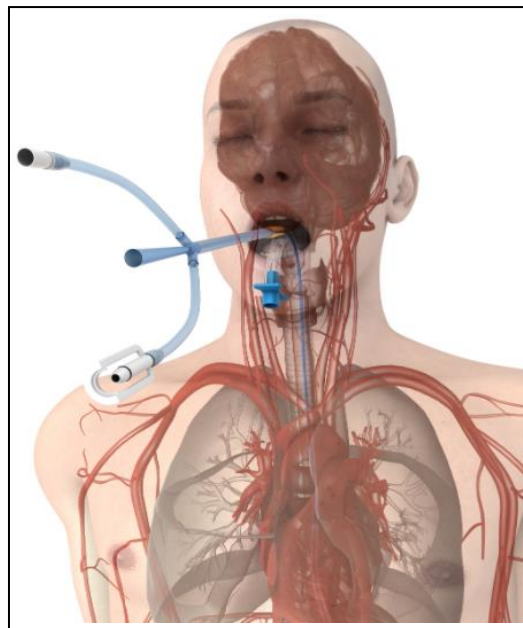


Figure 2.2: Oesophagus Measurement (Naiman *et al.*, 2017)

### 2.3 Comparison of Different Measurement Sites for Body Temperature

Table 2.2 shows the pros and cons of body temperature measurement based on different measurement sites and invasiveness.

Table 2.2: Comparison between Different Body Temperature Measurement Sites

<b>Invasiveness</b>	<b>Location</b>	<b>Pros</b>	<b>Cons</b>
Non-invasive	Axillary	<ul style="list-style-type: none"> <li>Easily accessible and safe</li> </ul>	<ul style="list-style-type: none"> <li>Unreliable measurement site due to the absence of prominent blood vessels</li> <li>Longer response time, usually 5 minutes with a mercury-in-glass thermometer and 40 to 80 seconds with an electronic thermometer (El-Radhi and Barry, 2006)</li> <li>Tendency to introduce errors and inaccuracies</li> </ul>
	Forehead Skin	<ul style="list-style-type: none"> <li>Easily accessible and safe</li> </ul>	<ul style="list-style-type: none"> <li>Sensitive to several factors such as exposure to the sun, cold air and perspiration (Tansey, Johnson and Johnson, 2015)</li> <li>Proper calibration is required to obtain a better estimation of body temperature</li> </ul>

Minimally invasive	Oral	<ul style="list-style-type: none"> <li>• Easy accessibility and convenient</li> <li>• Respond very quickly relative to the change in core body temperature (McCallum and Higgins, 2012)</li> </ul>	<ul style="list-style-type: none"> <li>• Oral temperature easily affected by foodstuffs, mucosal inflammation or circulating air (Drager Medical, no date)</li> </ul>
	Tympanic	<ul style="list-style-type: none"> <li>• Short measurement time</li> </ul>	<ul style="list-style-type: none"> <li>• Unreliable due to the incorrect placement of thermometer, lack of skill of the practitioner, and presence of cerumen in the ear canal that will disturb the measurement (El-Radhi and Barry, 2006)</li> <li>• Risk in perforating the tympanic membrane and cause potential discomfort due to misplacement of probe.</li> </ul>
	Rectal	<ul style="list-style-type: none"> <li>• Potential location for precise body temperature measurement as it directly reflects the core body temperature (Daniel S and Liran, 2002)</li> </ul>	<ul style="list-style-type: none"> <li>• Prolonged latency when there is a sudden fluctuation in core body temperature due to low blood circulation</li> <li>• Stressful, especially for children as it brings utter discomfort</li> </ul>

			<ul style="list-style-type: none"> <li>• Practical difficulties in keeping the rectal thermometer in position</li> <li>• Rectal thermometer without proper sanitisation can spread contamination found in the stool that causes contagious illness</li> <li>• Intestinal perforation might occur due to the placement of the probe is inserted too profoundly (Landsman <i>et al.</i>, 2012)</li> </ul>
Invasive	Oesophagus	<ul style="list-style-type: none"> <li>• High accuracy and quick response measurement</li> </ul>	<ul style="list-style-type: none"> <li>• Difficulties in term of insertion of a temperature probe, irritation of the nasal passage, and bleeding of oesophageal varices due to deep level insertion (Prabhakar, 2016)</li> <li>• Cause extreme discomfort for the conscious patient</li> </ul>
	Urinary Bladder	<ul style="list-style-type: none"> <li>• Useful for the patient that has required an indwelling catheter for continuous urinary drainage for their course of treatment</li> </ul>	<ul style="list-style-type: none"> <li>• Introduce inaccuracy as it is affected by the presence of the urine in the bladder</li> </ul>

			<ul style="list-style-type: none"> <li>• Impractical for clinical usage and useful for critically ill patients only (Fallis, 2002)</li> </ul>
	Pulmonary Artery	<ul style="list-style-type: none"> <li>• Gold-standard for core body temperature measurement</li> <li>• Fast response and better accuracy than oesophagus and urinary bladder (Wagner <i>et al.</i>, 2020)</li> </ul>	<ul style="list-style-type: none"> <li>• Impractical for clinical use</li> <li>• Incurred high risk during the insertion of the catheter as any mistakes may lead to death (Drager Medical, no date)</li> </ul>

## **2.4 Thermometer**

A thermometer is a measuring instrument that can evaluate temperature or temperature gradient to observe body malaise. In this 21<sup>st</sup> century, there are various types of thermometers for body temperature measurements such as digital electronic contact thermometer, alcohol thermometer, infrared thermometer, forehead thermometer and even old-style glass and mercury thermometer (Tang and Hung, 2017). The innovation of thermometer can be seen after several decades from its transformation from old type mercury-in-glass thermometer to digital thermometer and even contact or contactless infrared thermometer.

The thermometers for different measurement locations can be classified into two major categories, contact and contactless thermometer. The contact sensor in the contact thermometer required physical contact of invasive means with the measured object or individual as it uses heat conduction principle during measurement. On the other hand, a contactless thermometer used an infrared sensor to obtain the temperature of an object or individual non-invasively by referring to infrared emission level.

In brief, there are several basic requirements for an ideal thermometer. First, the accuracy level of a perfect thermometer must be only  $\pm 0.1$  °C. Next, the measurement of the thermometer should not be affected by the influence of environmental changes. The ideal thermometer must provide stable temperature readings, and the size of the thermometer must suit the site of measurement.

### **2.4.1 Comparison of Contact and Contactless Thermometer**

The mercury-in-glass thermometer as shown in Figure 2.3 is one of the oldest contact thermometers that has been the standard for human body temperature measurement for more than ten decades. However, since mercury is an environmentally hazard substance and extremely poisonous to the body, it has been recalled from the market and banned from medical usage (Sund-Levander and Grodzinsky, 2009). Next, an axillary thermometer is a contact and less invasive thermometer than oral or rectum thermometer. Even so, to obtain accurate measurement using an axillary thermometer, the axillary thermometer

has to be in place and hold for an extended time due to the slow temperature response from the measurement site.

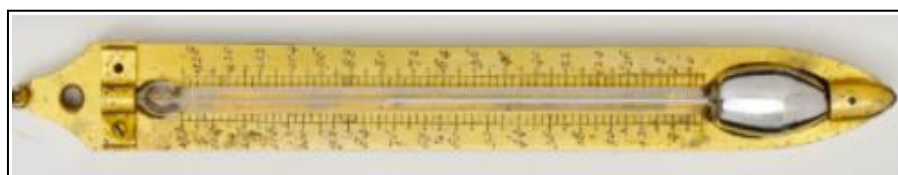


Figure 2.3: Mercury-in-glass thermometer (Rani, 2015)

Moreover, the infrared tympanic thermometer is another standard contact thermometer that provides a faster and convenient body temperature measurement method as the ear is readily reachable. Despite that, diversity still exists when comparing the temperature obtained from infrared tympanic thermometry to rectal thermometer. The main concern may be caused by the curve structure of ear canal and presence of cerumen that affects the accuracy and creates difficulties in measuring the tympanic membrane's temperature (Zhen *et al.*, 2014).

On the other hand, a contactless infrared thermometer can measure and provide accurate body temperature readings rapidly within seconds. Besides, the contactless infrared thermometer mostly measures the body temperature over the central forehead area, which is close to the temporal artery. The contactless infrared thermometer does not introduce any discomfort to the individual being accessed, and any physical body contact upon measurement is not required. Thus, the risk of infection due to contagious disease is minor and does not require regular sanitization.

Moreover, the contactless infrared thermometer temperature measurement significantly correlates with the rectal temperature using a mercury-in-glass thermometer. The temperature measured using contactless infrared thermometer has a correlation coefficient of 0.952 with the rectal temperature and the mean temperature was less than  $0.1^{\circ}\text{C}$  (Teran *et al.*, 2012).

However, the contactless infrared thermometer used in the study was a commercial product. Thus, the infrared thermometer has been well-calibrated using particular compensation technique to obtain the measurement close to the conventional measurement method. This hypothesis is originated and supported



by the research that proposed a cost-effective thermopile detectors array for close-range temperature screening (Sun *et al.*, 2014). According to the study, an average mean difference of 1.03°C and a standard deviation of 0.19°C were found based on the analysis of facial temperature obtained with axillary temperature as a reference. The result reveals that it is inevitable to include suitable correction factor and calibration if the estimation of body temperature from surfaces temperature is intended. On the flip side, the assessment of body temperature using forehead may not yield the best result as it is sensitive and highly influenced by the deviation of environment temperature.

In short, a contact thermometer still provides a more reliable temperature measurement based on the measurement site as compared to a contactless thermometer. However, proper calibration technique is required to improve the accuracy of measurement readings further. The response time of a contactless thermometer is shorter than a contact thermometer indicates good performance. Nevertheless, the contactless thermometer provides a much more hygiene measurement method than contact thermometers such as the rectum or axillary thermometer. The summary for the comparison between contact and the contactless thermometer is shown in Table 2.2.

Table 2.3: Comparison between Contact and Contactless Thermometer

<b>Aspects</b>	<b>Contactless Thermometer</b>	<b>Contact Thermometer</b>
<b>Speed</b>	Faster, normally within seconds	Slow, response time might differ based on measurement location
<b>Accuracy</b>	Less accurate, able to improve through proper calibration	High accuracy
<b>Hygiene</b>	More hygiene, no contact is required during measurement	Less hygiene, required physical contact during the measurement

#### 2.4.2 Comparison of Different Contactless Infrared Thermometer

Handheld infrared thermometer, automatic infrared thermometer, infrared thermography, and AI infrared thermometer are the common contactless type of infrared thermometers. All the mentioned contactless infrared thermometers work based on the same principle, detecting emitted infrared radiation and translating it into a temperature reading.

Nowadays, the handheld infrared thermometer available in the market can measure skin surface and body temperature. The provided selection offers flexibility to the user in terms of the type of temperatures to be measured. However, other contactless infrared thermometers only allow the measurement of body temperature. Also, all the contactless infrared thermometers measure the infrared radiation emitted from the prime surface it encounters. Thus, a proper adjustment must be made to the infrared thermometers by the manufacturer for better estimation of body temperature.

Next, the handheld infrared thermometer's person-in-charge does not need to be in contact with the individual to be evaluated. However, a few centimetres distance is unavoidable due to the limited distance of measurement from the infrared thermometer. Thus, the person-in-charge of the handheld infrared thermometer has to ensure the user is within the optimum measuring range and manually triggers the thermometer, as shown in Figure 2.4.



Figure 2.4: Handheld Infrared Thermometer (Kapoor, 2021)

As opposite to handheld infrared thermometer, others infrared thermometer allows the person-in-charge of the system to remain a certain

distance away from the targeted individual or object during measurement. The infrared thermometers will automatically measure the user's temperature if they are within the measuring range. Hence, the person-in-charge can monitor the process distance away from the user. As a result, the percentage of public disruption and cross-contamination are further reduced. Figure 2.5 indicates the automatic infrared thermometer that can measure the user's temperature automatically.



Figure 2.5: Automatic Infrared Thermometer (*Handsfree Non-contact Automatic Forehead Infrared Thermometer, no date*)

Moreover, all the contactless infrared thermometers can only obtain one measurement at once except for infrared thermography. The infrared thermography can measure the temperature of multiple people at once and estimate the temperature of individuals within the camera frame. Nevertheless, the lightweight and smaller size of the handheld, automatic, and AI infrared thermometer cause them to be portable compared to the infrared thermography. Generally, all the contactless infrared thermometers are equipped with an alarming system. However, only the AI infrared thermometer comes with features such as mask detection, face recognition, and data logging, which are not available in other contactless infrared thermometers. Figure 2.6 shows the AI infrared thermometer with face recognition capability.

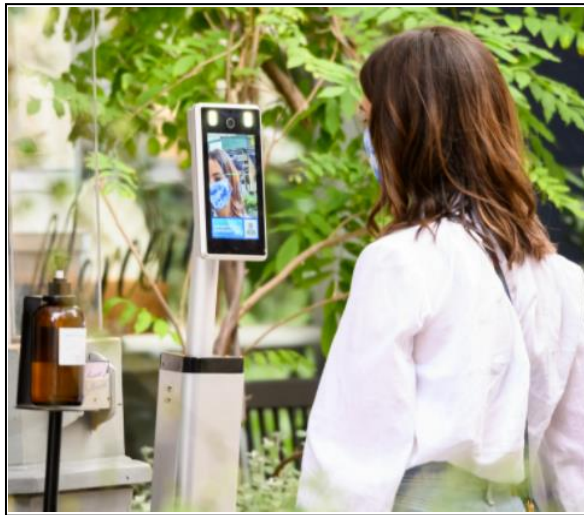


Figure 2.6: AI Infrared Thermometer (Smith, 2020)

Also, both the infrared thermometer's price is usually low as it consists of mainly a well-calibrated temperature sensor and its cover. On the other hand, the infrared thermography and AI infrared thermometer required expensive setup costs. Therefore, they are rarely used other than in larger companies, public services, and educational institutions. Figure 2.7 shows the deployment of infrared thermography for mass fever screening in the airport.



Figure 2.7: Deployment of Infrared Thermography (Glaser, 2020)

Lastly, the relatively lower price of handheld and automatic infrared thermometers caused them to be used extensively in many different body temperature screening places. Hence, the commercial handheld and automatic contactless infrared thermometer are reviewed in detail in the following section.

Table 2.4 shows the summarized table of comparison of different contactless infrared thermometers.

Table 2.4: Comparison of Different Contactless Infrared Thermometer

Aspect	Handheld	Automatic	Thermography	AI
Flexibility	Able to measure skin or body temperature	Measure body temperature only	Measure body temperature only	Measure body temperature only
Ease of use	Manual trigger and person-in-charge must be in close distance with user	Automatic detection and person-in-charge can monitor at a distance away from the user	Automatic detection and person-in-charge can monitor at a distance away from the user	Automatic detection and person-in-charge can monitor at a distance away from the user
Performance	One measurement at a time	One measurement at a time	Multiple measurements at once (within camera frame)	One measurement at a time
Additional Features	Alarming system	Alarming system	Alarming system	Alarming system, face recognition, data logging, and mask detection
Cost	Cheap	Medium	Expensive	Expensive

### 2.4.3 Commercially Available Handheld and Automatic Contactless Infrared Thermometer

There are various models of handheld and automatic infrared thermometers available in the market. However, in this section, only the most commonly deployed model found in different premises for temperature screening is reviewed. The selection of a specific model also depends on the highest sales performance in the various E-commerce platform. Moreover, the specified handheld and automatic infrared thermometer reviews are done based on the product's online technical datasheet. Table 2.5 indicates the summarized table of review for handheld and automatic infrared thermometers.

Table 2.5: Review of Handheld and Automatic Infrared Thermometer

Types	Handheld	Automatic
Model	UX-A-01	K3
Accuracy	$\pm 0.2^{\circ}\text{C}$	$\pm 0.2^{\circ}\text{C}$
Resolution	$0.1^{\circ}\text{C}$	$0.1^{\circ}\text{C}$
Response Time	1 second	0.5 second
Operating Temperature	32.0 to 42.9 $^{\circ}\text{C}$	34.0 to 45.0 $^{\circ}\text{C}$
Measuring Distance	5 to 15 cm	5 to 10 cm
Data Logging	Maximum of last 32 groups of temperature measured	Only available if connected to a computer for a maximum of 30 groups of temperature measured
Size (Length x Weight x Height)	105 x 55 x 160mm	200 x 150 x 180mm
Weight	115 grams	500 grams
Power Supply	2 x AA batteries	2 x AA batteries or USB power cable
Cost	Around RM30.00	Around RM 169.00

According to the table, both models have the same accuracy of  $\pm 0.2^{\circ}\text{C}$  with a resolution of  $0.1^{\circ}\text{C}$ . The response time of the automatic infrared thermometer is shorter as compared to the handheld infrared thermometer. The fast response time indicates that the automatic infrared thermometer can obtain more measurements than the handheld infrared thermometer within a specific time. In addition, both models have limited data logging capability. In terms of price, the automatic infrared thermometer is higher than the handheld type due to automatic measurement. Moreover, the operating temperature range for both infrared thermometers is different. However, both of them still provide a decent temperature range for body temperature measurement purposes.

Other than the aspects being reviewed in Table 2.5, the handheld infrared thermometer's accuracy relies on the measuring distance. The temperature measured changes with measuring distance. Hence, contributing to massive over reject and under reject. The over reject a phenomenon, which the object temperature is initially below the threshold value. Still, due to close distance measurement, the measured temperature is found to be above the threshold.

On the other hand, under reject occurs when the object temperature is initially above the threshold value, but the measured temperature is below the threshold duo to far distance measurement. Moreover, even though the automatic infrared thermometer specification mentioned that it could measure the temperature object within the measuring distance. However, it is discovered that the automatic infrared thermometer can only measure an object's temperature at a specific distance. Lastly, the specification of other models of the same thermometer in the market is almost identical.

## **2.5 Principle of Contactless Infrared Temperature Measurement**

In nature, all matters of temperature higher than absolute zero emit energy in the form of infrared radiation (Zhen *et al.*, 2014). An infrared thermometer utilized a lens to focus the infrared radiation from the targeted object onto a thermopile. The thermopile is a sensor used in an infrared thermometer to convert heat radiation from an object into an electrical signal for further processing. The accuracy of an infrared thermometer for temperature measurement is based on several factors. A strong understanding of these

essential factors, such as the distance to spot ratio, the field of view, and emissivity are vital in obtaining a precise body temperature measurement (Santoso and Dalu Setiaji, 2016).

### 2.5.1 Emissivity

All objects not only emit but also absorb and reflect heat, as shown in Figure 2.8. However, only the infrared energy emitted is used to indicate the temperature of the object. Emissivity is used as an indication for the ability of the object to emit infrared energy (Moon *et al.*, 2004). The emissivity values range from 0 to 1. The emissivity value of 0 is for a theoretical perfect thermal mirror and 1 for a theoretical object known as a blackbody that absorbed all the radiated energy. Measurement errors often cause by the reflected infrared energy or transmitted by the light source. If the object to be measured is visually reflective, not only the desired emitted radiation will be measured, but also the reflected radiation. The emissivity depends on the material of an object, surface and other factors. The higher the emissivity, the less influence of the reflected temperature, the easier the measurement generates a precise result. Thus, to measure a reflective an object with a reflective surface, definite compensation techniques must be applied to the infrared thermometer with permanent emissivity.

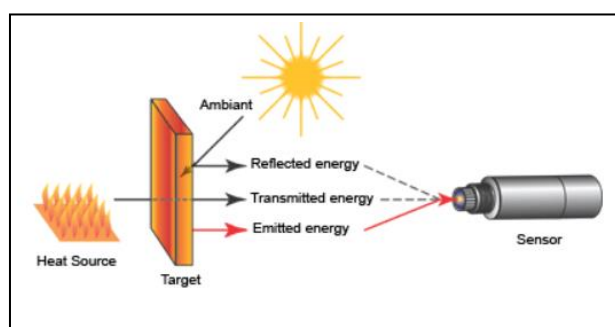


Figure 2.8: Difference forms of infrared energy (*What is Emissivity?* / Fluke Process Instruments, no date)

### 2.5.2 Field of View

The object's size and the distance of measure are crucial in order to obtain an accurate temperature measurement using an infrared thermometer. The field of



view is defined as the angle of vision, which the sensor will measure the average temperature of the object within the angle. Figure 2.9 indicates the field of view of an infrared thermometer. The narrower the field of angle, the better the accuracy of the measurement. Next, it is also essential that the object's to be measured fills the thermometer field of view. This allows the average temperature being measured is of the object but not from the surrounding. Thus, a relative closer distance of measurement is required if measured object is smaller in size to enhance accuracy. Equation 2.1 indicates the formula to calculate the measuring distance required based on the field of view and diameter of the object.

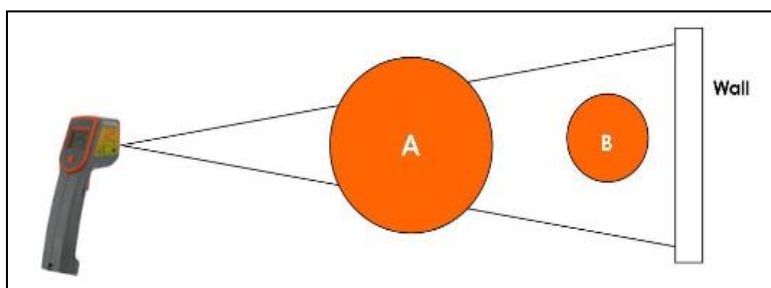


Figure 2.9: Field of View (*IR Thermometers explained - FireCraft / ir-thermometers-explained-firecraft.pdf / PDF4PRO*, no date)

$$D = \frac{S}{2 \times \tan\left(\frac{FOV}{2}\right)} \quad (2.1)$$

where

$D$  = measuring distance, cm

$S$  = diameter of object, cm

### 2.5.3 Distance to Spot Ratio

An infrared thermometer will collect the infrared energy emitted by the object from a circular measurement spot and divert it to the sensor. The distance to spot ratio indicates the relation between the size of the circular area and the measured object's distance, as shown in Figure 2.10. As the distance of measurement increases, the circular measurement spot also increases. The larger the distance to spot ratio, the higher the infrared thermometer's resolution. Thus, the thermometer can still measure the temperature of a smaller size object from a further distance.

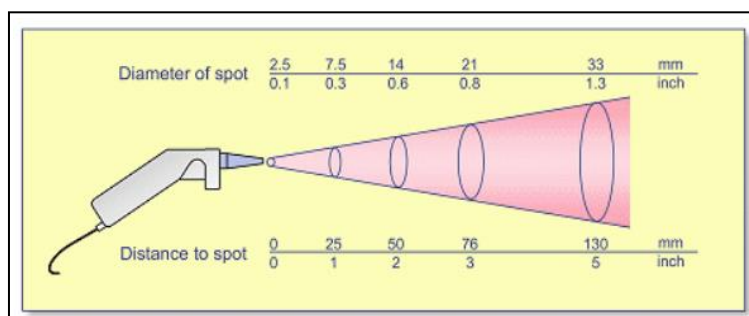


Figure 2.10: Relationship between Distance to Spot Area (Schneider, 2007)

## 2.6 Review of Existing Prototype

In this section, the existing prototypes of contactless temperature scanner system with different features are discussed.

### 2.6.1 Contactless Temperature Monitoring for Campus

An automated attendance recording and temperature measurement system is implemented (Tang and Hung, 2017). The invention's purposes are to prevent the outbreak of infectious disease and reduce the workforce for a repetitive task such as temperature logging. The system is established on a single board computer, FORLINX OK6410-A. The calibrated thermopile, namely the MLX90614, is used for contactless temperature measurement.

The access control system of the proposed system will verify the student's identity through a RFID card reader. After that, the thermopile will be initialized for temperature measuring and justify whether the user has a fever or not. The results obtained from the sensors are presented on the LED display and saved in the remote database, which governed by the authority. In order to ensure the accuracy of the system, the prototype is evaluated through several experiments with a commercial forehead thermometer, Beurer FT90. The experiments introduced proper calibration of the prototype and reduced the measurement error to within  $\pm 0.8^{\circ}\text{C}$  for the temperature ranges from  $32^{\circ}\text{C}$  to  $39^{\circ}\text{C}$ .

Even the prototype is well-calibrated with data being stored in the database, an alert system should be considered to alarm the people nearby if fever is identified. The system overview of the design is, as shown in Figure 2.11.

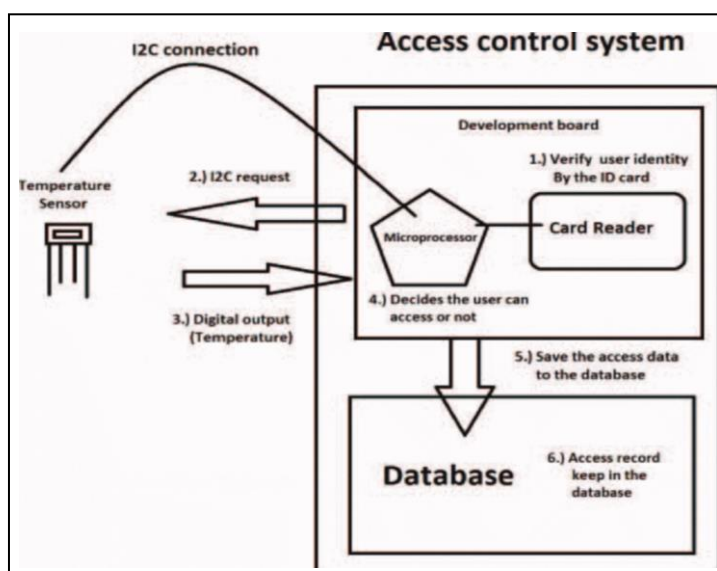


Figure 2.11: System Overview (Tang and Hung, 2017)

### 2.6.2 Contactless Portable Infrared Thermometer

A contactless portable infrared thermometer is designed for temperature scanning in clinical settings (Santoso and Dalu Setiaji, 2016). The proposed design is used as an indicator of infectious disease, especially for Influenza. The infrared thermometer can perform routine temperature scanning and allowed the user to input symptoms related to Influenza. Figure 2.12 illustrates the block diagram of the design.

The design is built on an AVR Atmega8A microcontroller with main components such as the MLX90614 infrared-sensitive thermopile detector, analogue joystick, LCD, buzzer and ultrasonic range sensor. The ultrasonic range sensor is used to limit the range of temperature measurement to 2cm to 3cm only. Once the temperature is measured, the user can input the information such as age category and symptoms through provided selection using a joystick. If the temperature is above average, the buzzer is triggered to draw attention. At the end of the process, an assessment ticket with all the information will be printed out by a mini thermal printer. The implementation of design using batteries and voltage regulators made the prototype to be portable.

The accuracy of the developed prototype is verified with Signstek 6802 II. The prototype can measure body temperature ranges between 35°C to 38°C with a measurement error of  $\pm 0.4^\circ\text{C}$ . Besides, the single complete process only

required around 1 minute, which is relatively time efficient. On the flip side, a data logging system should be included to store the user's temperature and symptoms as a record for future reference.

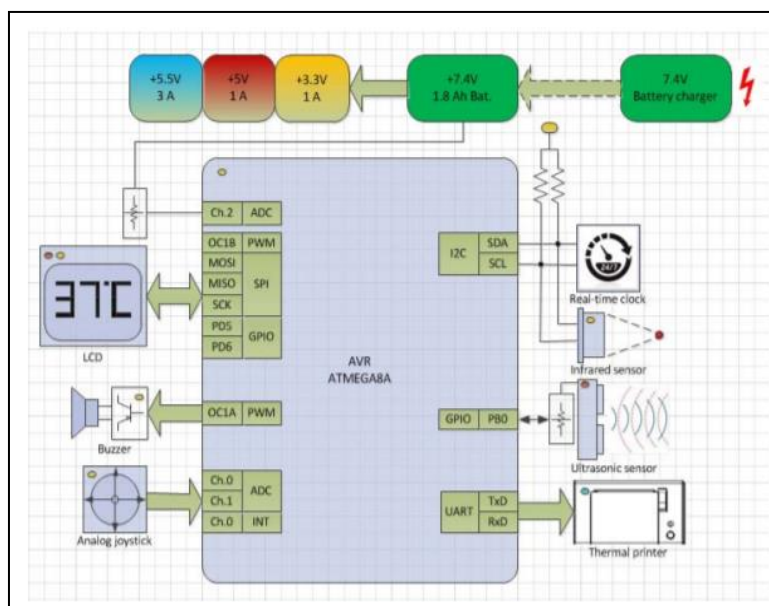


Figure 2.12: Block diagram (Santoso and Dalu Setiaji, 2016)

### 2.6.3 IoT Contactless Body Temperature Measurement System

The IoT contactless body temperature measurement system is designed to enable real-time remote body temperature monitoring via an open-source internet connection (Rahimoon, Abdullah and Taib, 2020). Figure 2.13 shows the functional block diagram of the system.

The Arduino CT-UNO controller is used as the microcontroller with two different temperature sensors attached to it. The two temperature sensors are the LM35 contact sensor and the MLX90614 contactless sensor. The LM35 temperature sensor is used to measure the ambient temperature, whereas the MLX90614 is responsible for human body temperature measurement. The measured temperatures will then be sent to the online portal through the additional ESP Wi-Fi Shield. The platform is wirelessly connected to enable the monitoring of collected data through an internet connection at anytime and anywhere.

The proposed system measure and record both the ambient and body temperature. The access to ESP Wi-Fi Shield enables remote temperature

monitoring to be possible. However, the authors did not mention any information related to the calibration works and the accuracy of the prototype.

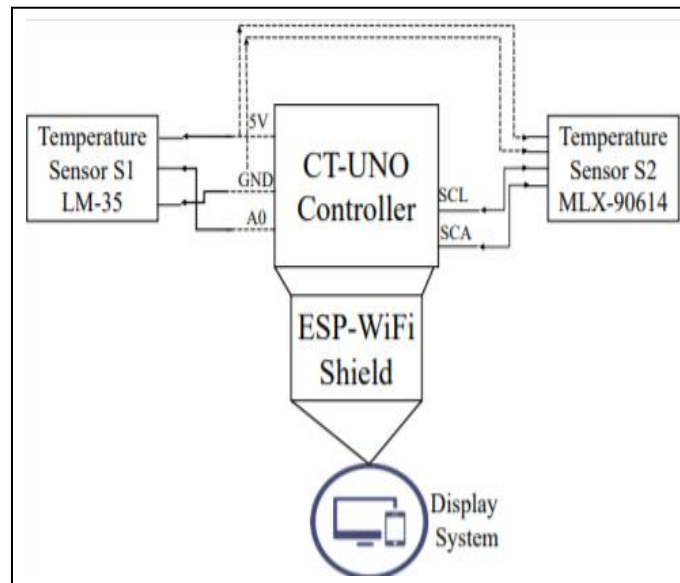


Figure 2.13: Function block diagram (Rahimoon, Abdullah and Taib, 2020)

## CHAPTER 3

### METHODOLOGY AND WORK PLAN

In this chapter, the methods and work plans involved in developing the prototype are explained in detail. The list and specifications of the required hardware and software will also be discussed.

#### 3.1 Project Planning and Management

In this section, the project workflow, schedule, and cost estimation are discussed. This ensures the effective allocation of resources such as time, money, and energy for the project.

##### 3.1.1 Workflow

Figure 3.1 indicates an overview of the project workflow. The project workflow consists of a series of subsequent tasks needed for the development of a working prototype. Table 3.1 shows the detailed descriptions of the tasks involved in the workflow.

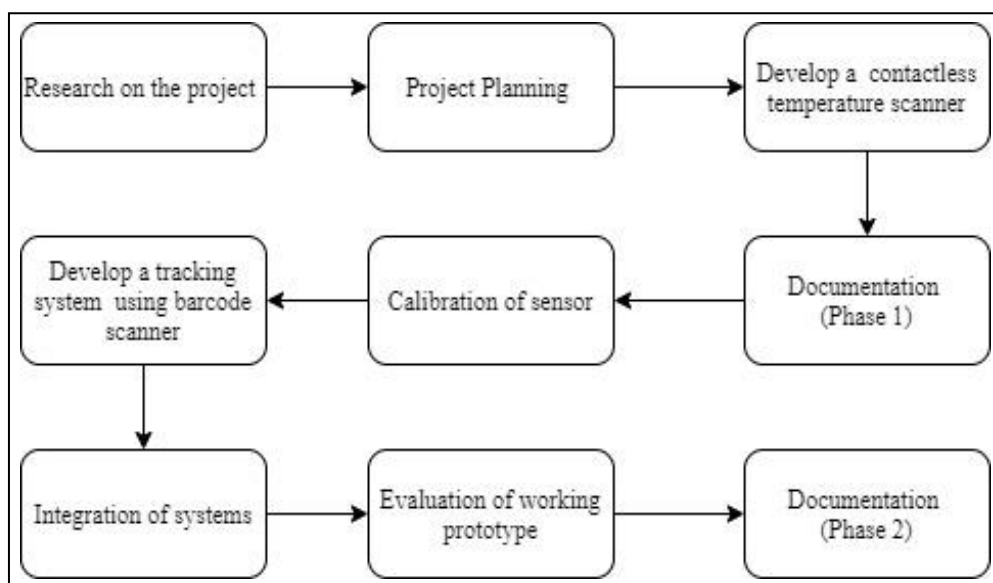


Figure 3.1: Project Workflow

Table 3.1: Task Description

<b>Task</b>	<b>Description</b>
<b>Research on the project</b>	<ul style="list-style-type: none"> <li>- Research on the information about smart contactless temperature scanner</li> <li>- Review of related works</li> <li>- Study and investigate the working principle of infrared thermometer</li> </ul>
<b>Project Planning</b>	<ul style="list-style-type: none"> <li>- Define the objectives and scopes of the project</li> <li>- Project scheduling and budgeting</li> <li>- Locate resources such as suitable sensors, microcontroller, and sensors</li> </ul>
<b>Develop a contactless temperature scanner system</b>	<ul style="list-style-type: none"> <li>- Design and construct the circuit for the contactless temperature scanner system</li> <li>- Code writing</li> </ul>
<b>Calibration of sensor</b>	<ul style="list-style-type: none"> <li>- Investigate suitable experiment setup for calibration</li> <li>- Calibration of infrared temperature sensor used with a commercial handheld infrared thermometer</li> </ul>
<b>Develop a tracking system</b>	<ul style="list-style-type: none"> <li>- Develop a tracking system with a barcode scanner</li> <li>- Design and construct the circuit for the tracking system</li> <li>- Code writing</li> </ul>
<b>Integration of systems</b>	<ul style="list-style-type: none"> <li>- Integrate both the contactless temperature scanner system and tracking system in term of hardware and software</li> </ul>
<b>Evaluation of the working prototype</b>	<ul style="list-style-type: none"> <li>- Test the functionality and accuracy of the prototype</li> <li>- Discussion of results</li> </ul>
<b>Documentation</b>	<ul style="list-style-type: none"> <li>- Report writing for the project</li> </ul>

### 3.1.2 Schedule

Gantt chart is used to schedule a suitable time frame for all the project workflow tasks. Figure 3.2 and Figure 3.3 indicate the Gantt chart for Phase 1 and Phase 2 of the project, respectively. The scheduling of activities is essential to avoid unwanted delays and ensure the project's completion on time. Nevertheless, planning and scheduling of activities can increase productivity.

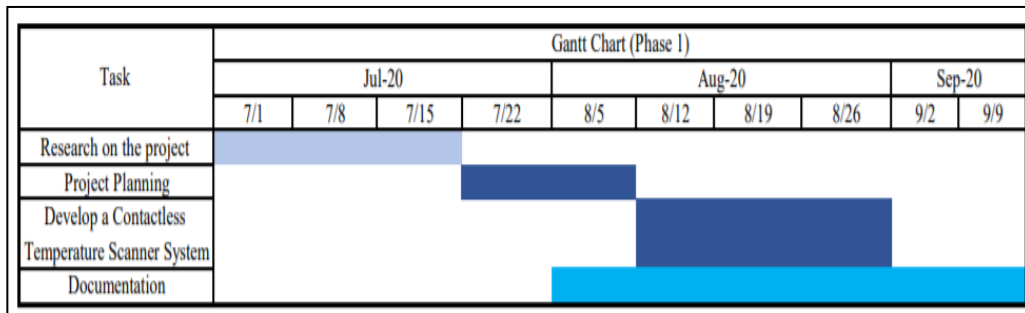


Figure 3.2 Gantt chart for Phase 1

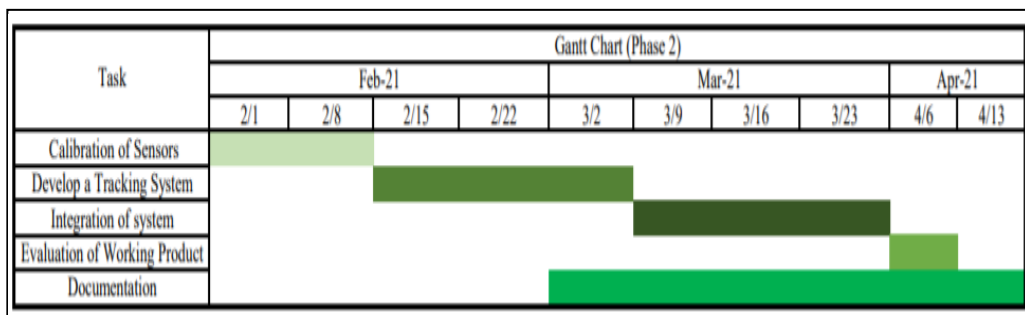


Figure 3.3 Gantt chart for Phase 2



### 3.1.3 Cost Estimation

As the project's main objective is to build a low-cost smart contactless temperature scanner system, cost estimation is relatively significant. Table 3.2 indicates the cost estimation based on the sensors, modules, and microcontroller used in this project.

Table 3.2: Estimated Cost

Components	Quantity	Price	Total Price
Arduino Mega 2560	1	RM 35.00	RM 35.00
USB Host Shield	1	RM 18.30	RM 18.30
16x2 LCD	1	RM 5.90	RM 5.90
Ultrasonic Sensor (HC-SR04)	1	RM 3.10	RM 3.10
Infrared Temperature Sensor (MLX69014)	1	RM 31.80	RM 31.80
RTC Module (DS321)	1	RM 2.90	RM 2.90
Buzzer	1	RM 0.75	RM 0.75
SD Card Module	1	RM 2.90	RM 2.90
Barcode Scanner (SSM)	1	RM 64.00	RM 64.00
Subtotal			RM 164.65

### 3.2 System Overview

The contactless temperature scanner system is built by integrating an infrared temperature sensor (MLX90614), ultrasonic sensor (HC-SR04), real-time clock module (DS321), LCD, buzzer, LED, SD card module, microcontroller (Arduino Mega), and barcode scanner. The block diagram of the proposed system is shown in Figure 3.4.

In this project, the microcontroller will first require barcodes from the user. Once the barcode is scanned through the barcode scanner, an ultrasonic sensor is used to limit the targeted object's measuring distance. The infrared temperature sensor will only be activated if the user is within the distance limit. Next, if the measured body temperature is not within the predefined range, the microcontroller will trigger the buzzer to alert the authority. On the other hand, if the measured body temperature is within the predefined range, the system will restart the process. The LCD is used to display all the collected information and provide a simple interface for the user. Besides, the LEDs are used to provide indication. Lastly, the information such as the current time and date, user's barcode on the identification card, and body temperature will be saved in an SD card as a record for the authority.

The proposed system will be separated into two subsystems to ease the sensor calibration and debugging process, which are the contactless temperature scanner system and tracking system. The circuits are designed and tested individually before integration to form the final working prototype.

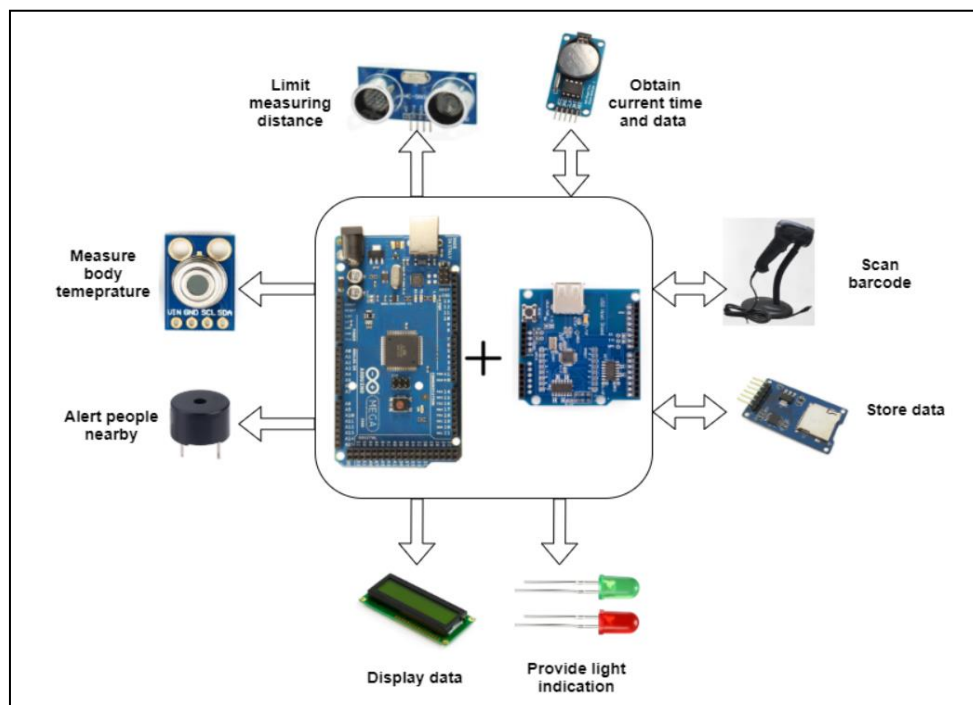


Figure 3.4: Block diagram of the proposed system

### 3.3 Hardware

The hardware selected for this project is standard and can be easily obtained from the market. All the hardware involved in the deployment of the proposed system will be discussed in the following subsections.

#### 3.3.1 Arduino Mega 2560

Arduino Mega 2560 is a microcontroller board founded on ATmega2560. It has 70 GPIO pins, which consist of 54 digital pins and 16 analog pins. The adequate pins, relatively larger sketch memory, and RAM of Arduino Mega 2560 cause it to be selected for this project. The larger RAM is needed for both the installed SPI and SD libraries responsible for reading and writing to the SD card in this project. The available components on the microcontroller and its specification are as shown in Figure 3.5 and Table 3.3.

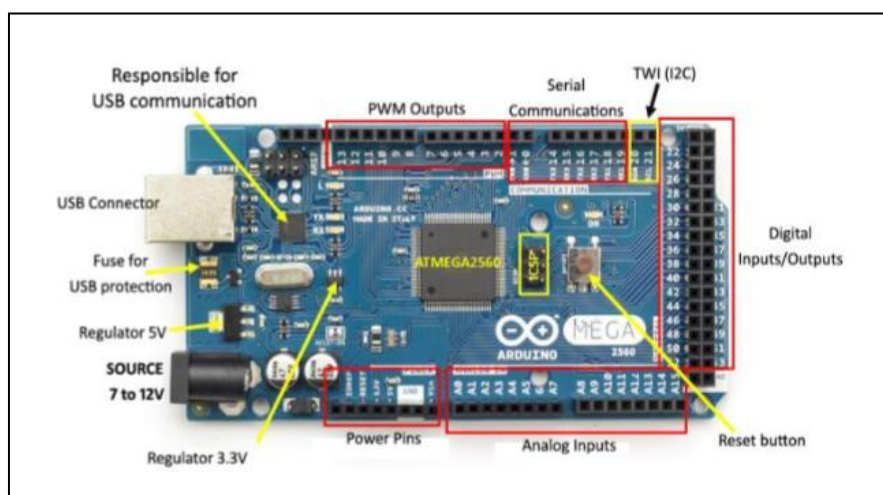


Figure 3.5: Arduino Mega 2560 (Kumar *et al.*, 2015)

Table 3.3: Specification of Arduino Mega 2560

<b>Specification</b>	
<b>Operating Voltage</b>	5V DC
<b>Recommended Input Voltage</b>	7 – 12V DC
<b>Number of Digital I/O Pins</b>	54
<b>Number of PMW Digital I/O Pins</b>	15 out of the 54 digital I/O pins
<b>Number of Analog Input Pins</b>	16
<b>DC Current per I/O Pins</b>	20mA
<b>DC Current per 3.3V Pins</b>	50mA
<b>SRAM</b>	8KB
<b>EEPROM</b>	4KB
<b>Flash Memory</b>	256KB
<b>Clock Speed</b>	16MHz
<b>Weight</b>	37g

### 3.3.2 USB Host Shield

The USB Host shield allows and provides communication between the Arduino Mega microcontroller and connected USB barcode scanner. Figure 3.6 shows the component available on the USB host shield.

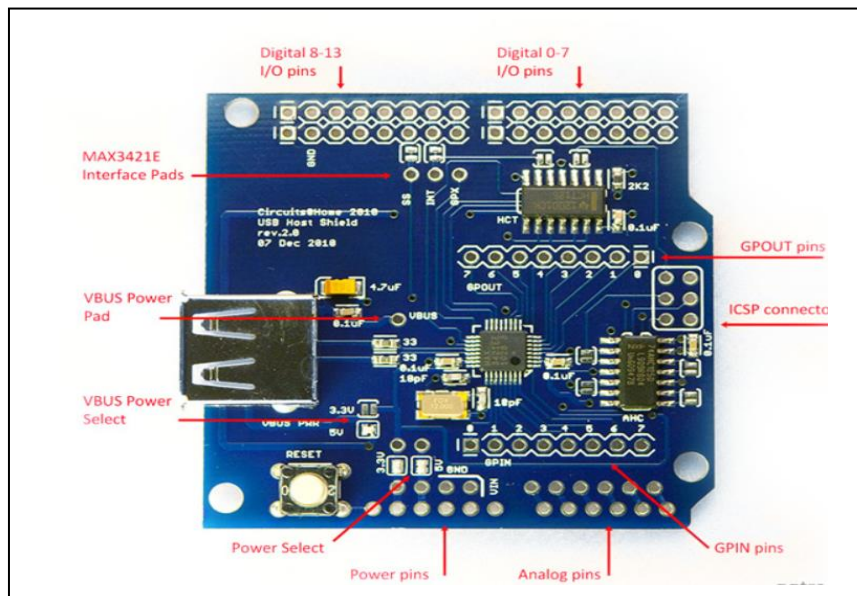


Figure 3.6: USB Host Shield (*USB Host Shield 2.0 - Arduino Compatible / QQ Online Trading, no date*)

### 3.3.3 HC-SR04 Ultrasonic Sensor

As shown in Figure 3.7, the ultrasonic sensor is used to limit the distance for body temperature measurement using ultrasonic waves. The pinout description and specification of the sensor are shown in Table 3.4 and Table 3.5, respectively.

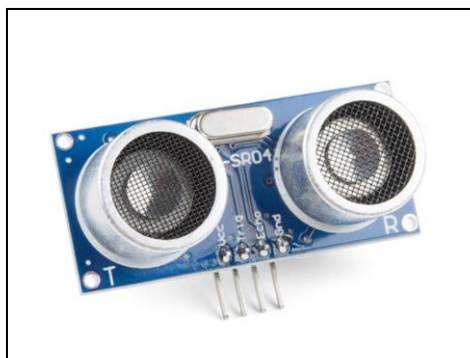


Figure 3.7: HS-SR04 Ultrasonic Sensor

Table 3.4: Pinout Description of HR-SR04

<b>Pin Name</b>	<b>Description</b>
<b>Vcc</b>	Connect to positive supply voltage
<b>Trig</b>	Input pin to trigger the ultrasonic pulse for object range detection
<b>Echo</b>	Output pin that produces a signal if and only if a reflected ultrasonic pulse is received from the object
<b>GND</b>	Connect to the ground

Table 3.5: Specification of Ultrasonic Sensor of HR-SR04

<b>Specification</b>	
<b>Operating Voltage</b>	5V DC
<b>Operating Current</b>	15mA
<b>Maximum Range</b>	400cm
<b>Minimum Range</b>	2cm
<b>Resolution</b>	0.3cm
<b>Measuring Angle</b>	<15°
<b>Operating Frequency</b>	40kHz

### 3.3.4 MLX90614 Non-Contact Infrared Temperature Sensor

The MLX90614 sensor, as shown in Figure 3.8, is an I2C based infrared temperature sensor specially designed for contactless body temperature measurements. The MLX90614 sensor integrates two different devices internally, which are infrared thermopile detector and application processor. Figure 3.9 indicates the internal block diagram of the MLX90614 sensor. Next, the infrared thermopile is responsible for sensing the infrared energy being emitted by the object within its field of view and generate the subsequent electrical signals. The electrical will then go through the application processor for signal processing before reaching the microcontroller board. The pinout description and specification of the infrared temperature sensor can be observed in Table 3.6 and Table 3.7.

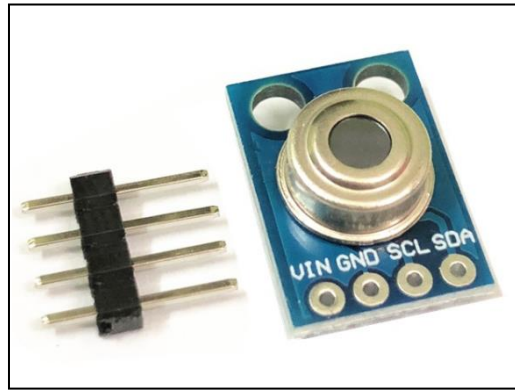


Figure 3.8: MLX96014 Infrared Temperature Sensor

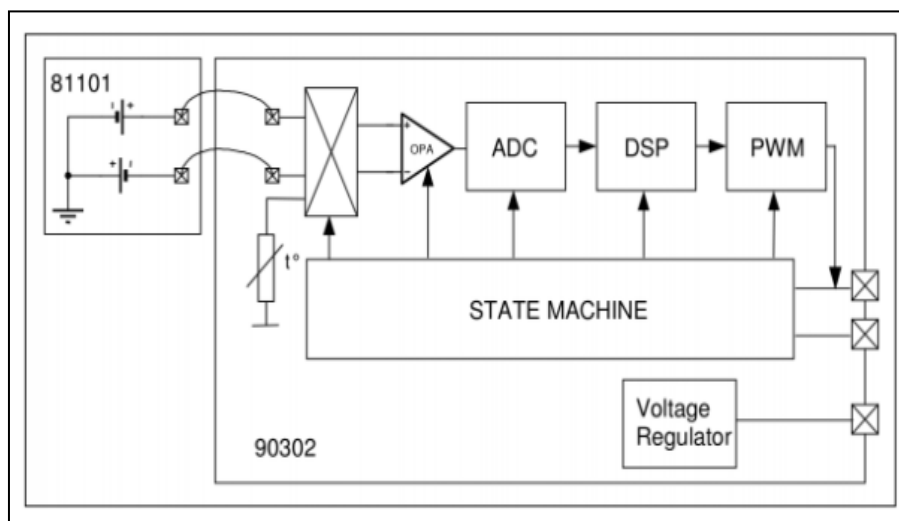


Figure 3.9: Internal block diagram of MLX96014 (*MLX90614 IR Thermometer Hookup Guide - learn.sparkfun.com, no date*)

Table 3.6: Pinout Description of MLX90614

Pin Name	Description
<b>Vdd</b>	Connect to positive supply voltage
<b>SCL</b>	Serial clock pin for I2C communication
<b>SDA</b>	Serial data pin for I2C communication
<b>GND</b>	Connect to the ground

Table 3.7: Specification of MLX90614

Specification	
<b>Operating Voltage</b>	5V DC
<b>Operating Current</b>	1.5mA
<b>Object Temperature Range</b>	-70° C to 382.2°C
<b>Ambient Temperature Range</b>	-40° C to 125°C
<b>Field of View</b>	90°
<b>Accuracy</b>	0.02°C
<b>Distance Range for Measurement</b>	Approximately 2cm – 5cm

### 3.3.5 16x2 LCD Module

The LCD module displays the measured temperature readings, barcode numbers on the identification card and provides a user interface. The pinout description and specification are as shown in Table 3.8 and Table 3.9, respectively. Figure 3.10 indicates a 16x2 LCD.

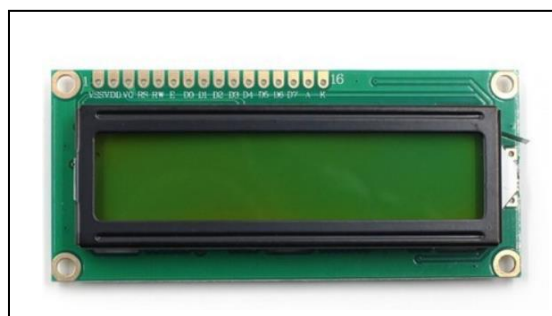


Figure 3.10: 16x2 LCD

Table 3.8: Pinout Description of 16x2 LCD

Pin Name	Description
<b>Vdd</b>	Connect to positive supply voltage
<b>V0</b>	Pin for contrast adjustment
<b>E</b>	Operation enable pin
<b>RS</b>	Data and command selection signal
<b>RW</b>	Read and write selection signal
<b>D0-D7</b>	Data pin
<b>A</b>	Anode for the LCD backlight



<b>K</b>	Cathode for the LCD backlight
<b>Vss</b>	Connect to the ground

Table 3.9: Specification of 16x2 LCD

Specification	
<b>Operating Voltage</b>	5V DC
<b>Controller</b>	Hitachi HD44780 LCD Controller
<b>Screen Resolution</b>	2 lines with 16 characters each
<b>Character resolution</b>	5 x 8 pixels

### 3.3.6 I2C Serial Interface Board Module

The I2C serial interface board module reduces the wire connection needed between the 16x2 LCD module and the Arduino Mega microcontroller. All the components on the I2C serial interface board and its specification are shown in Figure 3.11 and Table 3.10, respectively.

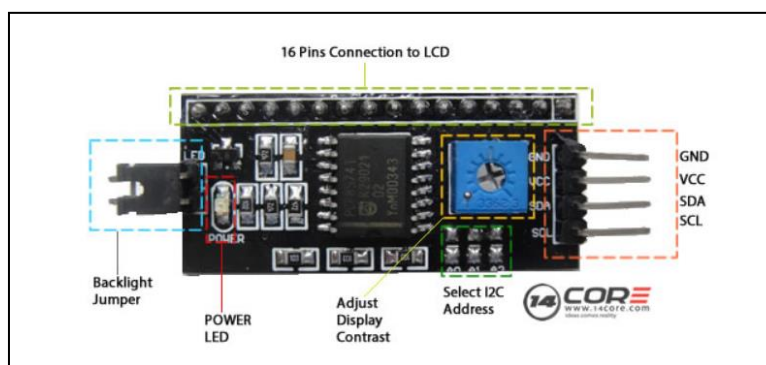


Figure 3.11: I2C Serial Interface Board Module (*Wiring I2C module on 16x2 LCD with SCL/SDA / 14core.com, no date*)

Table 3.10: Specification of I2C Serial Interface Board Module

Specification	
<b>Operating Voltage</b>	5V DC
<b>Compatibility</b>	Compatible with all Arduino board or another controller board that support I2C bus
<b>I2C Address</b>	0x20 – 0x27

### 3.3.7 DS3231 RTC Module

Figure 3.12 shows the RTC Module used to provide the current date and time for each body temperature measurement. The pinout description and specification are as shown below in Table 3.11 and Table 3.12.

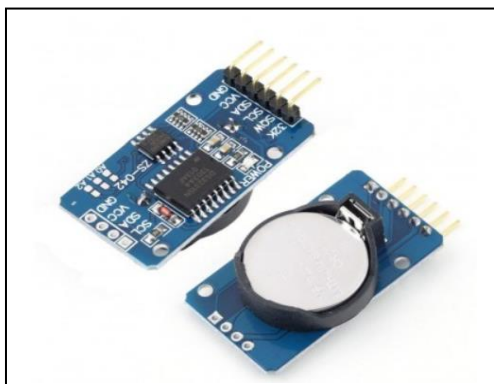


Figure 3.12: RTC Module

Table 3.11: Pinout Description of RTC Module

Pin Name	Description
Vcc	Connect to positive supply voltage
32K	Output pin for reference clock
SQW	Output pin for square wave
SCL	Serial clock pin for I2C interface
SDA	Serial data pin for I2C interface
GND	Connect to the ground

Table 3.12: Specification of RTC Module

Specification	
Operating Voltage	3.3V – 5.5V
Operating current	500nA
Operating temperature	-45°C to +80°C
Accuracy	+2ppm to -2ppm for 0°C to +40°C, +3.5ppm to -3.5ppm for -40°C to +85°C

### 3.3.8 SD Card Module

The SD card module is used to provide mass storage for the tracking system's data logging feature. Figure 3.13 indicates the SD card module used in the project. The module enables the operation such as read, write and create a file to the SD card. The pinout description and specification are as shown in Table 3.13 and Table 3.14.

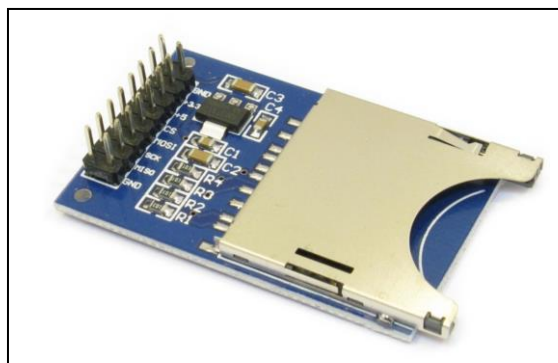


Figure 3.13: SD Card Module

Table 3.13: Pinout Description of SD Card Module

Pin Name	Description
Vcc	Connect to positive supply voltage
CS	Chip select pin
SCK	Serial clock pin
MOSI	SPI input pin to the module
MISO	SPI output pin from the module
GND	Connect to the ground

Table 3.14: Specification of SD Card Module

Specification	
Operating Voltage	3.3V or 5V
Interface	SPI
Compatible	Regular SD card

### 3.3.9 Buzzer

The function of the buzzer shown in Figure 3.14 is to alert the authority or nearby people when the user's temperature exceeds the predefined range of temperature. The specification of the buzzer is as shown in Table 3.15.



Figure 3.14: Buzzer

Table 3.15: Specification of Buzzer

Specification	
<b>Rated Voltage</b>	3 – 5V DC
<b>Frequency Range</b>	50 – 14000 Hz
<b>Resonant Frequency</b>	2048 Hz
<b>Sound Output</b>	≥85 dB
<b>Operating Temperature</b>	-20 – 60°C

### 3.3.10 LED

The LED is used to provide indication to the user. The green LED will light up to indicate normal body temperature. On the other hand, the red LED will light up to indicate abnormal body temperature. Figure 3.16 indicates the LED. The specification of LEDs used is as shown in Table 3.16.

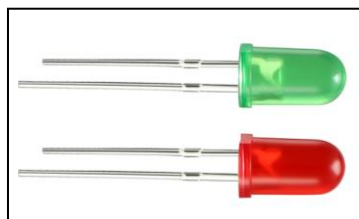


Figure 3.15: LED

Table 3.16: Specification of Red and Green LEDs

<b>Specification</b>	
<b>Red LED</b>	
<b>Forward Voltage</b>	1.8 – 2.2V DC
<b>Forward Current</b>	25mA
<b>Luminous Intensity</b>	100 – 200mcd
<b>Green LED</b>	
<b>Forward Voltage</b>	2.0 – 2.4V DC
<b>Forward Current</b>	20mA
<b>Luminous Intensity</b>	100 – 200mcd

### 3.3.11 SSM Wired 1D Barcode Scanner

The SSM wired barcode scanner is used to scan the barcode on an identification card, which is unique and represents the user's identity. Figure 3.16 illustrates the barcode scanner. The specification of the barcode is as shown in Table 3.17 below.



Figure 3.16: SSM Wired Barcode Scanner

Table 3.17: Specification of Barcode Scanner

<b>Specification</b>	
<b>Interface</b>	USB
<b>Operating Voltage</b>	5V DC
<b>Operating Current</b>	120mA
<b>Supported Symbology</b>	All types of 1D barcode
<b>Depth of Scan Field</b>	10 mm – 800mm
<b>Decode Error Rate</b>	Less than 1 in 5 million scans
<b>Scan Angle</b>	Skew $\pm 45^\circ$ ; Pitch $\pm 60^\circ$
<b>Precision</b>	4mil
<b>Operation</b>	Support both manual and automatic scanning

### 3.4 Software

All the software used to develop the prototype is discussed in the following subsections.

#### 3.4.1 Arduino IDE

Arduino IDE is the main text editor program that is written in C and C++ programming languages. It is a standard open-source software equipped with a simple programming environment and code compilation. The simple to use feature allows people with little prior programming knowledge to write code in that environment. Besides, the open-source software made the sharing of code possible and offered more convenient access to the public. Arduino IDE is often used to write and upload codes to different types of Arduino microcontroller boards. In this project, Arduino IDE is needed for writing and uploading code to Arduino Mega 2560.



Figure 3.17: Arduino IDE

### 3.4.2 Origin 2019b

Origin 2019b is an easy-to-use software for professional data presentation, data analysis, and scientific graphing. Origin 2019b supports various types of 2D and 3D plots. It also offers data analysis such as curve fitting, peak analysis, signal processing, and more. Origin 2019b is used for surface and curve fitting for the infrared temperature sensor's calibration in this project.



Figure 3.18: Origin 2019b

### 3.5 Circuit Design

This section will show both the circuit designs for the contactless temperature scanner system and the tracking system.

### 3.5.1 Contactless Temperature Scanner System

Figure 3.19 indicates the schematic diagram of the contactless temperature scanner system. It consists of the infrared temperature sensor (MLX90614), ultrasonic sensor (HC-SR04), and LCD (16x2) on the Arduino Mega microcontroller. The functional circuit is also used for sensor calibration setup, which will be discussed in Section 3.6.

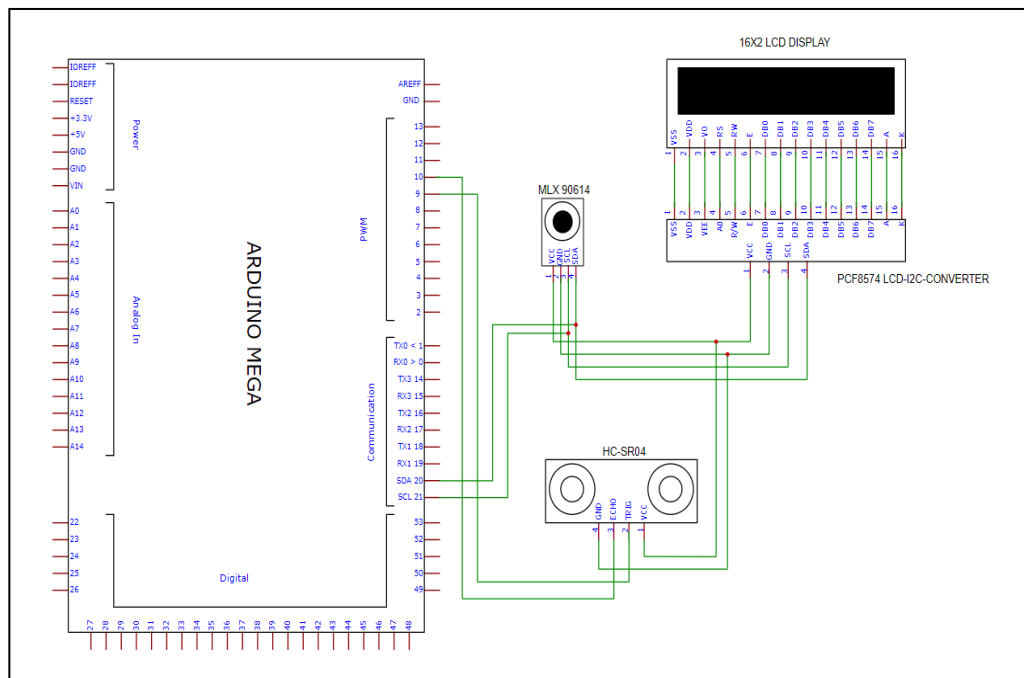


Figure 3.19: Temperature Scanner System Schematic Diagram

### 3.5.2 Tracking System

According to Figure 3.20, the tracking system integrates a USB host shield, RTC module, and SD card module on the Arduino Mega microcontroller. The USB host shield provides a USB port for the barcode scanner. Additionally, the check-in time and date are provided by the RTC module. The user's barcode, time, and date are saved in the SD card through the SD card module.



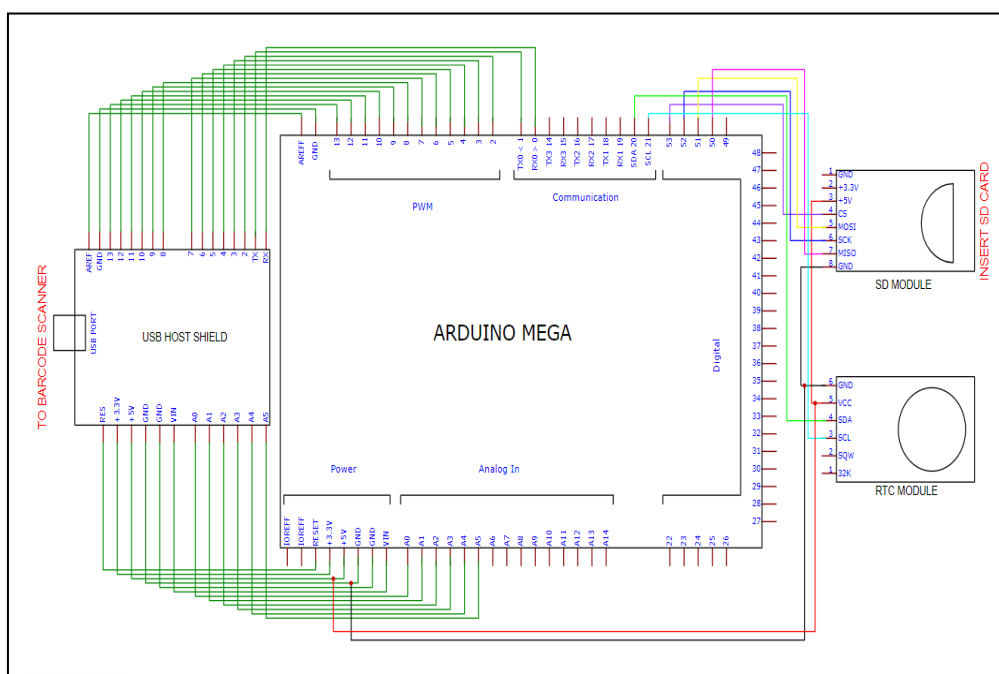


Figure 3.20: Tracking System Schematic Diagram

### 3.6 Sensor Calibration

The precise human body temperature measurement of the contactless temperature scanner system is crucial. Therefore, sensor calibration is an inevitable process conducted on the MLX90614 sensor to enable the sensor to operate as accurately as possible. The proposed sensor calibration setup is modified based on Tang and Hung (2017).

According to the study, a water balloon is heated to emulate a human's head using a temperature-controlled laboratory water bath. After that, the water balloon is used in the evaluation and calibration of the working prototype. In this project, the same approach will be taken. A water balloon is employed as the targeted object for the calibration of the MLX90614 sensor. The MLX90614 sensor is calibrated in several settings, at a fixed distance and multiple distances from the water balloon. The details of both the settings will be discussed in the following subsections.

#### 3.6.1 Fixed Distance Calibration Setup and Procedure

The MLX90614 sensor is calibrated a fixed distance from the water balloon in the fixed distance calibration setup. The functional circuit of a contactless temperature scanner system and a commercial contactless handheld infrared

thermometer gun, YNA-800, are involved. The thermometer gun is applied in calibration to make reference readings for compensation.

According to the datasheet, the thermometer gun's optimum measuring distance ranges from 3 cm to 5 cm. Contrary to the thermometer gun, the optimum measuring distance of the MLX90614 sensor ranges from 2 cm to 5 cm. Hence, the measuring distance of the targeted object is fixed at 3 cm, within the thermometer gun and MLX90614 sensor's measuring distance. Also, the measurement is most accurate at the nearest possible measuring distance. Besides, the body temperature measuring range of the thermometer gun stretches from 32.0 °C to 42.9 °C. Therefore, the MLX90614 sensor will only be calibrated based on the reference thermometer gun's allowable measuring range. For this setup, the manipulating variable is the temperature of the water balloon. The fixed variable is the measuring distance of the thermometer gun and MLX90614 sensor. Moreover, the responding variable is the temperature measured by both the thermometer gun and the MLX90614 sensor. The fixed distance calibration is conducted as described below.

Firstly, the water balloon is filled with the heated water of approximately 45 °C using a plastic pump bottle, as shown in Figure 3.21.



Figure 3.21: Filling the Water Balloon

The desired water balloon's diameter is calculated using Equation 2.1 to ensure the water balloon is within and filled the FOV of both the thermometer gun and MLX90614 sensor. The water balloon distance is 3 cm, and the field of view of the MLX 90614 sensor is 90 °. According to the calculation, the diameter of the water balloon has kept a minimum of 6 cm.

$$S = 3 \text{ cm} \times 2 \times \tan\left(\frac{90^\circ}{2}\right) = 6 \text{ cm}$$

Then, a porcelain dish is used to hold and support the heated water balloon throughout the calibration. A ruler is held perpendicularly to the water balloon's outermost surface at both sides, one after another, and the relative distance is marked as shown in Figure 3.22. The marked line acts as the starting point for the distance measurement. The porcelain dish with a water balloon is positioned on a ruler to justify measuring distance accuracy.

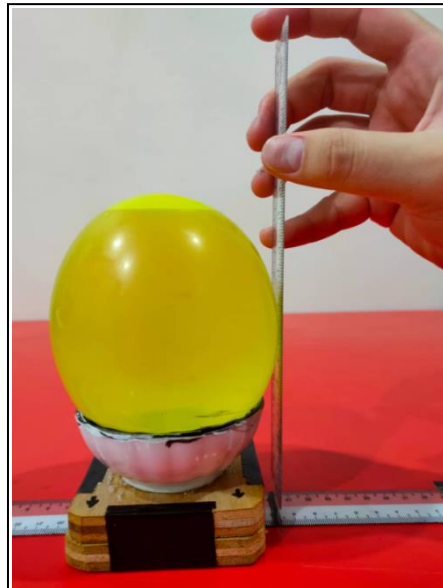


Figure 3.22: Marking of Reference Line

It is also verified that the temperature of water balloon from different surfaces of the same level is identical, using the thermometer gun. This also indicates that the temperature measured by both the thermometer gun and MLX90614 will be only the same if measurements are taken from surfaces of equal level. Thus, polystyrene foams and small-sized wooden boards are used

to provide subtle elevation to the thermometer gun, MLX90614 sensor, and water balloon. After that, the thermometer gun and MLX90614 sensor are situated 3 cm away from the marked line, as shown in Figure 3.23.

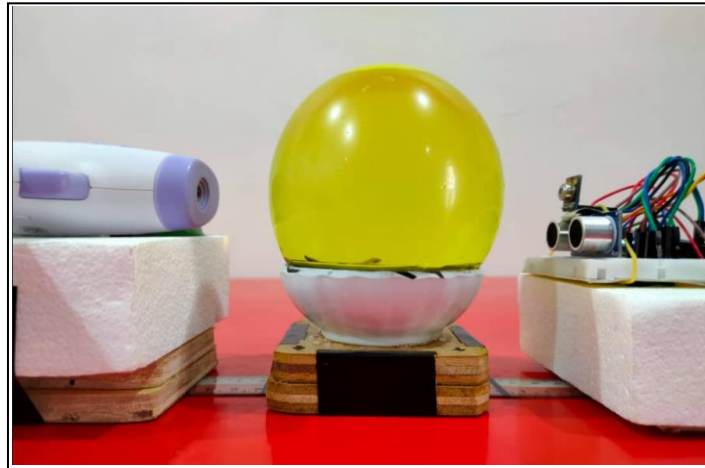


Figure 3.23: Fixed Distance Calibration Setup

The first reading is taken manually from both the thermometer gun and MLX90614 sensor as soon as the water balloon temperature drops slightly below 42.9 °C. However, it is discovered that the water balloon needs a longer amount of time, up to few hours, for its temperature to drop below 36 °C. Hence, a glass teapot is introduced. The water balloon temperature is controlled by immersing it into the teapot with water of the desired temperature for roughly 10 minutes. The water in the teapot is manipulated easily by adding hot or cold water. Moreover, a kitchen thermometer is used to indicate the water's temperature, as shown in Figure 3.24. A permanent marker is applied to the balloon's outer rim on the porcelain dish as an indication before the immersion. This is to ensure the correct placement of the water balloon after immersion.



Figure 3.24: Manipulating the Temperature of Water Balloon

Undoubtedly, the immersion method can lower the water balloon's temperature to approximately the desired temperature through thermal equilibrium. However, it requires human intervention during the immersion, which may draw human error and affect measurement accuracy. Hence, a different approach is adopted to manipulate a lower temperature of below 34 °C. The water balloon is first immersed in water below 30 °C for almost 10 minutes. After that, the water balloon is placed back on the porcelain dish. The measurement begins as soon as its temperatures rise slightly above 32 °C. However, the immersion method is also applied to a temperature above 34 °C. This is because the water balloon also required a longer time to rise for temperatures above 34 °C. Table 3.18 summarized the method applied to control the temperature of the water balloon.

Table 3.18: Method Applied to Manipulate the Temperature of Water Balloon

Temperature Range (°C)	Method Applied
42.9 – 36.0	Filled the water balloon with a temperature of approximately 45 °C and left the temperature to drop naturally until 36 °C

36.0 – 34.0	Immersion Method
34.0 – 32.0	Immersed the water balloon in water temperature of approximately 30 °C and left the temperature rise naturally until 34°C

Lastly, all the data collected is used to find a suitable curve fitting, and verification has been done to the MLX90614 sensor, which will be discussed in Chapter 4. The calibrated MLX90614 sensor will only provide accurate measurement if the targeted object is placed at 3 cm ( $\pm 0.2$  cm) from the sensor through fixed distance calibration.

### 3.6.2 Multiple Distances Calibration Setup and Procedure

The purpose of multiple distances calibration is to improve the measuring range of the calibrated MLX90614 sensor with a minimal trade-off with accuracy. With this, the temperature measured can be nearly consistent if measurement is made within the measuring distance. Therefore, the multiple distances calibration is conducted after the sensor is calibrated using the fixed distance calibration setup. Initially, the calibrated MLX90614 sensor only provided an accurate temperature measurement of the targeted object at a fixed distance of 3 cm ( $\pm 0.2$  cm). This causes the contactless temperature scanner system to experience measurement error once the targeted object is placed furtherer than 3 cm. The multiple distances calibration is conducted to ensure the contactless temperature scanner system can operate within 3 cm to 5 cm.

For multiple distances calibration setup, the water balloon temperature is taken at five different measuring distances, which are 3 cm, 3.5 cm, 4 cm, 4.5 cm, and 5 cm. The temperature measured by the calibrated MLX90614 sensor at 3 cm is used as a reference reading for other measuring distances. Moreover, this setup's responding variable is temperature measured by the MLX90614 sensor at different measuring distances. The manipulating variables are the temperature of the water balloon and the measuring distances of the MLX90614 sensor. Also, the fixed variable is the temperature of the water balloon during measurement at different measuring distances.

Generally, the multiple distances calibration setup and procedure are similar to the fixed distance calibration setup. However, the diameter of the water balloon is kept a minimum of 10 cm. This increase in diameter ensures the water balloon is still within the field of view of the MLX90614 sensor, even at 5 cm. The selection is justified by using Equation 2.1. Besides, an additional L-squared ruler is required to ensure proper alignment as the MLX90614 sensor is moved to acquire temperature at different measuring distances. The temperature data are collected similarly as in the fixed distance calibration setup. The temperature recorded will only be accepted if the water balloon's temperature remains constant after all the readings from different measuring distances are collected for a particular temperature. Therefore, a thermometer gun is placed at 3 cm from the water balloon to justify whether to accept or reject the collected data for a particular temperature. Figure 3.25 indicates the multiple distances calibration setup.

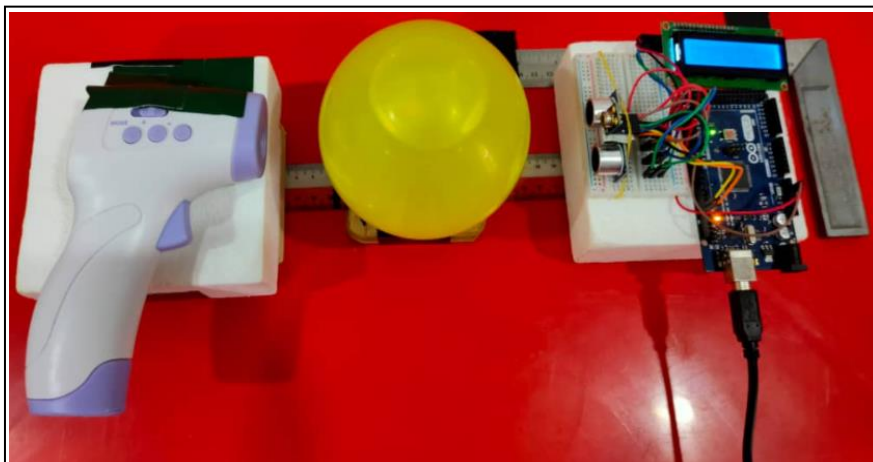


Figure 3.25: Multiple Distances Calibration Setup

Lastly, all the data collected is used to find a suitable surface fitting for the calibrated MLX90614 sensor alongside verification, which will be discussed further in Chapter 4.

### 3.7 System Integration

System integration is performed only after both the contactless temperature scanner system and the tracking system is verified. Section 3.7.1 shows the final

circuit design of the prototype. Furthermore, section 3.7.2 explains the overall system flowchart.

### 3.7.1 Final Circuit Design

The prototype's final circuit integrates individual functional circuits from a contactless temperature scanner system and tracking system. Additional piezoelectric buzzer and LEDs are included in the final circuit to alert and indicate the user. Figure 3.26 represents the final schematic of the final circuit.

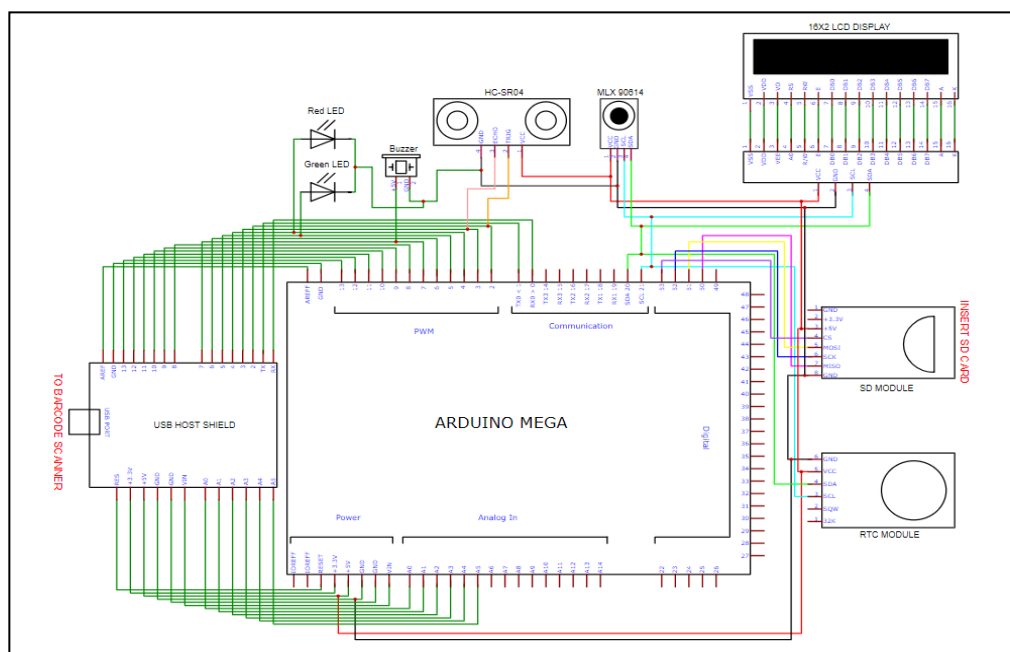


Figure 3.26: Schematic Circuit of Prototype

### 3.7.2 Overall System Flowchart

Based on the system flowchart in Figure 3.27, the system is activated only if both the SD card and USB Host are successfully initialized. After that, the system will proceed with barcode scanning. Once the barcode is scanned, the ultrasonic sensor will be triggered to obtain the user's distance. If the user's distance is within 3 cm to 5 cm, the infrared temperature sensor is activated. On the other hand, if the user's distance is not within the predefined range, instruction is given accordingly through the LCD.

Next, the infrared temperature sensor will obtain the average temperature of the user. The measured temperature is used to fit both the curve



and surface fitting equation obtained from the calibration setup. Lastly, the final temperature of the user is calculated. If the final temperature is within the predefined range, ranging from 35.5 °C to 36.5 °C, the user is granted access to the premise. This is indicated by the blinking of the green LED and buzzer with a low-frequency tone. In contrast, if the final temperature is outside the predefined range, red blinking led and high-frequency tone can alert the authority. All the information, such as measured temperature scanned the barcode, current time, and data are stored in the SD card for tracking purposes.

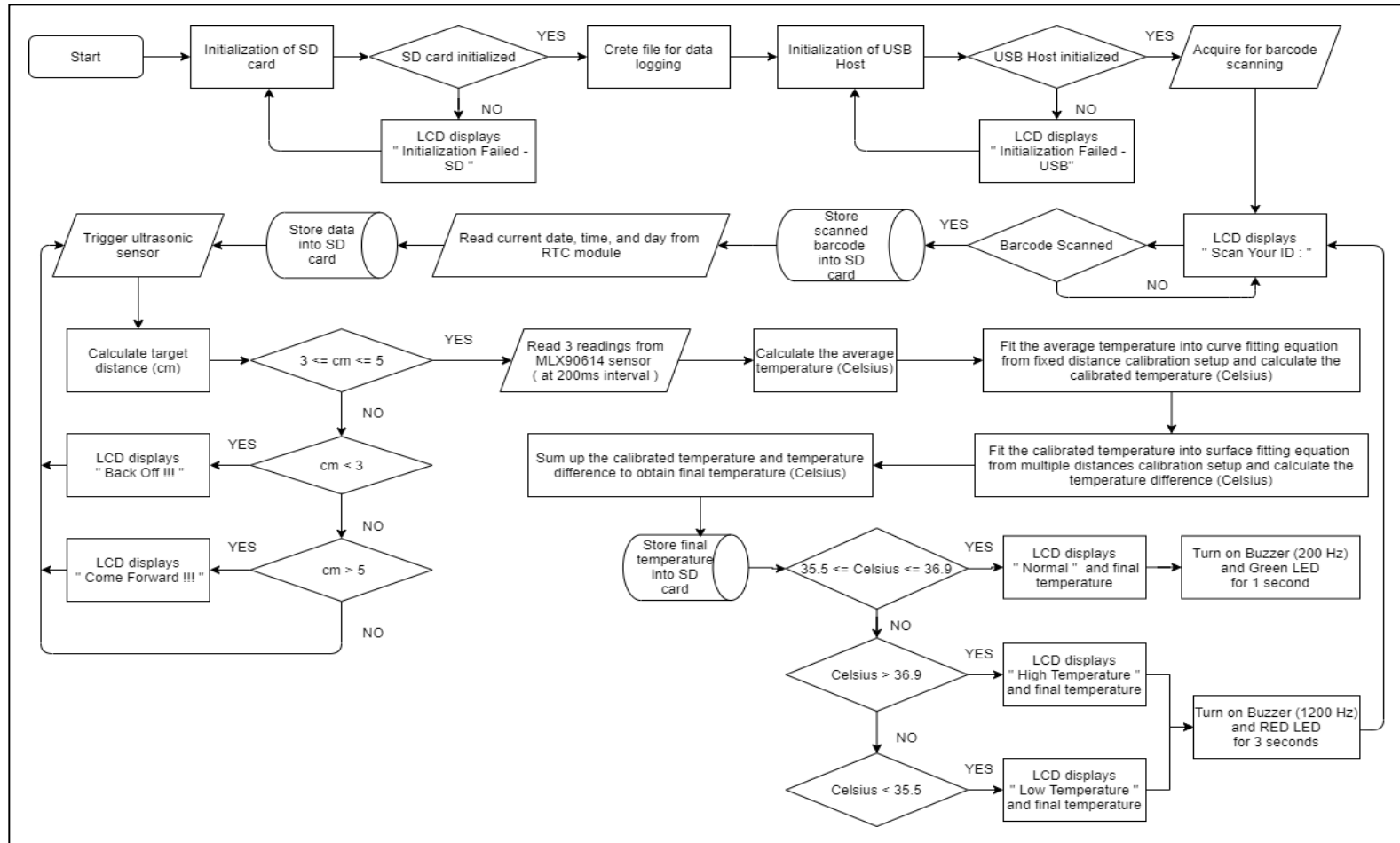


Figure 3.27: Flowchart of the System

## CHAPTER 4

### RESULTS AND DISCUSSION

#### 4.1 Introduction

This chapter shows and discusses the data collected from the fixed distance and multiple distances calibration setup. After that, the suitable curve and surface fitting performed to the temperature data collected through the mathematical model for calibration purposes are discussed. Next, the result obtained by the prototype is verified separately for each setup. Finally, a final evaluation is performed on the prototype.

#### 4.2 Fixed Distance Calibration Setup

The data collected, curve fitting, and verification for fixed distance calibration setup are discussed in sequence at the following subsections.

##### 4.2.1 Data Collected

Table 4.1 shows the temperature data collected from both the thermometer gun and MLX90614 infrared temperature sensor at room temperature. Three sets of readings are recorded manually, and the average is calculated for the MLX 90614 sensor. This is because the temperature measured by the MLX90614 sensor tends to fluctuate slightly for each temperature point during the measurement.

In addition, the MLX90614 sensor is adjusted to acquire measurement every one second through a microcontroller. This adjustment ensures that the MLX90614 sensor is fast enough to obtain three temperature readings consecutively of the water balloon at a particular temperature point before its temperature continues to drop. Furthermore, the total number of 29 temperature data points collected ranges from the maximum temperature of 42.4 °C to the minimum temperature of 32.1 °C. The surface temperature of the water balloon is measured. At least one data is collected for each degree Celsius interval to ensure sufficient data points are provided for calibration purpose.

After all the temperature data are collected, the error is calculated. The calculated error shows that the temperature measured by the MLX90614 sensor

is much lower than the thermometer gun, with a maximum value of -5.10 and a minimum value of -3.28. Therefore, calibration on MLX90614 is inevitable to compensate for the error.

Table 4.1: Data Collected from Fixed Distance Calibration Setup

Temperature Measured (°C)					
Reference (Thermometer Gun)	Prototype (MLX90614 Sensor)				
Thermometer Gun Reading	Reading 1	Reading 2	Reading 3	Average	Error
42.4	37.35	37.29	37.33	37.32	-5.08
41.6	36.81	36.79	36.77	36.79	-4.81
41.1	36.33	36.39	36.37	36.36	-4.74
40.6	35.91	35.99	35.97	35.96	-4.64
40.0	35.67	35.61	35.67	35.65	-4.35
39.4	35.47	35.45	35.43	35.45	-3.95
39.1	35.15	35.19	35.07	35.14	-3.96
38.7	34.91	34.93	34.91	34.92	-3.78
38.1	34.61	34.55	34.59	34.58	-3.52
37.8	34.43	34.37	34.31	34.37	-3.43
37.5	34.23	34.21	34.23	34.22	-3.28
37.2	33.83	33.87	33.93	33.88	-3.32
37.0	33.73	33.71	33.73	33.72	-3.28
36.8	33.43	33.51	33.49	33.48	-3.32
36.7	33.21	33.19	33.25	33.22	-3.48
36.6	32.99	32.97	33.05	33.00	-3.60
36.5	32.77	32.85	32.81	32.81	-3.69
36.3	32.39	32.41	32.45	32.42	-3.88
36.2	31.99	32.05	32.09	32.04	-4.16
36.1	31.47	31.43	31.41	31.44	-4.66
36.0	30.90	30.89	30.90	30.90	-5.10
35.4	30.29	30.29	30.31	30.30	-5.10

35.1	30.19	30.25	30.31	30.25	-4.85
34.5	29.75	29.71	29.69	29.72	-4.78
34.2	29.43	29.51	29.55	29.50	-4.70
34.0	29.35	29.37	29.35	29.36	-4.64
33.7	29.29	29.25	29.25	29.26	-4.44
32.4	28.19	28.17	28.11	28.16	-4.24
32.1	28.00	27.89	27.90	27.93	-4.17

#### 4.2.2 Curve Fitting

Once the temperature data are collected and analysed, the graph of reference (thermometer gun reading) versus prototype (average reading from MLX90614 sensor) is plotted as shown in Figure 4.1.

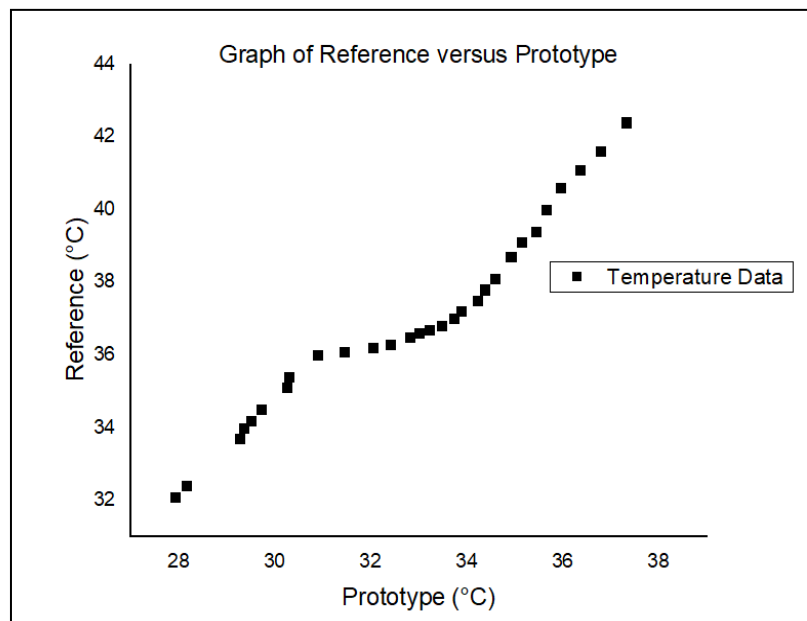


Figure 4.1: Graph of Reference Versus Prototype

Next, curve fitting is conducted to examine the relationship between the reference thermometer and the MLX90614 sensor. The Origin-Lab's curve fitting analysis tool is used to find the mathematical model that best described the relationship. After several trials and errors on different mathematical models, the relationship is best characterized with a polynomial model. As the initiative to select the most suitable polynomial model, statistical measures such as RSS,  $R^2$ , and adjusted  $R^2$  are considered. The best mathematical model is selected

based on the lowest value of RSS (close to 0), highest  $R^2$  and adjusted  $R^2$  value (close to 1). Therefore, all the available polynomial models, from 0<sup>th</sup> to 9<sup>th</sup> order in Origin Lab, are applied to the collected temperature data, and the respective statistical measures are obtained as shown in Table 4.2.

Table 4.2: Statistical Measures of Different Polynomial Models

Polynomial Models	RSS	$R^2$	Adjusted $R^2$
Linear (Degree 1)	10.0357986015	0.9480251876	0.9461001946
Quadratic (Degree 2)	7.1276473113	0.9630863326	0.9602468197
Cubic (Degree 3)	2.3041833585	0.9880667695	0.9866347819
Quartic (Degree 4)	1.6566608551	0.9914202506	0.9899902924
Quintic (Degree 5)	0.3864086005	0.9979988125	0.9975637718
Sextic (Degree 6)	0.2341410691	0.9987873971	0.9984566873
Septic (Degree 7)	0.1754054156	0.999091586	0.9987887809
Octic (Degree 8)	0.1744151258	0.9990967143	0.9987354000
Nonic (Degree 9)	0.1466856734	0.9992403235	0.9988804767

According to Table 4.2, the RSS reduces as the degree of polynomial order increases. On the other hand, the value of  $R^2$  and adjusted  $R^2$  increases as the degree of polynomial order increases. This trend indicates that the higher-order polynomial model results in a better fit to describe the relationship. However, to prevent the selection of an overcomplicated polynomial model, percentage error is also calculated. In this report, the percentage error is the percentage of the total number of errors, which is more than 0.20 difference from corresponding reference temperature across the total collected temperature data points. The percentage error is used to indicate that the suitable polynomial model will have a lower percentage error.

First, the polynomial equations of different orders are obtained using Origin-Lab before calculating the percentage error. Next, the average temperature measured by the MLX90614 sensor from the previously collected data is fitted into the polynomial equations to obtain calibrated temperature. The calibrated temperature is compared with the specified reference temperature, and the difference in value, also known as the error, is computed. The

percentage error is then figured out by allocating the number of errors, which is more than 0.2. Table 4.3 represents the calibrated temperature with percentage calculation after applying the 6<sup>th</sup> degree polynomial fitting equation to the collected data. The percentage error calculation of different polynomial models can be found in the Appendix B.

Table 4.3: Percentage Error for 6<sup>th</sup> Degree Polynomial Model

Sextic (Degree 6)		
Reference Temperature (°C)	Calibrated Temperature (°C)	Error
42.4	42.21	-0.19
41.6	41.63	0.03
41.1	41.02	-0.08
40.6	40.35	-0.25
40.0	39.81	-0.19
39.4	39.46	0.06
39.1	38.92	-0.18
38.7	38.55	-0.15
38.1	38.03	-0.07
37.8	37.73	-0.07
37.5	37.53	0.03
37.2	37.13	-0.07
37.0	36.98	-0.02
36.8	36.77	-0.03
36.7	36.59	-0.11
36.6	36.48	-0.12
36.5	36.39	-0.11
36.3	36.27	-0.03
36.2	36.19	-0.01
36.1	36.05	-0.05
36.0	35.80	-0.20
35.4	35.29	-0.11

35.1	35.24	0.14
34.5	34.51	0.01
34.2	34.15	-0.05
34.0	33.91	-0.09
33.7	33.75	0.05
32.4	32.21	-0.19
32.1	32.20	0.10
$\text{Percentage Error (\%)} = \frac{\text{Number Of Error}(> 0.2)}{\text{Total Data Point}} \times 100$ $= \frac{1}{29} \times 100 = 3.45$		

Before calculating percentage error, the polynomial fitting's coefficients for all the models are rounded off to 10 decimal places. This is because Arduino's microcontroller only supports a maximum of 7 digits of precision for both the float and double data types. The 7 digits of precision mean the total number of digits, including the number to the left of the decimal point. However, the percentage error obtained is relatively high. It is then concluded that selecting low decimal places for the coefficients will contribute distinctly to calibrated temperature inaccuracy. Therefore, an external library, namely the "Big Number" by Nick Gammon, is used to resolve the constraint. The particular library allows the microcontroller to deal with large decimal places that contribute to accuracy. However, the increment in decimal places will also slow down the microcontroller when performing the calculation. Therefore, Table 4.4, which shows the percentage error calculated using different decimal places for the polynomial fitting's coefficients, is constructed.

Table 4.4: Percentage Error Obtained using Different Decimal Places

Polynomial Models	Percentage Error (%)			
	7 digits of precision	7 decimal places	10 decimal places	14 decimal places
Linear	82.76	82.76	82.76	82.76
Quadratic	79.31	79.31	79.31	79.31



Cubic	48.28	48.28	48.28	48.28
Quartic	62.07	48.28	48.28	48.28
Quintic	100.00	100.00	6.90	6.90
Sextic	100.00	100.00	3.45	3.45
Septic	100.00	100.00	100.00	3.45
Octic	100.00	100.00	100.00	3.45
Nonic	100.00	100.00	100.00	3.45

According to Table 4.4, the fitting's coefficient's decimal places must not be lower than 10 decimal places to ensure accurate results for calibrated temperature. This can be seen as the lowest percentage error for fitting's coefficient with decimal places below 10 of the available polynomial models is only 48.28 %, which is still relatively high. The high percentage error indicates the inaccuracy of calibrated temperature. Moreover, it can also be seen that even with a further increment of decimal places to 14 decimal places, the lowest possible percentage error is still 3.45 %. Therefore, the fitting's coefficient for the polynomial model is rounded off to 10 decimal places, and the selection has been justified.

Lastly, the polynomial model of 6<sup>th</sup> degree is selected as it has high R2 and adjusted R2, close to 1. Nevertheless, it also has a relatively low RSS close to 0, according to Table 4.2. Besides, it also has the lowest percentage error of 3.45 % compared to other available polynomial models, with each coefficient of the fitting equation being rounded to 10 decimal places. In short, the selection of the best polynomial model does not depend solely on the statistical measures but also the percentage error in this case. Figures 4.2 and 4.3 represent the graph of reference versus prototype with the polynomial fitting of 6<sup>th</sup> degree and its fitting's coefficients, respectively. With that, the temperature measured by the prototype can be corrected through the polynomial equation. The polynomial fitting equations of the other models are attached in the Appendix A.

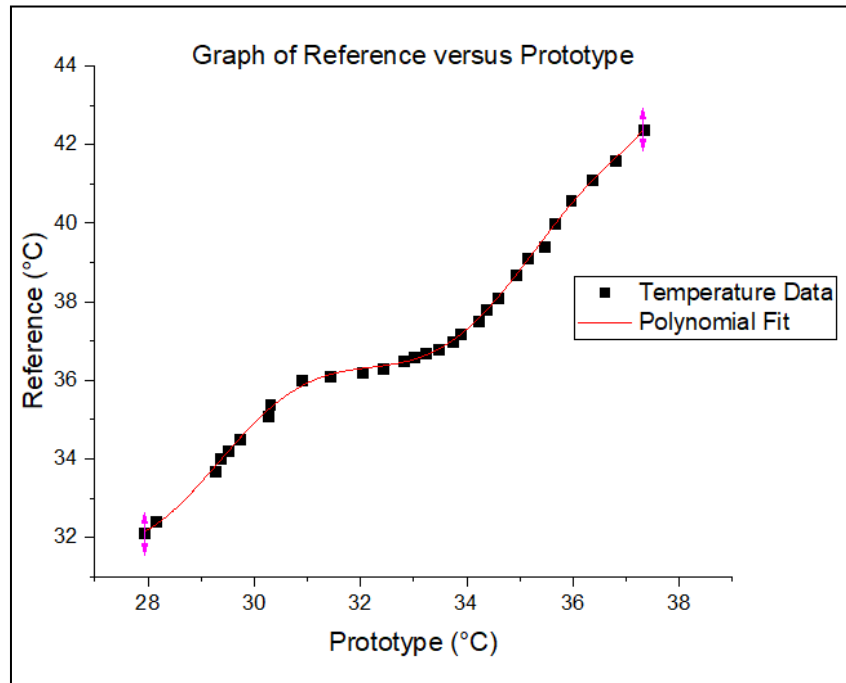


Figure 4.2: Polynomial Fitting for Graph of Reference Versus Prototype

Equation	$y = \text{Intercept} + B1*x^1 + B2*x^2 + B3*x^3 + B4*x^4 + B5*x^5 + B6*x^6$
Plot	Reference (°C)
Weight	No Weighting
Intercept	$489497.4381259961 \pm 109487.8993388349$
B1	$-88534.0889472121 \pm 20275.0691212701$
B2	$6648.1757721581 \pm 1561.4395541361$
B3	$-265.2889432816 \pm 64.0133859197$
B4	$5.9333044991 \pm 1.4734307289$
B5	$-0.0705219732 \pm 0.0180544938$
B6	$3.4802574946E-4 \pm 9.2010031969E-5$
Residual Sum of Squares	0.2341410691
R-Square (COD)	0.9987873971
Adj. R-Square	0.9984566873

Figure 4.3: 6<sup>th</sup> Polynomial Fitting's Coefficients

### 4.2.3 Verification

The experiment is reconducted in the same environment to verify the effectiveness of polynomial fitting on the prototype. Besides, the temperature data are also collected in the same manner as previous. The result is presented in a cluster bar chart with the error of each temperature data point labelled accordingly, as shown in Figure 4.4.

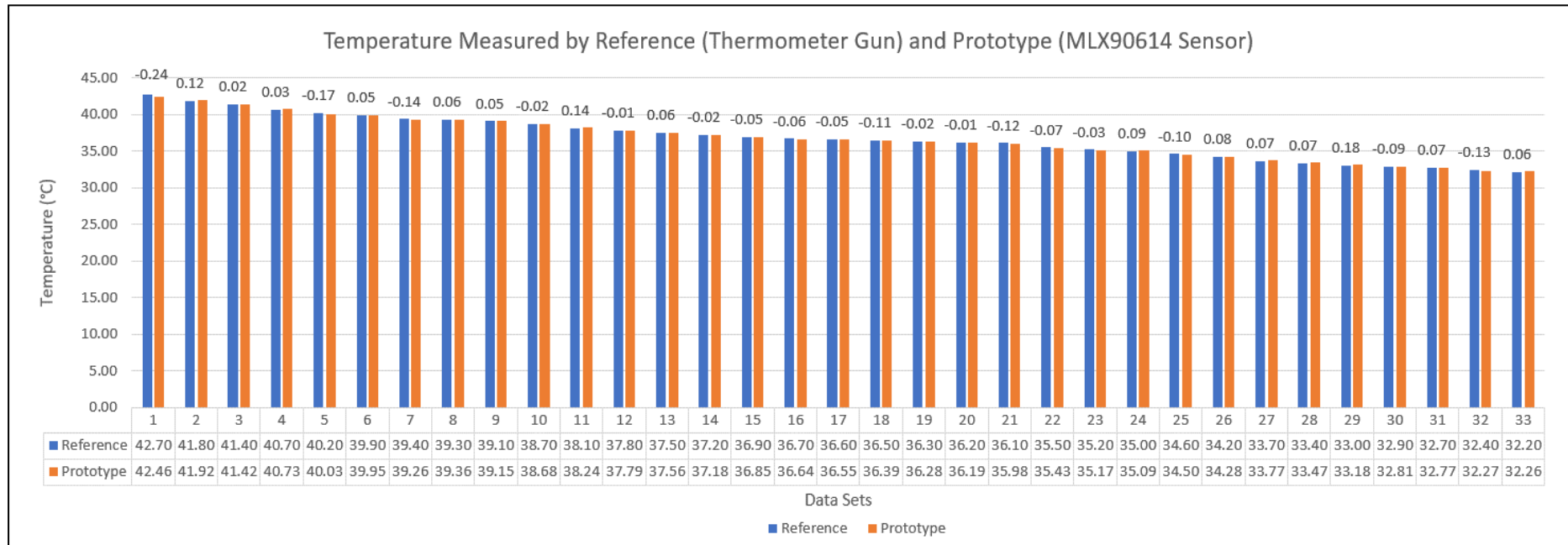


Figure 4.4: Verification for Temperature Measured by Reference and Prototype

According to Figure 4.4, the maximum error of the temperature measured by the calibrated prototype is -0.24. Next, the minimum error obtained is -0.01. The maximum and minimum error values are much lower than the previously collected data without calibration. This indicates that the prototype has been calibrated successfully through the polynomial fitting. The relatively low error provides the required accuracy for calibrated prototype to measure human body temperature.

### 4.3 Multiple Distances Calibration Setup

The data collected, surface fitting and verification for fixed distance calibration setup are discussed in sequence at the following subsections.

#### 4.3.1 Data Collected

Table 4.5 represents the calibrated prototype's temperature data at multiple distances from 3 cm to 5 cm with an interval distance increment of 0.5 cm. Aforementioned, in this setup, the temperature measured at 3 cm will act as a reference for temperature measured at other distances. Also, similar to the fixed distance calibration setup, three readings are taken consecutively for each temperature point, and at least 1 data point being collected for each degree Celsius interval. The temperature data shown in Table 4.5 is only the summary of the average temperature measured. All the readings for each measuring distance can be found in Appendix C.

Table 4.5: Average Temperature Measured at Different Measuring Distances

Average Temperature Measured (°C)				
Reference (3 cm)	3.5 cm	4 cm	4.5 cm	5 cm
42.66	41.28	40.07	39.79	38.78
40.51	39.27	38.33	37.93	37.75
38.26	37.63	37.08	36.75	36.66
37.20	36.67	36.47	36.35	36.25
36.87	36.54	36.36	36.26	36.14
36.40	36.14	36.04	35.96	35.80

35.90	35.68	35.63	35.56	35.45
35.34	35.17	35.10	35.05	34.97
34.52	34.38	34.33	34.30	34.23
33.60	33.50	33.46	33.44	33.37
32.55	32.47	32.44	32.40	32.35

Besides, Table 4.6 is generated to investigate the effect of measuring distance on temperature measurement accuracy. The difference in temperature measured in comparison to reference (3 cm) at multiple distances, which is denoted as delta, is calculated.

Table 4.6: Temperature Differences with Respect to Reference

Reference (3 cm)	Delta (°C)			
	3.5 cm	4 cm	4.5 cm	5 cm
42.66	-1.37	-2.59	-2.86	-3.88
40.51	-1.24	-2.18	-2.58	-2.76
38.26	-0.63	-1.17	-1.51	-1.60
37.20	-0.53	-0.73	-0.85	-0.95
36.87	-0.32	-0.51	-0.61	-0.73
36.40	-0.26	-0.36	-0.44	-0.60
35.90	-0.22	-0.28	-0.35	-0.46
35.34	-0.18	-0.25	-0.30	-0.37
34.52	-0.14	-0.19	-0.22	-0.28
33.60	-0.10	-0.15	-0.16	-0.23
32.55	-0.08	-0.11	-0.15	-0.20

#### 4.3.2 Surface Fitting

As shown in Figure 4.5, the surface graph is plotted to visualize better the relationship between temperature measured by calibrated prototype, measuring distances, and delta.

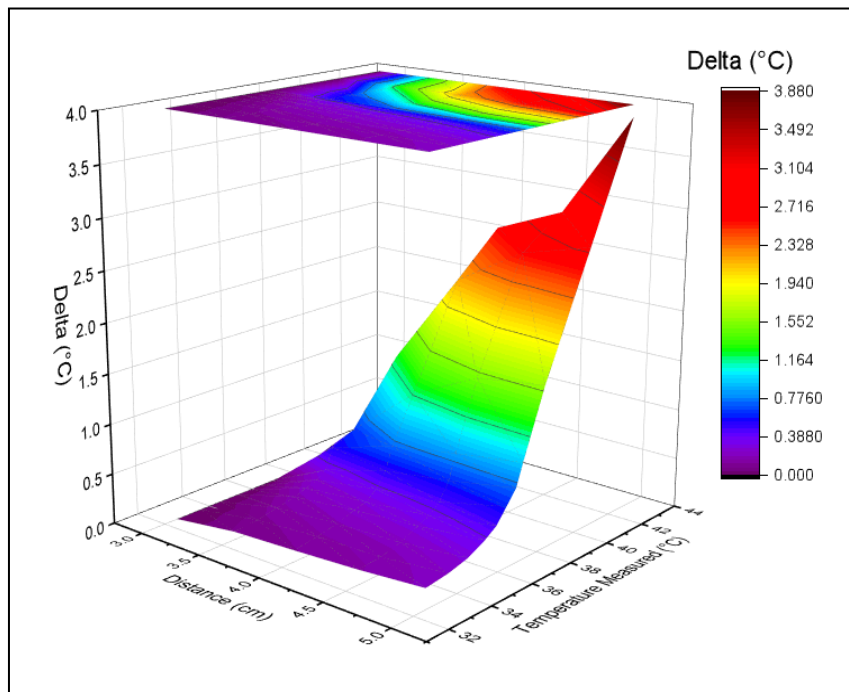


Figure 4.5: Plotted Surface Graph

According to Figure 4.5, it can be seen that the delta increases as both the temperature measured and measuring distance increase. This also indicates that the delta is at its peak value when the targeted object's temperature is highest and measured at the furthest measuring distance or vice versa. Next, the delta incurred also indicates that the measuring distance highly influences the calibrated prototype's accuracy. Therefore, surface fitting is conducted. The surface fitting is used to find the right equation that best described the temperature measured by calibrated prototype and measuring distance on the delta. After that, with the suitable surface fitting equation, the delta incurred can be calculated, and compensation can be made to the calibrated prototype.

The surface fitting is performed by accessing the non-linear surface fitting's function in Origin Lab. All the built-in functions available, 22 in total, are applied to the plotted surface graph, and analysis has been conducted to select the best-fit function. The available built-in functions are Chebyshev2D, Lorentz2D, Exponential2D, Gaussian2D, Parabola2D, and many more. Firstly, choosing a suitable built-in function is based on the same statistical measures mentioned in the previous fixed calibration setup. In this case, the surface fitting function that possesses high  $R^2$  and adjusted  $R^2$ , which is more than 0.95, and

low RSS, which is closer to 0, is chosen. Table 4.7 shows only the selected surface fitting functions with high statistical measures after applying all the available built-in functions.

Table 4.7: Statistical Measure of Selected Functions

Built-in functions	RSS	R <sup>2</sup>	Adjusted R <sup>2</sup>
GaussCum	0.0186596036	0.9779477842	0.9756975581
Gauss2D	0.0275770776	0.9674089719	0.9640833568
Gaussian2D	0.0293326474	0.9660416767	0.9617968863
Rational Taylor	0.0299957011	0.9674444325	0.9609333190
Voigt2D	0.0328102296	0.9620156896	0.9572676508

A further selection is carried out to find the most suitable function based on the function's percentage error and complexity. To calculate percentage error, the equation and coefficients of all selected surface fitting functions are obtained. The temperature measured and measuring distance collected previously are substituted into the equation to obtain the respective delta. With the known delta, the calibrated temperature is obtained by summing the delta and measured temperature. The calibrated temperature is compared with the specified reference temperature, and the difference in value is known as error.

Besides, all the surface fitting coefficients are left to 7 digits of precision. Even with the external “Big Number” library, there is still a limitation in term of the maximum number of data type, which is 12, can be declared under the library. Favourably, the number of decimal places does not have a vast effect on the calculated delta. This has been verified as the percentage error calculated using 7 significant figures and 10 decimal places for the surface fitting's coefficient is the same. Table 4.8 and 4.9 represent the example of percentage error calculation using the Rational Taylor function and the summarized percentage error of other selected surface fitting functions.

Table 4.8: Percentage Error Calculation using Rational Taylor function

Reference Temperature (°C)	Measured Temperature (°C)	Distance (cm)	Calculated Delta (°C)	Calibrated Temperature (°C)	Error
42.66	42.66	3.00	0.09	42.75	0.09
40.51	40.51	3.00	0.01	40.52	0.01
38.26	38.26	3.00	-0.05	38.20	0.05
37.20	37.20	3.00	-0.06	37.14	0.06
36.87	36.87	3.00	-0.06	36.81	0.06
36.40	36.40	3.00	-0.05	36.35	0.05
35.90	35.90	3.00	-0.04	35.86	0.04
35.34	35.34	3.00	-0.03	35.32	0.03
34.52	34.52	3.00	0.00	34.52	0.00
33.60	33.60	3.00	0.03	33.64	0.03
32.55	32.55	3.00	0.07	32.62	0.07
42.66	41.28	3.50	1.31	42.59	0.07
40.51	39.27	3.50	0.95	40.22	0.29
38.26	37.63	3.50	0.63	38.25	0.00
37.20	36.67	3.50	0.45	37.12	0.08
36.87	36.54	3.50	0.43	36.98	0.11
36.40	36.14	3.50	0.37	36.51	0.11
35.90	35.68	3.50	0.30	35.98	0.08
35.34	35.17	3.50	0.23	35.40	0.05
34.52	34.38	3.50	0.13	34.51	0.01
33.60	33.50	3.50	0.05	33.55	0.05
32.55	32.47	3.50	-0.04	32.43	0.12
42.66	40.07	4.00	1.62	41.69	0.97
40.51	38.33	4.00	1.07	39.40	1.11
38.26	37.08	4.00	0.73	37.81	0.44
37.20	36.47	4.00	0.58	37.05	0.15
36.87	36.36	4.00	0.56	36.92	0.05



36.40	36.04	4.00	0.48	36.52	0.12
35.90	35.63	4.00	0.40	36.03	0.12
35.34	35.10	4.00	0.30	35.39	0.05
34.52	34.33	4.00	0.17	34.50	0.02
33.60	33.46	4.00	0.04	33.50	0.10
32.55	32.44	4.00	-0.08	32.36	0.19
42.66	39.79	4.50	1.86	41.65	1.01
40.51	37.93	4.50	1.13	39.06	1.45
38.26	36.75	4.50	0.76	37.51	0.75
37.20	36.35	4.50	0.64	36.99	0.20
36.87	36.26	4.50	0.62	36.88	0.01
36.40	35.96	4.50	0.54	36.51	0.11
35.90	35.56	4.50	0.45	36.00	0.10
35.34	35.05	4.50	0.33	35.38	0.04
34.52	34.30	4.50	0.19	34.49	0.03
33.60	33.44	4.50	0.04	33.48	0.12
32.55	32.40	4.50	-0.10	32.30	0.25
42.66	38.78	5.00	1.63	40.40	2.25
40.51	37.75	5.00	1.19	38.94	1.57
38.26	36.66	5.00	0.81	37.47	0.79
37.20	36.25	5.00	0.69	36.94	0.26
36.87	36.14	5.00	0.65	36.79	0.08
36.40	35.80	5.00	0.56	36.36	0.04
35.90	35.45	5.00	0.47	35.91	0.01
35.34	34.97	5.00	0.35	35.32	0.02
34.52	34.23	5.00	0.19	34.42	0.09
33.60	33.37	5.00	0.03	33.40	0.20
32.55	32.35	5.00	-0.13	32.22	0.33
$\text{Percentage Error (\%)} = \frac{\text{Number of Errors (> 0.2)}}{\text{Total Data Points}} \times 100$ $= \frac{13}{55} \times 100 = 23.64$					

Table 4.9: Percentage Error of Different Built-in Functions

Built-in functions	Percentage Error (%)
Gauss Cum	32.73
Gauss2D	34.55
Gaussian2D	63.64
Rational Taylor	23.64
Voigt2D	43.64

According to Table 4.9, the Rational Taylor function has the lowest percentage error of 23.64 % compared to other selected functions. Therefore, the Rational Taylor function is chosen. Also, it has the simplest formula of all. This can be seen from Table 4.10, in which the definition of the selected functions is summarized. The Rational Taylor function's coefficient can be seen in Figure 4.6. Besides, the surface fitting equation and percentage error calculation of other selected functions are attached in Appendix D and E respectively.

Model	RationalTaylor
Equation	$z = (z_0 + A_01*x + B_01*y + B_02*y^2 + C_02*x*y)/(1 + A_1*x + B_1*y + A_2*x^2 + B_2*y^2 + C_2*x*y)$
Plot	Delta (°C)
z0	-6232.33 ± 22627.47
A01	1777.549 ± 6569.3
B01	208.8456 ± 751.0653
B02	-0.6475761 ± 2.192287
C02	-53.47685 ± 197.7926
A1	-1044.357 ± 4422.863
A2	17.71595 ± 75.74556
B1	93.73757 ± 397.2442
B2	-2.027365 ± 8.872121
C2	19.75493 ± 89.74824
Reduced Chi-Sqr	0.0299957
R-Square (COD)	0.9674444
Adj. R-Square	0.9609333

Figure 4.6: Rational Taylor's Fitting Coefficients

Table 4.10: Summarized Definition of Selected Functions

Built-in functions	Definition
Gauss Cum	$z = z_0 + 0.25B \left[ 1 + \operatorname{erf} \left\{ \frac{x-C}{\sqrt{2}D} \right\} \right] \left[ 1 + \operatorname{erf} \left\{ \frac{y-E}{\sqrt{2}F} \right\} \right]$ , where $z_0$ , B, C, D, E, and F are the coefficients of the function.
Gauss2D	$z = z_0 + A \exp \left\{ -\frac{1}{2} \left( \frac{x-x_c}{w_1} \right)^2 - \frac{1}{2} \left( \frac{y-y_c}{w_2} \right)^2 \right\}$ , where $z_0$ , A, $x_c$ , $y_c$ , $w_1$ , and $w_2$ are the coefficients of the function.
Gaussian 2D	$z = z_0 + A \exp \left\{ -\frac{1}{2} \left( \frac{x \cos(\theta) + y \sin(\theta) - x_c \cos(\theta) + y_c \sin(\theta)}{w_1} \right)^2 - \frac{1}{2} \left( \frac{-x \cos(\theta) + y \sin(\theta) + x_c \cos(\theta) - y_c \sin(\theta)}{w_2} \right)^2 \right\}$ , where $z_0$ , A, $x_c$ , $y_c$ , $w_1$ , $w_2$ and $\theta$ are the coefficients of the function.
Rational Taylor	$z = \frac{z_0 + A_0x + B_0y + B_0y^2 + C_0xy}{1 + A_1x + B_1y + A_2x^2 + B_2y^2 + C_2xy}$ , where $z_0$ , $A_0$ , $A_1$ , $A_2$ , $B_0$ , $B_1$ , $B_2$ , $C_0$ and $C_2$ are the coefficient of the function.
Voigt2D	$z = z_0 + A \left[ \frac{\mu}{\left[ 1 + \left( \frac{x-x_c}{w_1} \right)^2 \right] \left[ 1 + \left( \frac{y-y_c}{w_2} \right)^2 \right]} + (1 - \mu) \exp \left( -\frac{1}{2} \left( \frac{x-x_c}{w_1} \right)^2 - \frac{1}{2} \left( \frac{y-y_c}{w_2} \right)^2 \right) \right]$ , where $z_0$ , A, $x_c$ , $y_c$ , $w_1$ , $w_2$ , and $\mu$ are the coefficients of the function.

### 4.3.3 Verification

The same experiment is conducted to verify the effectiveness of error compensation on the temperature measured by calibrated prototype due to change in measuring distance. Figures 4.7 to 4.10 show the average temperature measured by the prototype with delta labelled after surface fitting at different measuring distance.

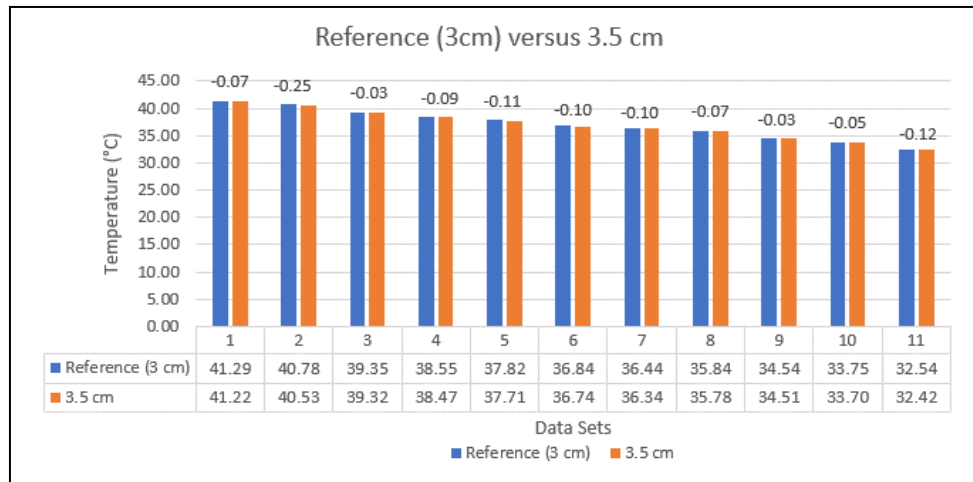


Figure 4.7: Temperature Measured at 3.5cm

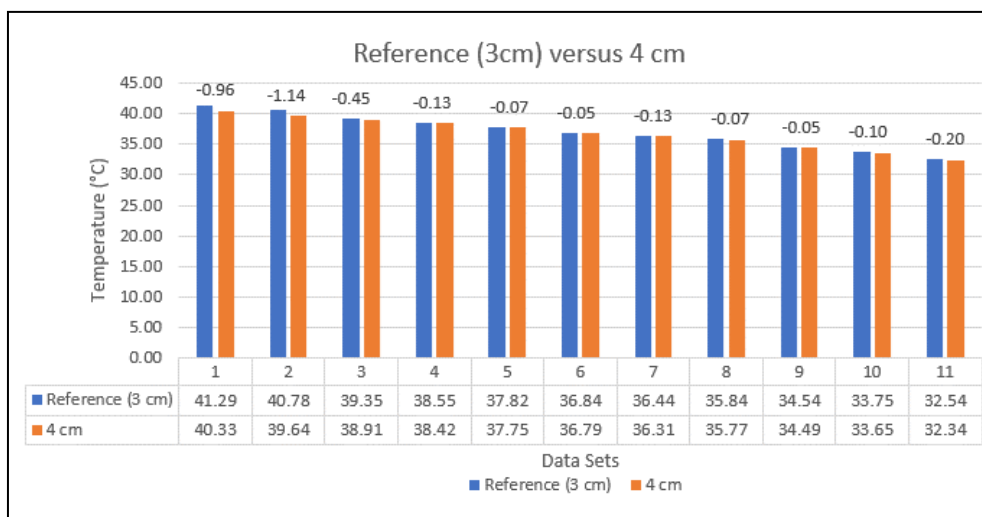


Figure 4.8: Temperature Measured at 4cm

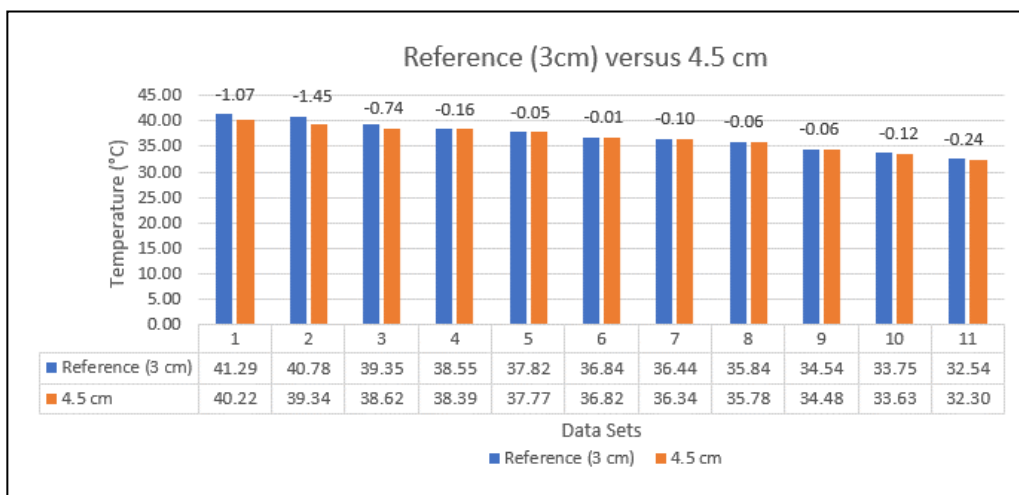


Figure 4.9: Temperature Measured at 4.5cm

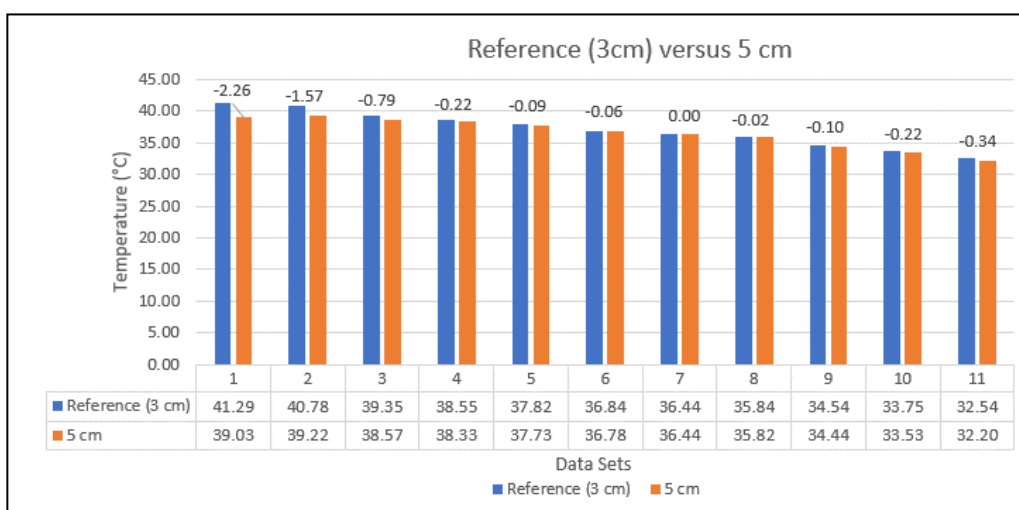


Figure 4.10: Temperature Measured at 5cm

According to Figure 4.7 to 4.10, the maximum delta for each measuring distance is successfully decreased as compared to Table 4.6. For example, the maximum error at 4 cm is reduced to  $-0.96\text{ }^{\circ}\text{C}$  from  $-2.59\text{ }^{\circ}\text{C}$  after surface fitting. Even though the verification is done based on the measuring distance of 3 cm. 3.5 cm, 4 cm. 4.5 cm and 5 cm, the prototype is still applicable at any distance from 3 cm to 5 cm.

#### 4.4 Prototype Evaluation

The prototype is used to perform body temperature measurements on humans as the subject to evaluate its functionality and accuracy as shown in Figure 4.11.

In addition, the evaluation is also used to find room for improvement for the prototype. The assessment is conducted by allowing the subjects to measure their temperature within the allowable measuring distance, from 3 cm to 5 cm. Besides, a hot or cold towel is placed on the subject's forehead to simulate abnormal temperatures. This is to mimic a sick individual with hypothermia or hyperthermia condition. In order to evaluate the prototype's performance, the body temperature measured with measuring distance is recorded in the SD card. After that, the subject's body temperature is also measured and recorded manually using a reference thermometer at a distance of approximately 3 cm. The result obtained are discussed accordingly in the following subsection.



Figure 4.11: Prototype Evaluation using Human as Subject

#### 4.4.1 Percentage of Escapees

The collected data are studied, and the presence of under reject (UR) and over reject (OR) conditions are spotted. Over rejection occurs when the object's temperature is within the normal range, but the measured temperature is found to be out of the normal range due to the measurement being done at a close or far distance. Next, under rejection occurs when the object's temperature is out of the normal range. Still, the measured temperature is within the normal range due to the measurement being done closer or farther. The under rejection can contribute to the perception of risk as the temperature scanner is not able to

detect the person with abnormal temperature. In the industry, under rejection is also referred to as an escapee. Table 4.11 represents the guideline followed to catch any under rejection and over rejection.

Table 4.11: Reference Table to Detect Escapee

Result: Reference Temperature	Result: Measured Temperature	OR / UR / Valid	Consequences
High (>36.9°C)	High	Valid	-
	Normal	UR (High)	Escaped (Risk)
	Low	UR (High)	Retest
Normal (35.5°C - 36.9°C)	High	OR	Retest
	Normal	Valid	-
	Low	OR	Retest
Low (<35.5°C)	High	UR (Low)	Retest
	Normal	UR (Low)	Escaped (Risk)
	Low	Valid	-

Generally, both conditions occurred due to the imperfection of calibration. Therefore, the percentage of escapees is calculated, and suitable mitigation is proposed. Table 4.12 shows the calculation of percentage escapees.

Table 4.12: Data collected with Percentage Escapee Calculation

Distance (cm)	Reference Temperature (°C)	Measured Temperature (°C)	Error (°C)	Result: Reference Temperature	Result: Measured Temperature	OR/UR/Valid
3.61	39.30	39.16	-0.14	High	High	Valid
4.57	38.80	37.49	-1.31	High	High	Valid
4.37	38.60	38.45	-0.15	High	High	Valid
4.89	38.30	36.89	-1.41	High	Normal	UR (High)
4.52	38.10	36.83	-1.27	High	Normal	UR (High)
4.59	37.60	36.36	-1.24	High	Normal	UR (High)
4.63	37.90	36.53	-1.37	High	Normal	UR (High)
3.83	37.70	37.51	-0.19	High	High	Valid
4.82	37.30	36.88	-0.42	High	Normal	UR (High)
3.41	37.00	37.04	0.04	High	High	Valid
3.42	36.90	36.76	-0.14	Normal	Normal	Valid
3.91	36.40	36.26	-0.14	Normal	Normal	Valid
4.55	36.30	36.26	-0.04	Normal	Normal	Valid
3.62	36.30	36.28	-0.02	Normal	Normal	Valid



4.86	36.40	36.33	-0.07	Normal	Normal	Valid
4.83	36.30	36.41	0.11	Normal	Normal	Valid
3.58	36.30	36.35	0.05	Normal	Normal	Valid
4.97	36.30	36.29	-0.01	Normal	Normal	Valid
3.31	36.40	36.32	-0.08	Normal	Normal	Valid
4.98	36.50	36.37	-0.13	Normal	Normal	Valid
3.87	36.20	36.14	-0.06	Normal	Normal	Valid
4.71	36.50	36.44	-0.06	Normal	Normal	Valid
4.98	36.30	36.23	-0.07	Normal	Normal	Valid
4.86	36.20	36.31	0.11	Normal	Normal	Valid
3.78	36.40	36.32	-0.08	Normal	Normal	Valid
4.91	36.50	36.32	-0.18	Normal	Normal	Valid
4.98	36.30	36.29	-0.01	Normal	Normal	Valid
4.88	36.30	36.28	-0.02	Normal	Normal	Valid
4.93	36.30	36.25	-0.05	Normal	Normal	Valid
3.30	36.60	36.66	0.06	Normal	Normal	Valid
3.23	36.30	36.35	0.05	Normal	Normal	Valid

4.98	36.30	36.23	-0.07	Normal	Normal	Valid
3.67	36.20	36.19	-0.01	Normal	Normal	Valid
4.50	36.30	36.30	0.00	Normal	Normal	Valid
4.88	36.30	36.25	-0.05	Normal	Normal	Valid
3.88	36.30	36.24	-0.06	Normal	Normal	Valid
4.91	36.30	36.16	-0.14	Normal	Normal	Valid
4.97	36.60	36.72	0.12	Normal	Normal	Valid
3.91	36.30	36.22	-0.08	Normal	Normal	Valid
4.71	36.30	36.27	-0.03	Normal	Normal	Valid
4.81	36.60	36.61	0.01	Normal	Normal	Valid
4.86	36.60	36.59	-0.01	Normal	Normal	Valid
3.55	36.60	36.55	-0.05	Normal	Normal	Valid
4.86	36.60	36.79	0.19	Normal	Normal	Valid
4.91	36.60	36.52	-0.08	Normal	Normal	Valid
3.11	36.60	36.65	0.05	Normal	Normal	Valid
4.81	36.60	36.64	0.04	Normal	Normal	Valid
4.83	36.60	36.66	0.06	Normal	Normal	Valid

4.97	36.60	36.71	0.11	Normal	Normal	Valid
3.21	36.60	36.55	-0.05	Normal	Normal	Valid
4.91	36.60	36.50	-0.10	Normal	Normal	Valid
3.97	36.70	36.68	-0.02	Normal	Normal	Valid
4.81	36.70	36.75	0.05	Normal	Normal	Valid
4.91	36.30	36.37	0.07	Normal	Normal	Valid
3.71	36.30	36.41	0.11	Normal	Normal	Valid
4.91	36.30	36.41	0.11	Normal	Normal	Valid
4.97	36.30	36.52	0.22	Normal	Normal	Valid
3.51	36.60	36.55	-0.05	Normal	Normal	Valid
4.64	36.00	35.45	-0.55	Normal	Low	OR
3.32	35.70	35.59	-0.11	Normal	Normal	Valid
4.75	35.40	36.22	0.82	Low	OK	UR (Low)
4.63	35.00	35.78	0.78	Low	OK	UR (Low)
3.78	34.80	34.69	-0.11	Low	Low	Valid
4.89	34.50	35.56	1.06	Low	OK	UR (Low)
4.56	34.30	35.53	1.23	Low	OK	UR (Low)

4.67	34.00	35.21	1.21	Low	OK	UR (Low)
3.33	33.90	33.78	-0.12	Low	Low	Valid
3.12	33.40	33.55	0.15	Low	Low	Valid
$\text{Percentage of escapee (\%)} = \frac{\text{Total Count (UR (High and Low))}}{\text{Total Sample}} \times 100\% = \frac{10}{70} \times 100\% = 14.29\%$						

According to Table 4.12, under rejection can be seen when the measuring distance is more than 4.5cm. This result also indicates that there is a minor flaw in the multiples distance calibration setup. The reason is that water balloon's inability to remain perfectly round after being inflated to a bigger diameter of approximately 10 cm to fill the FOV of an infrared sensor. Therefore, the surrounding temperatures are included during the multiple distances calibration when the balloon is placed at 5 cm. The prototype is modified to operate with a maximum measuring distance of 4.5 cm instead of 5 cm to reduce the escapee percentage. The overall error is relatively small, which is less than  $\pm 0.2$  °C for measuring distance of less than 4.5 cm. Hence, the latest maximum measuring distance is modified to 4.5 cm. This modification can ensure accuracy and reduce the percentage of escapees of the prototype.

#### 4.4.2 Limitation of Operating Temperature Range

During the prototype evaluation, it is found that the prototype is unable to provide accurate measurement for the temperature outside 32.0 °C to 42.9 °C. The limitation is because of the 6<sup>th</sup> order polynomial equation usage for error compensation in fixed distance calibration. The curve fitting is solely based on the temperature data collected, within 32.0 °C to 42.9 °C. Therefore, the 6<sup>th</sup> degree polynomial equation can only provide subtle compensation for temperature within the specified range. Once the temperature measured is outside the predefined range, the polynomial equation will contribute to inaccurate calibrated temperature. As expected, the incorrect calibrated temperature will also lead to the wrong final temperature after it went through the surface fitting equation from multiple distances calibration. Table 4.13 indicates the calibrated temperature obtained based on random substitution of the measured temperature.

Table 4.13: Estimation of Allowable Measured Temperature Range

Measured Temperature (°C)	Calibrated Temperature (°C)
21	1031.127594
22	594.8886956
23	326.3530216
24	171.0209618
25	88.47134555
26	49.78740011
27	35.23328735
28	32.18121883
29	33.28914948
30	34.92904973
31	35.86575617
32	36.1864007
33	36.48041821
34	37.27013271
35	38.69192202
36	40.42796095

37	41.88854296
38	42.64498032
39	43.11308287
40	45.4872151
41	54.92493194
42	80.98219289
43	139.2991548
44	253.5365428
45	457.5626006

Table 4.13 is constructed to provide an estimate of the temperature range, which is supported by the 6<sup>th</sup> order polynomial equation. According to Table 4.13, the prototype will only give the correct calibrated temperature for the measured temperature ranges from 28.0 °C to 38.0 °C. The corresponding calibrated temperature outside that range will give rise to the inaccurate calibrated temperature, which is significantly outside 32.0 °C to 42.9 °C. Hence, the prototype is modified to check and ensure the initial measured temperature is within the temperature range from 28.0 °C to 38.0 °C before feeding it to the polynomial equation. If the measured temperature is less or equal to 27.0 °C, the system will display “EXTREME LOW TEMPERATURE” on the LCD instead of the wrong final temperature. On the other hand, if the measured temperature is more or equal to 39.0 °C, the system will display “EXTREME HIGH TEMPERATURE” on the LCD. The operating temperature range of the prototype is limited.

## 4.5 Final Prototype

The final prototype's result and hardware, which consists of the contactless temperature scanner system and barcode tracking system, are shown in the following subsections.

### 4.5.1 Contactless Temperature Scanner System

Figure 4.12 indicates the display of normal temperature reading on the LCD with the flashing green LED.



Figure 4.12: Normal Temperature

Next, Figures 4.13 and 4.14 show the high and low temperature reading on the LCD with the blinking of a red LED.



Figure 4.13: High Temperature Within the Operating Range



Figure 4.14: Low Temperature Within the Operating Range

Figure 4.15 and 4.16 represent the display of extreme high and low temperature, which is outside the operating temperature range of 32.0 °C to 42.9 °C.



Figure 4.15: High Temperature Outside the Operating Range





Figure 4.16: Low Temperature Outside the Operating Range

#### 4.5.2 Barcode Tracking System

Figure 4.17 indicates the prototype's barcode inquiry through the LCD.

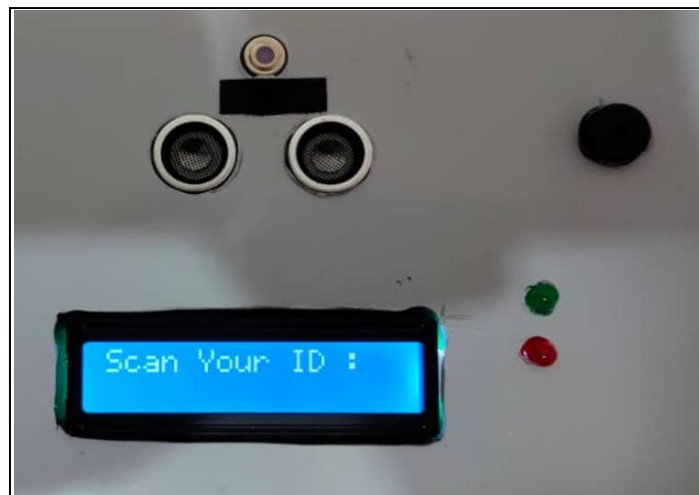


Figure 4.17: System Inquiry of Barcode

Figure 4.18 shows the scanned barcode is displayed on the LCD.



Figure 4.18: Display of Scanned Barcode

Figure 4.19 shows the data stored in the SD card.

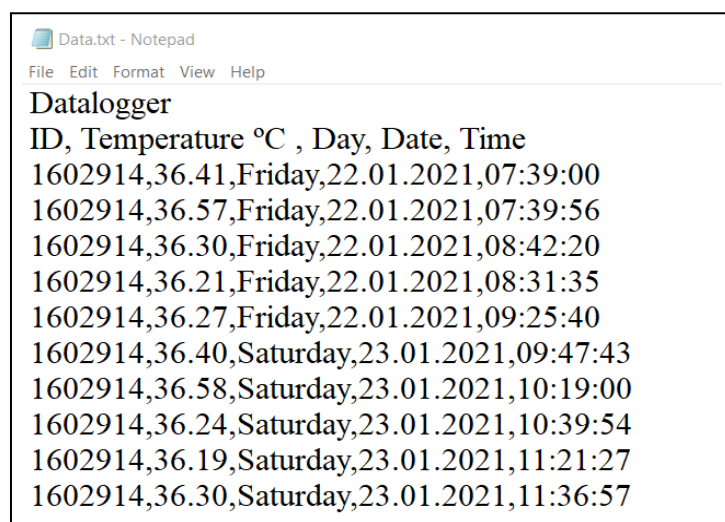


Figure 4.19: Sample of Data Stored

### 4.5.3 Prototype Setup

Figure 4.20 represents the final setup of the prototype.



Figure 4.20: Overview of Final Prototype

## CHAPTER 5

### CONCLUSIONS AND RECOMMENDATIONS

#### 5.1 Conclusion

This project's primary purpose is to develop a low-cost functional distance independent contactless temperature scanner system equipped with alarming and data logging features. The prototype can provide accurate body temperature measurement after fixed distance calibration with a reference infrared thermometer. The 6<sup>th</sup> degree polynomial model is selected as the mathematical model to describe the relationship between reference and calibrated temperature based on the statistical measure obtained. Moreover, the effect of measuring distance towards the accuracy of the prototype is discovered and compensated through surface fitting using the Rational Taylor function in multiple distances calibration. Hence, a minimum trade-off has been achieved to the prototype while increasing its measuring range. The result obtained from both the fixed distance and multiple distances calibration setup is discussed and verified. The prototype can provide an accuracy of  $\pm 0.2$  °C for measuring distance ranges from 3 cm to 4.5 cm through prototype evaluation. This indicates that a feasible calibration method for distance-independent temperature measurement has been introduced. Lastly, the prototype can automatically record information such as barcode, temperature, check-in time, and date.

#### 5.2 Recommendations for Future Works

The future works of this project can be improved in three aspects. These aspects are accuracy, design, and additional features. The prototype's accuracy can be further enhanced by using professional equipment such as the blackbody radiation source and infrared temperature sensor with longer distance coverage. The blackbody can provide perfect emission and zero reflection. This characteristic allows uniform temperature and acts as an ideal source for the Next, in this project, the measuring distance is modified from 5 cm to 4.5 cm due to water balloons' inability to remain in a perfect circle. The blackbody radiation source typically comes as a circular plate, and the user can adjust the diameter of it according to the FOV of an infrared sensor. The professional

equipment can ensure the blackbody source filled the FOV. This can prevent the involvement of surrounding temperature, which can affect the accuracy during the calibration process. Next, the use of infrared temperature sensor with more extended distance coverage can further enhance the allowable measuring distance.

Besides, the design, especially on the circuit, can be improved. For example, the PCB can replace the breadboard once all the testing and experimenting have been done. The design of PCB can reduce the weight and size of the prototype. Even though the current prototype can function flawlessly, a PCB connection is said to be more secure than a breadboard. Hence, it makes the prototype to be durable. For casing, a 3D printer can produce a design with a suitable dimension and holes for the sensor and power cable. The current prototype is developed using the specified casing's dimension available in the market. Therefore, it causes it to be more prominent in size if compared to the commercial product. The specified design can also ensure the sensor attaches perfectly to the casing.

Next, the extra functionality such as real-time virtual monitoring can be achieved in future works using a Wi-Fi module. This functionality allows the user to monitor the data collected anywhere and anytime. Also, the system can generate an email to alert the user if anyone with an abnormal temperature is detected. This virtual monitoring feature allows users to monitor the whole process remotely and only take subsequent action if an alert message is received. Furthermore, the system can include a database in future work. With the database, the user can save the employees' barcode beforehand, and access is granted only to the individual with a barcode kept in the database. Thus, provide security enhancement to the premisses.

## REFERENCES

Anuar, H. and Leow, P. L. (2019) 'Non-invasive core body temperature sensor for continuous monitoring', in *2019 IEEE International Conference on Sensors and Nanotechnology, SENSORS and NANO 2019*. Institute of Electrical and Electronics Engineers Inc. doi: 10.1109/SENSORSNANO44414.2019.8940040.

*Coronavirus: Comparing COVID-19, SARS and MERS | News | Al Jazeera* (no date). Available at: <https://www.aljazeera.com/news/2020/04/coronavirus-comparing-covid-19-sars-mers-200406165555715.html> (Accessed: 9 September 2020).

Daniel S, M. and Liran, M. (2002) *Core temperature measurement: Methods and current insights*. Available at: [https://www.researchgate.net/publication/8107409\\_Core\\_temperature\\_measurement\\_Methods\\_and\\_current\\_insights](https://www.researchgate.net/publication/8107409_Core_temperature_measurement_Methods_and_current_insights) (Accessed: 2 September 2020).

Drager Medical (no date) *The significance of core temperature-Pathophysiology and measurement methods*.

El-Radhi, A. S. and Barry, W. (2006) 'Thermometry in paediatric practice', *Archives of Disease in Childhood*. BMJ Publishing Group, pp. 351–356. doi: 10.1136/ad.2005.088831.

Fallis, W. M. (2002) 'Monitoring urinary bladder temperature in the intensive care unit: State of the science', *American Journal of Critical Care*. American Association of Critical Care Nurses, 11(1), pp. 38–47. doi: 10.4037/ajcc2002.11.1.38.

Geneva, I. I. *et al.* (2019) 'Normal body temperature: A systematic review', *Open Forum Infectious Diseases*. Oxford University Press, 6(4). doi: 10.1093/ofid/ofz032.

Glaser, A. (2020) '*Fever detection*' cameras to fight coronavirus? Experts say they don't work. Available at: <https://www.nbcnews.com/tech/security/fever-detection-cameras-fight-coronavirus-experts-say-they-don-t-n1170791> (Accessed: 22 March 2021).

*Handsfree Non-contact Automatic Forehead Infrared Thermometer* (no date). Available at: [https://www.kartpul.store/index.php?route=product/product&product\\_id=77](https://www.kartpul.store/index.php?route=product/product&product_id=77) (Accessed: 22 March 2021).

Heng Yew Ling, T. *et al.* (2015) 'Non-Intrusive Human Body Temperature Acquisition and Monitoring System'. doi: 10.1109/ISMS.2015.17.

*IR Thermometers explained - FireCraft / ir-thermometers-explained-firecraft.pdf / PDF4PRO* (no date). Available at: <https://pdf4pro.com/view/ir-thermometers-explained-firecraft-5b8aba.html> (Accessed: 9 September 2020).

Kapoor, A. (2021) *Infrared Thermometers to measure body temperature from a distance | Most Searched Products - Times of India*. Available at: <https://timesofindia.indiatimes.com/most-searched-products/health-and-fitness/health-care/infrared-thermometer-popular-ones-to-measure-body-temperature-in-a-non-contact-way/articleshow/71180035.cms> (Accessed: 22 March 2021).

Kumar, Ma. *et al.* (2015) *Automated Color Recognition System for Visually Challenged and Achromatopsia People using Arduino and Mobile App, International Journal of Advanced Research in Electronics and Communication Engineering (IJARECE)*.

Landsman, I. S. *et al.* (2012) 'Pediatric Anesthesia', in *Pediatric Surgery*. Elsevier Inc., pp. 201–226. doi: 10.1016/B978-0-323-07255-7.00013-1.

McCallum, L. and Higgins, D. (2012) *Measuring body temperature | Nursing Times*. Available at: <https://www.nursingtimes.net/clinical-archive/assessment-skills/measuring-body-temperature-06-11-2012/> (Accessed: 2 September 2020).

*MLX90614 IR Thermometer Hookup Guide - learn.sparkfun.com* (no date). Available at: <https://learn.sparkfun.com/tutorials/mlx90614-ir-thermometer-hookup-guide/all> (Accessed: 12 September 2020).

Moon, K. S. *et al.* (2004) 'Lead-free solder interconnect by variable frequency microwave (VFM)', in *Proceedings - Electronic Components and Technology Conference*, pp. 1989–1995. doi: 10.1109/ectc.2004.1320400.

Naiman, M. I. *et al.* (2017) 'Esophageal heat transfer for patient temperature control and targeted temperature management', *Journal of Visualized Experiments*. Journal of Visualized Experiments, 2017(129). doi: 10.3791/56579.

*Normal body temperature | definition of Normal body temperature by Medical dictionary* (no date). Available at: <https://medical-dictionary.thefreedictionary.com/Normal+body+temperature> (Accessed: 12 September 2020).

Prabhakar, H. (2016) *Complications in Neuroanesthesia, Complications in Neuroanesthesia*. Elsevier Inc. doi: 10.1016/C2015-0-00811-5.

Rahimoon, A. A., Abdullah, M. N. and Taib, I. (2020) 'Design of a contactless body temperature measurement system using Arduino', *Indonesian Journal of Electrical Engineering and Computer Science*. Institute of Advanced

Engineering and Science, 19(3), pp. 1251–1258. doi: 10.11591/ijeecs.v19.i3.pp1251-1258.

Rani, M. (2015) *Evolution Of Inventions: THERMOMETER*. Available at: <http://inventionevolution.blogspot.com/2015/02/thermometer.html> (Accessed: 22 March 2021).

Ritchie, H. *et al.* (2021) *Coronavirus (COVID-19) Cases - Statistics and Research - Our World in Data*. Available at: <https://ourworldindata.org/covid-cases> (Accessed: 21 March 2021).

Santoso, D. and Dalu Setiaji, F. (2016) ‘Non-contact portable infrared thermometer for rapid influenza screening’, in *Proceedings of the 2015 International Conference on Automation, Cognitive Science, Optics, Micro Electro-Mechanical System, and Information Technology, ICACOMIT 2015*. Institute of Electrical and Electronics Engineers Inc., pp. 18–23. doi: 10.1109/ICACOMIT.2015.7440147.

Schneider, F. (2007) *Advances in IR Temperature Measurement | FierceElectronics*. Available at: <https://www.fierceelectronics.com/components/advances-ir-temperature-measurement> (Accessed: 9 September 2020).

Sessler, D. I. (2008) ‘Temperature monitoring and perioperative thermoregulation’, *Anesthesiology*. Lippincott Williams and Wilkins, pp. 318–338. doi: 10.1097/ALN.0b013e31817f6d76.

Smith, T. (2020) *The Rise of Covid-19 Temperature Scanners That Can Also Capture and Store Your Face | by Thomas Smith | Mar, 2021 | OneZero*. Available at: <https://onezero.medium.com/those-covid-19-temperature-scanning-kiosks-use-scary-powerful-facial-recognition-8cc8ada0c595> (Accessed: 22 March 2021).

Sun, G. *et al.* (2014) ‘Fever screening of seasonal influenza patients using a cost-effective thermopile array with small pixels for close-range thermometry’, *International Journal of Infectious Diseases*. Elsevier, 25, pp. 56–58. doi: 10.1016/j.ijid.2014.03.1398.

Sund-Levander, M. and Grodzinsky, E. (2009) ‘Time for a change to assess and evaluate body temperature in clinical practice’, *International Journal of Nursing Practice*. John Wiley & Sons, Ltd, 15(4), pp. 241–249. doi: 10.1111/j.1440-172X.2009.01756.x.

Tang, H. F. and Hung, K. (2017) ‘Design of a non-contact body temperature measurement system for smart campus’, in *2016 IEEE International Conference on Consumer Electronics-China, ICCE-China 2016*. Institute of Electrical and Electronics Engineers Inc. doi: 10.1109/ICCE-China.2016.7849773.



Teo, A. K. J., Tan, R. K. J. and Prem, K. (2020) 'Concealment of potential exposure to COVID-19 and its impact on outbreak control: Lessons from the HIV response', *American Journal of Tropical Medicine and Hygiene*. American Society of Tropical Medicine and Hygiene, 103(1), pp. 35–37. doi: 10.4269/ajtmh.20-0449.

Teran, C. G. *et al.* (2012) 'Clinical accuracy of a non-contact infrared skin thermometer in paediatric practice', *Child: Care, Health and Development*. John Wiley & Sons, Ltd, 38(4), pp. 471–476. doi: 10.1111/j.1365-2214.2011.01264.x.

*USB Host Shield 2.0 - Arduino Compatible | QQ Online Trading* (no date). Available at: <http://qqtrading.com.my/usb-host-shield-2-arduino-compatible> (Accessed: 9 September 2020).

Wagner, M. *et al.* (2020) 'Comparison of a Continuous Noninvasive Temperature to Monitor Core Temperature Measures During Targeted Temperature Management', *Neurocritical Care*. Springer, pp. 1–7. doi: 10.1007/s12028-020-01036-9.

*What is Emissivity? | Fluke Process Instruments* (no date). Available at: <https://www.flukeprocessinstruments.com/en-us/service-and-support/knowledge-center/infrared-technology/what-is-emissivity> (Accessed: 9 September 2020).

*Wiring I2C module on 16x2 LCD with SCL/SDA | 14core.com* (no date). Available at: <https://www.14core.com/wiring-i2c-module-on-16x2-lcd-with-sclsda/> (Accessed: 12 September 2020).

Zhen, C. *et al.* (2014) 'Accuracy of infrared ear thermometry in children: A meta-analysis and systematic review', *Clinical Pediatrics*. SAGE Publications Inc., 53(12), pp. 1158–1165. doi: 10.1177/0009922814536774.

## APPENDICES

### APPENDIX A: Polynomial Curve Fitting Equation

Equation	$y = \text{Intercept} + B1 \cdot x^1$
Plot	Reference ( $^{\circ}\text{C}$ )
Weight	No Weighting
Intercept	$5.8632200567 \pm 1.4077817859$
B1	$0.9484698711 \pm 0.0427393768$
Residual Sum of Squares	10.0357986015
R-Square (COD)	0.9480251876
Adj. R-Square	0.9461001946

Figure A - 1: First Degree Polynomial Fitting's Coefficient

Equation	$y = \text{Intercept} + B1 \cdot x^1 + B2 \cdot x^2$
Plot	Reference ( $^{\circ}\text{C}$ )
Weight	No Weighting
Intercept	$56.1692276866 \pm 15.4925968391$
B1	$-2.163707126 \pm 0.9562300661$
B2	$0.0478111009 \pm 0.0146793448$
Residual Sum of Squares	7.1276473113
R-Square (COD)	0.9630863326
Adj. R-Square	0.9602468197

Figure A - 2: Second Degree Polynomial Fitting's Coefficient

Equation	$y = \text{Intercept} + B1 \cdot x^1 + B2 \cdot x^2 + B3 \cdot x^3$
Plot	Reference ( $^{\circ}\text{C}$ )
Weight	No Weighting
Intercept	$-754.1196383411 \pm 112.36760205$
B1	$72.8873785736 \pm 10.3892768159$
B2	$-2.2593316931 \pm 0.3190348192$
B3	$0.0235423559 \pm 0.00325431$
Residual Sum of Squares	2.3041833585
R-Square (COD)	0.9880667695
Adj. R-Square	0.9866347819

Figure A - 3: Third Degree Polynomial Fitting's Coefficient

Equation	$y = \text{Intercept} + B1*x^1 + B2*x^2 + B3*x^3 + B4*x^4$
Plot	Reference (°C)
Weight	No Weighting
Intercept	$-4528.0038757939 \pm 1236.0061476292$
B1	$541.0446531047 \pm 153.1177507649$
B2	$-23.9672727087 \pm 7.0930275442$
B3	$0.4694673795 \pm 0.1456219461$
B4	$-0.0034241089 \pm 0.001117973$
Residual Sum of Squares	1.6566608551
R-Square (COD)	0.9914202506
Adj. R-Square	0.989902924

Figure A - 4: Fourth Degree Polynomial Fitting's Coefficient

Equation	$y = \text{Intercept} + B1*x^1 + B2*x^2 + B3*x^3 + B4*x^4 + B5*x^5$
Plot	Reference (°C)
Weight	No Weighting
Intercept	$76313.0542413619 \pm 9317.0534144026$
B1	$-11966.8281703953 \pm 1440.4425872702$
B2	$748.1300880091 \pm 88.8635246015$
B3	$-23.2998296344 \pm 2.7345178074$
B4	$0.3615206783 \pm 0.0419738831$
B5	$-0.0022356685 \pm 2.5711172922E-$
Residual Sum of Squares	0.3864086005
R-Square (COD)	0.9979988125
Adj. R-Square	0.9975637718

Figure A - 5: Fifth Degree Polynomial Fitting's Coefficient

Equation	$y = \text{Intercept} + B1*x^1 + B2*x^2 + B3*x^3 + B4*x^4 + B5*x^5 + B6*x^6 + B7*x^7$
Plot	Reference (°C)
Weight	No Weighting
Intercept	$-3177741.9621809083 \pm 1386327.3712079362$
B1	$703610.728340472 \pm 299260.366403074$
B2	$-66562.1384852836 \pm 27642.5227436514$
B3	$3487.4586551554 \pm 1416.3112951073$
B4	$-109.2959764712 \pm 43.473004670$
B5	$2.0488954852 \pm 0.7994004766$
B6	$-0.0212737216 \pm 0.0081540513$
B7	$9.438132808E-5 \pm 3.5591560764E-5$
Residual Sum of Squares	0.1754054156
R-Square (COD)	0.9990915856
Adj. R-Square	0.9987887809

Figure A - 6: Seventh Degree Polynomial Fitting's Coefficient

Equation	$y = \text{Intercept} + B1*x^1 + B2*x^2 + B3*x^3 + B4*x^4 + B5*x^5 + B6*x^6 + B7*x^7 + B8*x^8$
Plot	Reference (°C)
Weight	No Weighting
Intercept	$-9166673.5145860091 \pm 1.7828730571E7$
B1	$2184177.9271691977 \pm 4404263.6792132454$
B2	$-226469.5003261906 \pm 475370.6334478649$
B3	$13342.4279315693 \pm 29280.7561678307$
B4	$-488.3560276975 \pm 1125.7508895818$
B5	$11.3670169606 \pm 27.6639180058$
B6	$-0.1642350049 \pm 0.4243244904$
B7	$0.0013459727 \pm 0.0037143199$
B8	$-4.7871779531E-6 \pm 1.4206120513E-5$
Residual Sum of Squares	0.1744151258
R-Square (COD)	0.9990967143
Adj. R-Square	0.9987354

Figure A - 7: Eighth Degree Polynomial Fitting's Coefficient

Equation	$y = \text{Intercept} + B1*x^1 + B2*x^2 + B3*x^3 + B4*x^4 + B5*x^5 + B6*x^6 + B7*x^7 + B8*x^8 + B9*x^9$
Plot	Reference (°C)
Weight	No Weighting
Intercept	$-4.4053913666E8 \pm 2.2823123136E8$
B1	$1.2249584429E8 \pm 6.3617625803E8$
B2	$-1.5120817258E7 \pm 7871728.2327452106$
B3	$1087562.9053844565 \pm 567482.1772527602$
B4	$-50230.2110112737 \pm 26267.6819090116$
B5	$1544.9328930127 \pm 809.6054112091$
B6	$-31.6443357651 \pm 16.6152900972$
B7	$0.4162334477 \pm 0.2189435015$
B8	$-0.0031903725 \pm 0.001680929$
B9	$1.0857144997E-5 \pm 5.7287786231E-6$
Residual Sum of Squares	0.1466856734
R-Square (COD)	0.9992403235
Adj. R-Square	0.9988804767

Figure A - 8: Ninth Degree Polynomial Fitting's Coefficient

APPENDIX B: Percentage Error Calculation for Curve Fitting  
(10 decimal places)

Callibration Temperature (1 order)	Error (1 order)
41.26	-1.14
40.76	-0.84
40.35	-0.75
39.97	-0.63
39.68	-0.32
39.49	0.09
39.19	0.09
38.98	0.28
38.66	0.56
38.46	0.66
38.32	0.82
37.99	0.79
37.85	0.85
37.61	0.81
37.37	0.67
37.17	0.57
36.98	0.48
36.61	0.31
36.26	0.06
35.68	-0.42
35.17	-0.83
34.60	-0.80
34.55	-0.55
34.05	-0.45
33.84	-0.36
33.71	-0.29
33.62	-0.08
32.57	0.17
32.35	0.25
Percentage Error (%) = $24/29 \times 100 = 82.76$	

Figure B - 1: Percentage Error for First Degree Polynomial Model

Callibration Temperature (2 order)	Error (2 order)
42.01	-0.39
41.28	-0.32
40.71	-0.39
40.18	-0.42
39.80	-0.20
39.55	0.15
39.17	0.07
38.91	0.21
38.52	0.42
38.28	0.48
38.12	0.62
37.74	0.54
37.58	0.58
37.32	0.52
37.05	0.35
36.84	0.24
36.65	0.15
36.27	-0.03
35.93	-0.27
35.40	-0.70
34.96	-1.04
34.50	-0.90
34.47	-0.63
34.09	-0.41
33.95	-0.25
33.85	-0.15
33.79	0.09
33.15	0.75
33.03	0.93
Percentage Error (%) = $23/29 \times 100 = 79.31$	

Figure B - 2: Percentage Error for Second Degree Polynomial Model

Calibrated Temperature (3 order)	Error (3 order)
42.99	0.59
41.69	0.09
40.80	-0.30
40.05	-0.55
39.55	-0.45
39.24	-0.16
38.81	-0.29
38.53	-0.17
38.15	0.05
37.93	0.13
37.78	0.28
37.46	0.26
37.33	0.33
37.14	0.34
36.95	0.25
36.80	0.20
36.67	0.17
36.41	0.11
36.18	-0.02
35.81	-0.29
35.45	-0.55
35.00	-0.40
34.96	-0.14
34.48	-0.02
34.26	0.06
34.11	0.11
34.00	0.30
32.48	0.08
32.09	-0.01
Percentage Error (%) = $14/29 \times 100 = 48.28$	

Figure B - 3: Percentage Error for Third Degree Polynomial Model

Calibrated Temperature (4 order)	Error (4 order)
42.64	0.24
41.67	0.07
40.92	-0.18
40.23	-0.37
39.73	-0.27
39.42	0.02
38.95	-0.15
38.65	-0.05
38.21	0.11
37.95	0.15
37.78	0.28
37.41	0.21
37.25	0.25
37.02	0.22
36.80	0.10
36.64	0.04
36.50	0.00
36.24	-0.06
36.03	-0.17
35.72	-0.38
35.44	-0.56
35.09	-0.31
35.06	-0.04
34.65	0.15
34.44	0.24
34.29	0.29
34.18	0.48
32.36	-0.04
31.83	-0.27
Percentage Error (%) = $14/29 \times 100 = 48.28$	

Figure B - 4: Percentage Error for Fourth Degree Polynomial Model

Calibrated Temperature (5 order)	Error (5 order)
42.23	-0.17
41.87	0.27
41.24	0.14
40.49	-0.11
39.90	-0.10
39.51	0.11
38.93	-0.17
38.56	-0.14
38.04	-0.06
37.75	-0.05
37.57	0.07
37.20	0.00
37.07	0.07
36.88	0.08
36.72	0.02
36.61	0.01
36.53	0.03
36.39	0.09
36.28	0.08
36.06	-0.04
35.75	-0.25
35.23	-0.17
35.18	0.08
34.53	0.03
34.22	0.02
34.01	0.01
33.87	0.17
32.32	-0.08
32.12	0.02
Percentage Error (%) = $2/29 * 100 = 6.90$	

Figure B - 5: Percentage Error for Fifth Degree Polynomial Model

Callibrated Temperature (7 order)	Error (7 order)
39.47	-2.93
39.01	-2.59
38.65	-2.45
38.22	-2.38
37.84	-2.16
37.57	-1.83
37.13	-1.97
36.83	-1.87
36.39	-1.71
36.14	-1.66
35.99	-1.51
35.68	-1.52
35.57	-1.43
35.43	-1.37
35.34	-1.36
35.29	-1.31
35.27	-1.23
35.28	-1.02
35.30	-0.90
35.27	-0.83
35.07	-0.93
34.60	-0.80
34.56	-0.54
33.91	-0.59
33.61	-0.59
33.41	-0.59
33.27	-0.43
31.92	-0.48
31.75	-0.35
Percentage Error (%) = $29/29 * 100 = 100$	

Figure B - 6: Percentage Error for Seventh Degree Polynomial Model

Callibrated Temperature (8 order)	Error (8 order)
-45.94	-88.34
-52.05	-93.65
-55.79	-96.89
-58.58	-99.18
-60.23	-100.23
-61.10	-100.50
-62.17	-101.27
-62.69	-101.39
-63.15	-101.25
-63.22	-101.02
-63.18	-100.68
-62.79	-99.99
-62.49	-99.49
-61.84	-98.64
-60.97	-97.67
-60.12	-96.72
-59.25	-95.75
-57.24	-93.54
-55.09	-91.29
-51.29	-87.39
-47.77	-83.77
-43.89	-79.29
-43.59	-78.69
-40.20	-74.70
-38.82	-73.02
-37.94	-71.94
-37.35	-71.05
-30.10	-62.50
-28.55	-60.65
Percentage Error (%) = 29/29*100 =100	

Figure B - 7: Percentage Error for Eighth Degree Polynomial Model

Callibrated Temperature (9 order)	Error (9 order)
7963.63	7921.23
7002.83	6961.23
6310.33	6269.23
5707.78	5667.18
5287.89	5247.89
5029.11	4989.71
4646.39	4607.29
4393.46	4354.76
4033.70	3995.60
3817.55	3779.75
3675.04	3637.54
3357.03	3319.83
3224.45	3187.45
3021.02	2984.22
2819.19	2782.49
2662.76	2626.16
2527.81	2491.31
2272.14	2235.84
2051.35	2015.15
1733.63	1697.53
1488.99	1452.99
1254.02	1218.62
1237.23	1202.13
1059.18	1024.68
992.75	958.55
952.47	918.47
926.45	892.75
664.12	631.72
619.63	587.53
Percentage Error (%) = 29/29*100 =100	

Figure B - 8: Percentage Error for Ninth Degree Polynomial Model

## APPENDIX C: Data Collected for Multiple Distances Calibration



Reference (3cm)	Reading 1	Reading 2	Reading 3	Average
	42.64	42.66	42.67	42.66
	40.58	40.44	40.51	40.51
	38.25	38.28	38.24	38.26
	37.21	37.19	37.19	37.20
	36.92	36.85	36.83	36.87
	36.58	36.31	36.31	36.40
	35.89	35.90	35.92	35.90
	35.33	35.37	35.33	35.34
	34.54	34.49	34.52	34.52
	33.62	33.57	33.62	33.60
	32.56	32.54	32.55	32.55

Figure C - 1: Temperature Data Collected at 3cm

3.5 cm	Reading 1	Reading 2	Reading 3	Average	Error
	41.29	41.29	41.27	41.28	1.37
	39.29	39.29	39.23	39.27	1.24
	37.65	37.68	37.55	37.63	0.63
	36.65	36.68	36.67	36.67	0.53
	36.57	36.54	36.52	36.54	0.32
	36.17	36.15	36.11	36.14	0.26
	35.69	35.67	35.69	35.68	0.22
	35.17	35.16	35.17	35.17	0.18
	34.38	34.38	34.37	34.38	0.14
	33.49	33.52	33.50	33.50	0.10
	32.47	32.47	32.46	32.47	0.08

Figure C – 2: Temperature Data Collected at 3.5cm

4 cm	Reading 1	Reading 2	Reading 3	Average	Error
	40.09	40.09	40.03	40.07	2.59
	38.38	38.32	38.29	38.33	2.18
	37.11	37.03	37.11	37.08	1.17
	36.45	36.48	36.47	36.47	0.73
	36.38	36.35	36.35	36.36	0.51
	36.06	36.03	36.02	36.04	0.36
	35.61	35.64	35.63	35.63	0.28
	35.08	35.11	35.10	35.10	0.25
	34.33	34.33	34.33	34.33	0.19
	33.44	33.48	33.45	33.46	0.15
	32.45	32.44	32.42	32.44	0.11

Figure C – 3: Temperature Data Collected at 4cm

4.5 cm	Reading 1	Reading 2	Reading 3	Average	Error
	39.85	39.78	39.75	39.79	2.86
	37.95	37.92	37.92	37.93	2.58
	36.74	36.74	36.77	36.75	1.51
	36.36	36.35	36.34	36.35	0.85
	36.27	36.24	36.27	36.26	0.61
	35.97	35.96	35.96	35.96	0.44
	35.55	35.58	35.54	35.56	0.35
	35.04	35.05	35.05	35.05	0.30
	34.28	34.26	34.36	34.30	0.22
	33.43	33.46	33.43	33.44	0.16
	32.41	32.39	32.40	32.40	0.15

Figure C – 4: Temperature Data Collected at 4.5cm

5 cm	Reading 1	Reading 2	Reading 3	Average	Error
	38.71	38.78	38.84	38.78	3.88
	37.72	37.76	37.77	37.75	2.76
	36.67	36.65	36.65	36.66	1.60
	36.26	36.25	36.24	36.25	0.95
	36.11	36.12	36.18	36.14	0.73
	35.80	35.80	35.81	35.80	0.60
	35.42	35.48	35.44	35.45	0.46
	34.99	34.99	34.93	34.97	0.37
	34.22	34.23	34.25	34.23	0.28
	33.37	33.39	33.35	33.37	0.23
	32.36	32.34	32.34	32.35	0.20

Figure C - 5: Temperature Data Collected at 5cm

## APPENDIX D: Surface Fitting Equation

Model	GaussCum
Equation	$z = z_0 + 0.25*B*(1 + \text{erf}((x - C)/(\text{sqrt}(2)*D)))*(1 + \text{erf}((y - \text{Delta})/(\text{sqrt}(2)*E)))$
Plot	Delta (°C)
z0	0.04013092 ± 0.03526239
B	3.588038 ± 0.1747741
C	3.670114 ± 0.03504687
D	0.4674541 ± 0.04610148
E	38.80761 ± 0.1941929
F	2.352108 ± 0.1922247
Reduced Chi-	0.0186596
R-Square (C	0.9779478
Adj. R-Square	0.9756976

Figure D - 1: GaussCum Fitting's Coefficient

Model	Gauss2D
Equation	$z=z_0+A*\exp(-0.5*((x-xc)/w1)^2-0.5*((y-yc)/w2)^2)$ ;
Plot	Delta (°C)
z0	0.004971383 ± 0.04661152
A	3.589607 ± 0.1248485
xc	4.849041 ± 0.08016061
w1	0.9234207 ± 0.07143432
yc	42.6744 ± 0.3628917
w2	3.373876 ± 0.2508043
Reduced Chi-	0.02757708
R-Square (C	0.967409
Adj. R-Square	0.9640834

Figure D - 2: Gauss2D Fitting's Coefficient

Model	Gaussian2D
Equation	$z=z_0+A*\exp(-0.5*((x*\cos(\theta)+y*\sin(\theta)-xc*\cos(\theta)-yc*\sin(\theta))/w1)^2-0.5*((-x*\sin(\theta)+y*\cos(\theta)+xc*\sin(\theta)-yc*\cos(\theta))/w2)^2)$ ;
Plot	Delta (°C)
z0	-0.01321502 ± 0.0517838
A	3.658769 ± 0.1648616
xc	4.896854 ± 0.1037408
w1	0.9388223 ± 0.07966259
yc	42.83252 ± 0.4429635
w2	3.441803 ± 0.2828241
theta	0 ± 0.02509911
Reduced Chi-Sqr	0.02933265
R-Square (COD)	0.9660417
Adj. R-Square	0.9617969

Figure D - 3: Gaussian2D Fitting's Coefficient

Model	Voigt2D
Equation	$z=z_0+A*(\mu/((1+((x-xc)/w1)^2)*(1+((y-yc)/w2)^2))+(1-\mu)*\exp(-0.5*((x-xc)/w1)^2-0.5*((y-yc)/w2)^2)$
Plot	Delta (°C)
z0	0.04169849 ± 0.07023484
A	3.589507 ± 0.2247197
xc	4.930282 ± 0.1498527
w1	0.9595903 ± 0.1031847
yc	43.32424 ± 1.080528
w2	3.743999 ± 0.6059128
mu	0 ± 0.3883463
Reduced Chi-S	0.03281023
R-Square (COD)	0.9620157
Adj. R-Square	0.9572677

Figure D - 4: Voigt2D Fitting's Coefficient

### APPENDIX E: Percentage Error Calculation for Surface Fitting

Temperature (Reference)	Temperature (Before)	Distance	Delta ( From Equation)	Error(Before)	Temperature (After)	Error (After)
42.66	42.66	3.00	0.30	0.00	42.96	0.30
40.51	40.51	3.00	0.25	0.00	40.76	0.25
38.26	38.26	3.00	0.15	0.00	38.41	0.15
37.20	37.20	3.00	0.11	0.00	37.30	0.11
36.87	36.87	3.00	0.10	0.00	36.96	0.10
36.40	36.40	3.00	0.08	0.00	36.48	0.08
35.90	35.90	3.00	0.07	0.00	35.97	0.07
35.34	35.34	3.00	0.06	0.00	35.40	0.06
34.52	34.52	3.00	0.05	0.00	34.57	0.05
33.60	33.60	3.00	0.04	0.00	33.65	0.04
32.55	32.55	3.00	0.04	0.00	32.59	0.04
42.66	41.28	3.50	1.14	1.37	42.42	0.24
40.51	39.27	3.50	0.78	1.24	40.05	0.46
38.26	37.63	3.50	0.44	0.63	38.06	0.19
37.20	36.67	3.50	0.27	0.53	36.94	0.26
36.87	36.54	3.50	0.26	0.32	36.80	0.07
36.40	36.14	3.50	0.21	0.26	36.35	0.05
35.90	35.68	3.50	0.16	0.22	35.84	0.06
35.34	35.17	3.50	0.12	0.18	35.28	0.06
34.52	34.38	3.50	0.08	0.14	34.46	0.06
33.60	33.50	3.50	0.06	0.10	33.56	0.04
32.55	32.47	3.50	0.04	0.08	32.51	0.04
42.66	40.07	4.00	1.96	2.59	42.03	0.63
40.51	38.33	4.00	1.18	2.18	39.51	1.00
38.26	37.08	4.00	0.67	1.17	37.76	0.50
37.20	36.47	4.00	0.48	0.73	36.94	0.25
36.87	36.36	4.00	0.45	0.51	36.81	0.06
36.40	36.04	4.00	0.37	0.36	36.40	0.00
35.90	35.63	4.00	0.28	0.28	35.91	0.00
35.34	35.10	4.00	0.20	0.25	35.29	0.05
34.52	34.33	4.00	0.12	0.19	34.45	0.07
33.60	33.46	4.00	0.07	0.15	33.53	0.08
32.55	32.44	4.00	0.05	0.11	32.49	0.06
42.66	39.79	4.50	2.33	2.86	42.12	0.54
40.51	37.93	4.50	1.26	2.58	39.19	1.32
38.26	36.75	4.50	0.70	1.51	37.45	0.81
37.20	36.35	4.50	0.55	0.85	36.90	0.30
36.87	36.26	4.50	0.52	0.61	36.78	0.09
36.40	35.96	4.50	0.43	0.44	36.39	0.01
35.90	35.56	4.50	0.33	0.35	35.88	0.02
35.34	35.05	4.50	0.23	0.30	35.28	0.07
34.52	34.30	4.50	0.14	0.22	34.44	0.08
33.60	33.44	4.50	0.08	0.16	33.52	0.08
32.55	32.40	4.50	0.05	0.15	32.45	0.10
42.66	38.78	5.00	1.81	3.88	40.59	2.07
40.51	37.75	5.00	1.21	2.76	38.96	1.55
38.26	36.66	5.00	0.69	1.60	37.34	0.91
37.20	36.25	5.00	0.54	0.95	36.79	0.41
36.87	36.14	5.00	0.50	0.73	36.64	0.23
36.40	35.80	5.00	0.40	0.60	36.20	0.20
35.90	35.45	5.00	0.31	0.46	35.76	0.14
35.34	34.97	5.00	0.22	0.37	35.19	0.15
34.52	34.23	5.00	0.13	0.28	34.37	0.15
33.60	33.37	5.00	0.08	0.23	33.45	0.16
32.55	32.35	5.00	0.05	0.20	32.40	0.15
Percentage Error (%) = 18/55*100 = 32.73						

Figure E - 5.1: GaussCum's Percentage Error Calculation

Temperature (Reference)	Temperature (Before)	Distance	Delta ( From Equation)	Error(Before)	Temperature (After)	Error (After)
42.66	42.66	3.00	0.49	0.00	43.15	0.49
40.51	40.51	3.00	0.40	0.00	40.91	0.40
38.26	38.26	3.00	0.21	0.00	38.47	0.21
37.20	37.20	3.00	0.13	0.00	37.33	0.13
36.87	36.87	3.00	0.11	0.00	36.98	0.11
36.40	36.40	3.00	0.09	0.00	36.49	0.09
35.90	35.90	3.00	0.07	0.00	35.97	0.07
35.34	35.34	3.00	0.05	0.00	35.39	0.05
34.52	34.52	3.00	0.03	0.00	34.55	0.03
33.60	33.60	3.00	0.02	0.00	33.62	0.02
32.55	32.55	3.00	0.01	0.00	32.56	0.01
42.66	41.28	3.50	1.14	1.37	42.42	0.23
40.51	39.27	3.50	0.75	1.24	40.02	0.49
38.26	37.63	3.50	0.41	0.63	38.03	0.22
37.20	36.67	3.50	0.26	0.53	36.92	0.27
36.87	36.54	3.50	0.24	0.32	36.79	0.08
36.40	36.14	3.50	0.19	0.26	36.34	0.06
35.90	35.68	3.50	0.15	0.22	35.83	0.07
35.34	35.17	3.50	0.11	0.18	35.28	0.07
34.52	34.38	3.50	0.06	0.14	34.44	0.08
33.60	33.50	3.50	0.04	0.10	33.54	0.06
32.55	32.47	3.50	0.02	0.08	32.48	0.07
42.66	40.07	4.00	1.75	2.59	41.82	0.84
40.51	38.33	4.00	1.03	2.18	39.36	1.15
38.26	37.08	4.00	0.60	1.17	37.68	0.57
37.20	36.47	4.00	0.44	0.73	36.90	0.29
36.87	36.36	4.00	0.41	0.51	36.77	0.09
36.40	36.04	4.00	0.34	0.36	36.38	0.02
35.90	35.63	4.00	0.27	0.28	35.90	0.01
35.34	35.10	4.00	0.19	0.25	35.29	0.05
34.52	34.33	4.00	0.12	0.19	34.45	0.07
33.60	33.46	4.00	0.06	0.15	33.52	0.09
32.55	32.44	4.00	0.03	0.11	32.47	0.08
42.66	39.79	4.50	2.33	2.86	42.12	0.54
40.51	37.93	4.50	1.25	2.58	39.18	1.33
38.26	36.75	4.50	0.72	1.51	37.47	0.79
37.20	36.35	4.50	0.58	0.85	36.93	0.26
36.87	36.26	4.50	0.55	0.61	36.81	0.05
36.40	35.96	4.50	0.47	0.44	36.43	0.03
35.90	35.56	4.50	0.37	0.35	35.92	0.02
35.34	35.05	4.50	0.26	0.30	35.31	0.03
34.52	34.30	4.50	0.16	0.22	34.46	0.06
33.60	33.44	4.50	0.08	0.16	33.52	0.08
32.55	32.40	4.50	0.04	0.15	32.44	0.11
42.66	38.78	5.00	1.82	3.88	40.60	2.06
40.51	37.75	5.00	1.23	2.76	38.98	1.53
38.26	36.66	5.00	0.73	1.60	37.38	0.87
37.20	36.25	5.00	0.58	0.95	36.83	0.36
36.87	36.14	5.00	0.55	0.73	36.68	0.18
36.40	35.80	5.00	0.45	0.60	36.25	0.15
35.90	35.45	5.00	0.36	0.46	35.81	0.09
35.34	34.97	5.00	0.27	0.37	35.24	0.11
34.52	34.23	5.00	0.16	0.28	34.39	0.12
33.60	33.37	5.00	0.08	0.23	33.45	0.15
32.55	32.35	5.00	0.04	0.20	32.38	0.17
				Percentage Error (%) = 19/55*100 = 34.55		

Figure E - 5.2: Gauss2D's Percentage Error Calculation

Temperature (Reference)	Temperature (Before)	Distance	Delta ( From Equation)	Error(Before)	Temperature (After)	Error (After)
42.66	42.66	3.00	-0.01	0.00	42.64	0.01
40.51	40.51	3.00	-0.01	0.00	40.50	0.01
38.26	38.26	3.00	-0.01	0.00	38.24	0.01
37.20	37.20	3.00	-0.01	0.00	37.18	0.01
36.87	36.87	3.00	-0.01	0.00	36.85	0.01
36.40	36.40	3.00	-0.01	0.00	36.39	0.01
35.90	35.90	3.00	-0.01	0.00	35.89	0.01
35.34	35.34	3.00	-0.01	0.00	35.33	0.01
34.52	34.52	3.00	-0.01	0.00	34.50	0.01
33.60	33.60	3.00	-0.01	0.00	33.59	0.01
32.55	32.55	3.00	-0.01	0.00	32.54	0.01
42.66	41.28	3.50	-0.01	1.37	41.27	1.39
40.51	39.27	3.50	-0.01	1.24	39.26	1.25
38.26	37.63	3.50	-0.01	0.63	37.61	0.64
37.20	36.67	3.50	-0.01	0.53	36.65	0.54
36.87	36.54	3.50	-0.01	0.32	36.53	0.34
36.40	36.14	3.50	-0.01	0.26	36.13	0.27
35.90	35.68	3.50	-0.01	0.22	35.67	0.23
35.34	35.17	3.50	-0.01	0.18	35.15	0.19
34.52	34.38	3.50	-0.01	0.14	34.36	0.15
33.60	33.50	3.50	-0.01	0.10	33.49	0.11
32.55	32.47	3.50	-0.01	0.08	32.45	0.10
42.66	40.07	4.00	-0.01	2.59	40.06	2.60
40.51	38.33	4.00	-0.01	2.18	38.32	2.19
38.26	37.08	4.00	-0.01	1.17	37.07	1.19
37.20	36.47	4.00	-0.01	0.73	36.45	0.74
36.87	36.36	4.00	-0.01	0.51	36.35	0.52
36.40	36.04	4.00	-0.01	0.36	36.02	0.38
35.90	35.63	4.00	-0.01	0.28	35.61	0.29
35.34	35.10	4.00	-0.01	0.25	35.08	0.26
34.52	34.33	4.00	-0.01	0.19	34.32	0.20
33.60	33.46	4.00	-0.01	0.15	33.44	0.16
32.55	32.44	4.00	-0.01	0.11	32.42	0.13
42.66	39.79	4.50	-0.01	2.86	39.78	2.88
40.51	37.93	4.50	-0.01	2.58	37.92	2.59
38.26	36.75	4.50	-0.01	1.51	36.74	1.52
37.20	36.35	4.50	-0.01	0.85	36.34	0.86
36.87	36.26	4.50	-0.01	0.61	36.25	0.62
36.40	35.96	4.50	-0.01	0.44	35.95	0.45
35.90	35.56	4.50	-0.01	0.35	35.54	0.36
35.34	35.05	4.50	-0.01	0.30	35.03	0.31
34.52	34.30	4.50	-0.01	0.22	34.29	0.23
33.60	33.44	4.50	-0.01	0.16	33.43	0.18
32.55	32.40	4.50	-0.01	0.15	32.39	0.16
42.66	38.78	5.00	-0.01	3.88	38.76	3.89
40.51	37.75	5.00	-0.01	2.76	37.74	2.77
38.26	36.66	5.00	-0.01	1.60	36.64	1.61
37.20	36.25	5.00	-0.01	0.95	36.24	0.96
36.87	36.14	5.00	-0.01	0.73	36.12	0.74
36.40	35.80	5.00	-0.01	0.60	35.79	0.61
35.90	35.45	5.00	-0.01	0.46	35.43	0.47
35.34	34.97	5.00	-0.01	0.37	34.96	0.39
34.52	34.23	5.00	-0.01	0.28	34.22	0.30
33.60	33.37	5.00	-0.01	0.23	33.36	0.25
32.55	32.35	5.00	-0.01	0.20	32.33	0.22
				Percentage Error (%) = 35/55*100 = 63.64		

Figure E - 5.3: Gaussian2D's Percentage Error Calculation

Temperature (Reference)	Temperature (Before)	Distance	Delta (From Equation)	Error(Before)	Temperature (After)	Error (After)
42.66	42.66	3.00	2.93	0.00	45.58	2.93
40.51	40.51	3.00	2.25	0.00	42.76	2.25
38.26	38.26	3.00	1.21	0.00	39.47	1.21
37.20	37.20	3.00	0.81	0.00	38.01	0.81
36.87	36.87	3.00	0.70	0.00	37.57	0.70
36.40	36.40	3.00	0.57	0.00	36.97	0.57
35.90	35.90	3.00	0.45	0.00	36.36	0.45
35.34	35.34	3.00	0.34	0.00	35.69	0.34
34.52	34.52	3.00	0.23	0.00	34.74	0.23
33.60	33.60	3.00	0.14	0.00	33.75	0.14
32.55	32.55	3.00	0.09	0.00	32.64	0.09
42.66	41.28	3.50	2.81	1.37	44.09	1.44
40.51	39.27	3.50	1.83	1.24	41.10	0.59
38.26	37.63	3.50	1.05	0.63	38.68	0.42
37.20	36.67	3.50	0.70	0.53	37.37	0.17
36.87	36.54	3.50	0.66	0.32	37.21	0.34
36.40	36.14	3.50	0.55	0.26	36.70	0.30
35.90	35.68	3.50	0.44	0.22	36.13	0.22
35.34	35.17	3.50	0.34	0.18	35.51	0.16
34.52	34.38	3.50	0.23	0.14	34.60	0.09
33.60	33.50	3.50	0.14	0.10	33.65	0.04
32.55	32.47	3.50	0.09	0.08	32.56	0.01
42.66	40.07	4.00	2.39	2.59	42.46	0.20
40.51	38.33	4.00	1.45	2.18	39.78	0.73
38.26	37.08	4.00	0.90	1.17	37.98	0.28
37.20	36.47	4.00	0.68	0.73	37.15	0.05
36.87	36.36	4.00	0.65	0.51	37.01	0.14
36.40	36.04	4.00	0.56	0.36	36.59	0.19
35.90	35.63	4.00	0.46	0.28	36.08	0.18
35.34	35.10	4.00	0.35	0.25	35.44	0.10
34.52	34.33	4.00	0.23	0.19	34.56	0.05
33.60	33.46	4.00	0.15	0.15	33.60	0.00
32.55	32.44	4.00	0.09	0.11	32.53	0.02
42.66	39.79	4.50	2.32	2.86	42.11	0.54
40.51	37.93	4.50	1.30	2.58	39.23	1.28
38.26	36.75	4.50	0.80	1.51	37.55	0.70
37.20	36.35	4.50	0.67	0.85	37.02	0.18
36.87	36.26	4.50	0.64	0.61	36.90	0.03
36.40	35.96	4.50	0.56	0.44	36.52	0.12
35.90	35.56	4.50	0.45	0.35	36.01	0.11
35.34	35.05	4.50	0.35	0.30	35.40	0.05
34.52	34.30	4.50	0.24	0.22	34.54	0.02
33.60	33.44	4.50	0.15	0.16	33.59	0.01
32.55	32.40	4.50	0.09	0.15	32.49	0.06
42.66	38.78	5.00	1.76	3.88	40.53	2.12
40.51	37.75	5.00	1.23	2.76	38.98	1.53
38.26	36.66	5.00	0.78	1.60	37.43	0.82
37.20	36.25	5.00	0.64	0.95	36.89	0.30
36.87	36.14	5.00	0.61	0.73	36.75	0.12
36.40	35.80	5.00	0.52	0.60	36.32	0.08
35.90	35.45	5.00	0.43	0.46	35.88	0.02
35.34	34.97	5.00	0.34	0.37	35.31	0.03
34.52	34.23	5.00	0.23	0.28	34.46	0.05
33.60	33.37	5.00	0.15	0.23	33.52	0.09
32.55	32.35	5.00	0.09	0.20	32.44	0.11

Percentage Error (%) =  $24/55 \times 100 = 43.64$

Figure E - 5.4: Voigt2D's Percentage Error Calculation

## APPENDIX F: Arduino Source Code

```
#include <Wire.h>
#include <LiquidCrystal_I2C.h>
#include <LiquidCrystal.h>
#include "math.h"
#include "BigNumber.h"
#include "FormatDouble.h"
#include <Adafruit_MLX90614.h>
#include <usbhid.h>
#include <usbhub.h>
#include <hiduniversal.h>
#include <hidboot.h>
#include <SPI.h>
#include <SD.h>
#include <DS3231.h>
const int en = 2, rw = 1, rs = 0, d4 = 4, d5 = 5, d6 = 6, d7 = 7, bl = 3; // Define
LCD pinout
const int i2c_addr = 0x3F; // Define I2C Address - change if required
LiquidCrystal_I2C lcd(i2c_addr, en, rw, rs, d4, d5, d6, d7, bl, POSITIVE);
DS3231 rtc(SDA, SCL);
Adafruit_MLX90614 mlx = Adafruit_MLX90614();
File MyData;
const int CS = 53; //chipselect
int LED_G = 5; // Define LED pin
int LED_R = 4;
int trigPin = 2; // Define Ultrasonic sensor pins
int echoPin = 3;
boolean process = false;
double duration, cm ,delta_1, delta_2 ;
double sensorReading0, average_temperature, delta_avg, final_temperature,
sensorReading1,sensorReading2,sensorReading3, sensorReading;
BigNumber ans;
```



```

class MyParser : public HIDReportParser {
public:
    MyParser();
    void Parse(USBHID *hid, bool is_rpt_id, uint8_t len, uint8_t *buf);
protected:
    uint8_t KeyToAscii(bool upper, uint8_t mod, uint8_t key);
    virtual void OnKeyScanned(bool upper, uint8_t mod, uint8_t key);
    virtual void OnScanFinished();
};

MyParser::MyParser() {}

void MyParser::Parse(USBHID *hid, bool is_rpt_id, uint8_t len, uint8_t *buf)
{
    // If error or empty, return
    if (buf[2] == 1 || buf[2] == 0) return;
    for (uint8_t i = 7; i >= 2; i--) {
        // If empty, skip
        if (buf[i] == 0) continue;
        // If enter signal emitted, scan finished
        if (buf[i] == UHS_HID_BOOT_KEY_ENTER) {
            OnScanFinished();
        }
        // If not, continue normally
        else {
            // If bit position not in 2, it's uppercase words
            OnKeyScanned(i > 2, buf, buf[i]);
        }
    }
    return;
}

uint8_t MyParser::KeyToAscii(bool upper, uint8_t mod, uint8_t key) {
    // Letters
    if (VALUE_WITHIN(key, 0x04, 0x1d)) {
        if (upper) return (key - 4 + 'A');
    }
}

```

```

    else return (key - 4 + 'a');
}
// Numbers
else if (VALUE_WITHIN(key, 0x1e, 0x27)) {
    return ((key == UHS_HID_BOOT_KEY_ZERO) ? '0' : key - 0x1e + '1');
}
return 0;
}

void MyParser::OnKeyScanned(bool upper, uint8_t mod, uint8_t key) {
    uint8_t ascii = KeyToAscii(upper, mod, key);
    Serial.print((char)ascii);
    lcd.print((char)ascii);
    MyData = SD.open("Data.txt", FILE_WRITE);
    if (MyData) {
        MyData.print((char)ascii);
    }
    MyData.close();
}

void MyParser::OnScanFinished() {
    MyData = SD.open("Data.txt", FILE_WRITE);
    if (MyData) {
        MyData.print(',');
    }
    MyData.close();
    process = true ;
}

USB      Usb;
USBHub   Hub(&Usb);
HIDUniversal Hid(&Usb);
MyParser  Parser;

void setup() {
    //Define LED
    pinMode (LED_G, OUTPUT);

```

```
pinMode (LED_R, OUTPUT);
rtc.begin();
// The following lines can be uncommented to set the date and time
//rtc.setDOW(WEDNESDAY); // Set Day-of-Week to SUNDAY
//rtc.setTime(01, 50, 00); // Set the time to 12:00:00 (24hr format)
//rtc.setDate(24, 3, 2021); // Set the date to January 1st, 2014
// change - upload - uncomment - re upload
//Define input and output pins for ultrasonic sensor
pinMode(trigPin, OUTPUT);
pinMode(echoPin, INPUT);
// boot up the sensor
mlx.begin();
Serial.begin(9600);
if (SD.begin(CS))
{
  Serial.println("Initilization successful.Ready to use");

} else
{
  Serial.println("Inilization failed. Check your connection");
  return;
}
MyData = SD.open("Data.txt", FILE_WRITE);
if (MyData) {
  Serial.println(F("File opened ok"));
  // print the headings for our data
  MyData.println("ID, Temperature °C , Day, Date, Time ");
}
MyData.close();
Serial.println (F("Datalogger"));
Serial.println (F("ID, Temperature °C , Day, Date, Time "));
// Set display type as 16 char, 2 rows
lcd.clear();
```

```

lcd.begin(16, 2);
lcd.setBacklight(HIGH); //Lighting backlight
//barcode initialization
lcd.setCursor(0, 0);
lcd.print("Scan Your ID :");
lcd.setCursor(0, 1);
if (Usb.Init() == -1) {
  Serial.println("OSC did not start.");
}
delay( 200 );
Hid.SetReportParser(0, &Parser);
}
//Main functions will be placed under here
// Logging_details
void logging_details()
{
  //delay(1000);
  MyData = SD.open("Data.txt", FILE_WRITE);
  if (MyData) {
    MyData.print(rtc.getDOWStr()); //Day
    MyData.print(',');
    MyData.print(rtc.getDateStr()); //Date
    MyData.print(',');
    MyData.println(rtc.getTimeStr()); //Time
  }
  MyData.close();
}
// logging temperature
void logging_temperature()
{
  average_temperature = Polynomial_Fitting (); //temeprature from fixed
distance calibration
  float z = 6232.330;

```

```

float a = 1777.549;
float b = 208.8456;
float c = 0.647576;
float d = 53.47685;
float e = 1044.357;
float f = 17.71595;
float g = 93.73757;
float h = 2.027365;
float i = 19.75493;
float j = pow(average_temperature, 2);
float k = pow(cm, 2);
float l = cm * average_temperature ;
delta_1 = (-z + a * (cm) + b * (average_temperature) - (c * j) - (d * l) );
delta_2 = (1 - e * (cm) + g * (average_temperature) + (f * k) - (h * j) + (i *
l) );
delta_avg = delta_1 / delta_2 ; // delta incurred due to the change in
measuring distance
final_temperature = average_temperature + delta_avg ; // final temeprature
from multiple calibration setup
MyData = SD.open("Data.txt", FILE_WRITE);
if (MyData) {
MyData.print(final_temperature);
MyData.print(',');
}
MyData.close();
if ( final_temperature >= 35.50 && final_temperature <= 36.90 ) //normal
{
lcd.clear();
lcd.setCursor(0, 0);
lcd.print("Temperature:");
lcd.setCursor(0, 1);
lcd.print(final_temperature);
lcd.print(" Celcius");
}

```

```
digitalWrite(LED_G, HIGH);
tone(7, 500, 300);
delay(1000);
digitalWrite(LED_G, LOW);
}
else if ( final_temperature > 36.90) //high temperature
{
  lcd.clear();
  lcd.setCursor(0, 0);
  lcd.print("High Temperature");
  lcd.setCursor(0, 1);
  lcd.print(final_temperature);
  lcd.print(" Celcius");
  digitalWrite(LED_R, HIGH);
  tone(7, 1200, 2000);
  delay(10000);
  digitalWrite(LED_R, LOW) ;
}
else if ( final_temperature < 35.50 )//low temperature
{
  lcd.clear();
  lcd.setCursor(0, 0);
  lcd.print("Low Temperature");
  lcd.setCursor(0, 1);
  lcd.print(final_temperature);
  lcd.print(" Celcius");
  digitalWrite(LED_R, HIGH);
  tone(7, 1200, 2000);
  delay(10000);
  digitalWrite(LED_R, LOW) ;
}
}
float Polynomial_Fitting () {
```

```

BigNumber::setScale (10);
sensorReading1 = mlx.readObjectTempC();
delay(100);
sensorReading2 = mlx.readObjectTempC();
delay(100);
sensorReading3 = mlx.readObjectTempC();
sensorReading = sensorReading1 + sensorReading2 + sensorReading3;
char buf [20];
fmtDouble (sensorReading, 2, buf, sizeof buf);
BigDecimal data = BigDecimal (buf);
BigDecimal a ("0.0003480257");
BigDecimal b ("0.0705219732");
BigDecimal c ("5.9333044991");
BigDecimal d ("265.2889432816");
BigDecimal e ("6648.1757721581");
BigDecimal f ("88534.0889472121");
BigDecimal g ("489497.4381259961");
BigDecimal six = data.pow(6);
BigDecimal five = data.pow(5);
BigDecimal four = data.pow(4);
BigDecimal three = data.pow(3);
BigDecimal two = data.pow(2);
BigDecimal one = data.pow(1);
ans = a * (six) - b * (five) + c * (four) - d * (three) + e * (two) - f * (one) + g ;
//Polynomial Fitting equation
char * s = ans.toString ();
float temp = atof (s);
free (s);
return temp;
}
void loop() {
  Usb.Task(); //keep in loop until the process is TRUE (after barcode scanned)
  if (process) {

```

```
digitalWrite(trigPin, LOW);
delayMicroseconds(5);
digitalWrite(trigPin, HIGH);
delayMicroseconds(10);
digitalWrite(trigPin, LOW);
pinMode(echoPin, INPUT);
duration = pulseIn(echoPin, HIGH);
// Convert the time into a distance
cm = (duration / 2) / 29.1; // Divide by 29.1 or multiply by 0.0343
delay(300);
if (cm >= 3 && cm <= 4.5 ) {
  sensorReading0 = mlx.readObjectTempC();
  if (sensorReading0 >= 39) { //limit high boundary
    lcd.clear();
    lcd.print("Warning");
    lcd.setCursor(0, 1);
    lcd.print("Extreme High");
    digitalWrite(LED_R, HIGH);
    tone(7, 1200, 2000);
    delay(2000);
    digitalWrite(LED_R, LOW);
    MyData = SD.open("Data.txt", FILE_WRITE);
    if (MyData) {
      MyData.print("Extreme High");
      MyData.print(',');
    }
    MyData.close();
    logging_details();
    delay(500);
    lcd.clear();
    lcd.print("Scan Your ID:");
    lcd.setCursor(0, 1);
    process = false; //reset process
```



```
}  
else if (sensorReading0 <= 27) { //limit low boundary  
  lcd.clear();  
  lcd.print("Warning");  
  lcd.setCursor(0, 1);  
  lcd.print("Extreme Low");  
  digitalWrite(LED_R, HIGH);  
  tone(7, 1200, 2000);  
  delay(2000);  
  digitalWrite(LED_R, LOW);  
  MyData = SD.open("Data.txt", FILE_WRITE);  
  if (MyData) {  
    MyData.print("Extreme Low");  
    MyData.print(',');  
  }  
  MyData.close();  
  logging_details();  
  delay(500);  
  lcd.clear();  
  lcd.print("Scan Your ID:");  
  lcd.setCursor(0, 1);  
  process = false;  
}  
else {  
  logging_temperature();  
  logging_details();  
  delay(500); //3000  
  lcd.clear();  
  lcd.print("Scan Your ID:");  
  lcd.setCursor(0, 1);  
  process = false;  
}  
}
```

```
else if (cm < 3 ) {  
    lcd.setCursor(0, 0);  
    lcd.print("Time: ");  
    lcd.print(rtc.getTimeStr());  
    lcd.setCursor(0, 1);  
    lcd.print("Back Off  ");  
}  
else if (cm > 4.5 ) {  
    lcd.setCursor(0, 0);  
    lcd.print("Time: ");  
    lcd.print(rtc.getTimeStr());  
    lcd.setCursor(0, 1);  
    lcd.print("Come Forward ");  
}  
}  
}
```